MODELING AND OPTIMIZATION OF THE MICROSPHERE GENERATION PROCESS

A Thesis Submitted to the

College of Graduate Studies and Research

in Partial Fulfillment of the Requirements

for the Degree of Doctor of Philosophy

in the Department of Mechanical Engineering

University of Saskatchewan

Saskatoon

By

Lei Lei

©Lei Lei, April 2016. All rights reserved.

PERMISSION TO USE

In presenting this thesis in partial fulfillment of the requirements for a Postgraduate degree from the University of Saskatchewan, I agree that the Libraries of this University may make it freely available for inspection. I further agree that permission for copying of this thesis in any manner, in whole or in part, for scholarly purposes may be granted by the professor or professors who supervised my thesis work or, in their absence, by the Head of the Department or the Dean of the College in which my thesis work was done. It is understood that any copying or publication or use of this thesis or parts thereof for financial gain shall not be allowed without my written permission.

It is also understood that due recognition shall be given to me and to the University of Saskatchewan in any scholarly use which may be made of any material in my thesis.

Requests for permission to copy or to make other use of material in this thesis in whole or part should be addressed to:

Head of the Department of Mechanical Engineering
University of Saskatchewan
57 Campus Drive, Saskatoon, SK S7N 5A9, Canada

ABSTRACT

Microspheres (< 1000 μm) have applications in various fields (e.g., drug delivery, cosmetics, food, etc.). Microspheres can be generated by the micro-fluidic technique, in which microspheres are produced from one fluid under the action of another immiscible fluid in a network of channels. There are four performance indexes associated with a microsphere generation process with a device, namely (1) the size of microspheres (as small as possible), (2) the uniformity of size distributions (as high as possible), and (3) the flexibility of devices (i.e., the size range of microspheres that can be generated with one device), and (4) the efficacy of the microspheres generation process (mass production or not).

Two operating principles along with their corresponding devices, the modified T-junction device and membrane emulsification device, are studied in this dissertation, because of their unique features, with the former having an excellent task flexibility and the latter having an excellent efficacy. The study defined three objectives, namely (1) understanding the mechanism of the microsphere generation process with the modified T-junction by both numerical investigation and experimental investigation, (2) optimizing the microsphere generation process with any micro-fluidic device in general and the modified T-junction device in particular (optimization: the size and uniformity), and (3) designing and fabricating a new emulsification membrane by tackling the shortcoming (i.e., fragile with the membrane) with the existing emulsification membrane.

For objective (1), a simulation model was built first, validated by the experiment, and then the simulation model was employed to study the regimes. For objective (2), a new optimization procedure was first proposed for general micro-fluidic systems and then applied to the modified T-junction system. For objective (3), a new membrane was designed and fabricated and tested.

The following conclusions can be drawn from the study: (1) the modified T-junction device works based on a combined operating principle (flow focusing and conventional T-junction) and there are three regimes (instead of the four regimes in the conventional T-junction) in the flow; (2) the optimization of the microsphere generation process makes sense for the micro-fluidic device in general and the modified T-junction in particular (the optimal modified T-junction is: the mean size: 16.1 μm and 24.8 μm, and

the uniformity (Standard Deviation (SD)): 0.2 μm and 0.7 μm); (3) the shortcoming with emulsification membrane can be overcome with a multi-layer membrane architecture.

There are several contributions made by this dissertation in the field of micro-fluidic. First is the provision of an accurate Computational Fluid Dynamics (CFD) model for the modified T-junction. Second is the new knowledge discovered regarding the mechanism of microsphere generation with the modified T-junction device. Third is the provision of an effective optimization approach for any micro-fluidic device in general and for the modified T-junction device in particular. Fourth is the design with the successful fabrication of the membrane emulsification device based on new system architecture (i.e., multi-layer structure). From an application's perspective, this dissertation has provided evidence that with the micro-fluidic technique, the smallest size of microspheres can be 2.3 μm ; the highest uniformity (SD) can be 0.8 μm. Further, if an application puts emphasis on the task flexibility, the modified T-junction device is an excellent choice, and if an application puts emphasis on the mass production, the multi-layer membrane device is an excellent choice.

ACKNOWLEDGEMENTS

I would like to express my deepest gratitude to my supervisor, Professor Wenjun (Chris) Zhang, who brings me to the graduate study. Not only has he provided me suggestions on my research and life, but also his patience, conscientious, and encouragement has given me great support during my PhD study. His emphasis on methodology of research on graduate students is beneficial to me so much.

I also would like to express my gratitude to my co-supervisor, Prof. Donald J. Bergstrom, who has led me to the field of fluid dynamics. His expertise has greatly improved my knowledge in fluid mechanics, and his meticulous and critical approach to my work has impressed me.

I would like to thank my committee member, Prof. Fangxiang Wu, Prof. Xiongbiao (Daniel) Chen, and Prof. Jane Alcorn, who have provided me great advice during this research.

I would like to thank my friends Bing Zhang, Xue Yong, Lin Cao, Rob Arthur, Zhen Wang, Ying Yan, Bing Han, Ang Chen, Dong He, Feng Dai, Xiaohua Hu, Yu Zhao, Mengya Cai, Jun Di, who have offered me great encouragements during these years.

I would like to thank the Synchrotron Laboratory for Micro and Nano Devices (SyLMAND) at the Canadian Light Source (CLS) and all the team members in there, especially Dr. Sven Achenbach, Michael Jacobs, and Garth Wells, and they offered me great help, suggestion, assistance, and support for the membrane fabrication process.

I would like to thank my parents for their love, support, and encouragements every single day during these years when I am far away from them. This dissertation can never be completed without them.

I also would like to thank the scholarship from China Scholarship Council (CSC).

This dissertation is dedicated to
my parents and Bing.

CONTENTS

LIST OF TABLES

LIST OF FIGURES

LIST OF ABBREVIATIONS

ABS	Acrylonitrile Butadiene Styrene
CFD	Computational Fluid Dynamics
CCD	Charge-Coupled Device
CMC	Carboxymethylcellulose
DCM	Dichloromethane
DI water	Distilled water
FDA	Food and Drug Administration
IPA	Isopropyl Alcohol
LB	Lattice Boltzmann
LS	Level Set
MD	Molecular Dynamics
N-S	Naviers Stokes
ODM	Orthogonal Design Method
PDMS	Polydimethylsiloxane
PTFE	Polytetrafluoroethylene
PVA	Polyvinyl Alcohol
SD	Standard Deviation
SPG	Shirasu Porous Glass
VOF	Volume of Fluid

CHAPTER 1. INTRODUCTION

This dissertation presents the investigation of a modified T-junction device and an emulsification membrane to make microspheres. This chapter introduces the background and motivation of this research. After that, the objectives are given, followed by the organization of the dissertation.

1.1 Background and motivation

Microspheres are small particles with their diameters in the range typically from 1 μm to 1000 μm. The manufacturing system or device for making microspheres is evaluated in four areas: (1) the size of microspheres (the smaller, the better), (2) the uniformity of microspheres in terms of size (the more uniform, the better), (3) the flexibility – i.e. the capability to make microspheres of different size with one device (the larger the size range, the better), and (4) the efficacy of the microspheres generation process (mass production or not). Production and encapsulation of microspheres are the two most important steps in drug delivery technology, food science, cosmetics, electronics, and pharmaceuticals（Maan *et al.* 2015, Perez-Moral *et al.* 2014, Samimi *et al.* 2014, Sosnik 2014）. Microspheres can be produced by agitation, vibration, fluid interaction, and other techniques such as with an electromagnetic field. This dissertation only focused on fluid interaction techniques.

In fluid interaction techniques, two fluids (fluid-A and fluid-B) are presented and configured. The two fluids must be immiscible when they are put together for a sufficiently long time. Emulsification along with an external energy input leads to the situation of fluid-A encapsulating fluid-B. To facilitate the emulsion process, a special material is usually added, which is called a surfactant, to separate microspheres.

There are several ways to make fluid-A and fluid-B interact with each other to produce microspheres from fluid A (A is called the dispersed flow and B is called the continuous flow), which includes the T-junction（Arias *et al.* 2012, Balabel 2012, Bashir *et al.* 2011, Chen *et al.* 2012, Li *et al.* 2012, Li *et al.* 2014, Raj *et al.* 2010, Schneider *et al.* 2011, Ushikubo *et al.* 2014, Wang *et al.* 2011, Yeom and Lee

2011), the flow focusing (Chen *et al.* 2014, Cohen *et al.* 2014, Liu and Zhang 2011, Mulligan and Rothstein 2012, Tarameshlou *et al.* 2014), the membrane emulsification (Akamatsu *et al.* 2010, Holdich *et al.* 2010, Lloyd *et al.* 2014, Piacentini *et al.* 2013, Santos *et al.* 2015, Vladisavljevic and Schubert 2002, Wagdare *et al.* 2010, Zhou *et al.* 2007), and variations of the foregoing three, such as the modified T-junction (Song 2011), and multi-emulsification devices (Chiu and Chen 2011, Fu *et al.* 2005, Lin *et al.* 2010, Nurumbetov *et al.* 2012, Vladisavljević *et al.* 2012, Wang *et al.* 2010). Characteristics of each device will be discussed in Chapter 2.

In order to have a better understanding of the microsphere formation process, such as the flow patterns and the size distribution of microspheres, many studies have been performed computationally and experimentally (Anna *et al.* 2003, Anna and Mayer 2006, Castro-Hernández *et al.* 2009, Glawdel and Ren 2012, Guillot *et al.* 2008, Moon *et al.* 2014, Nunes *et al.* 2013, Ong *et al.* 2007, Utada *et al.* 2008, Utada *et al.* 2007, Ward *et al.* 2005). These studies focused on devices with the conventional operating principles but not on the devices that are based on a combination of two or three conventional operating principles, such as the modified T-junction device. Therefore, adding this missing element to the knowledge of micro-fluidic devices became the first motivation of this dissertation.

Another motivation came from some missing elements of knowledge of the membrane emulsification device. Conventional membranes are usually made of silicon (Lloyd *et al.* 2014, Song 2011, Thanh Ha *et al.* 2013, Van der Graaf *et al.* 2004), Shirasu Porous Glass (SPG) (Liu *et al.* 2012, Liu *et al.* 2012, Nakashima *et al.* 1987, Oh *et al.* 2011, Vladisavljevic and Schubert 2002, Vladisavljević and Schubert 2003), or metal materials (Aryanti *et al.* 2006, Holdich *et al.* 2013, Piacentini *et al.* 2013, Vladisavljevic and Williams 2006). The silicon membrane is cost-effective, easy to set up and able to produce small microspheres (close to nanometer) but has poor strength, which may lead to the membrane being broken when the pressure added is high (Song 2011). The SPG membrane has high strength and accuracy but can be easily contaminated during the microsphere generation process (which compromises its application in the area of biology). Further, the SPG membrane is relatively expensive compared with the membranes made of other materials (Nakashima *et al.* 1987, Oh *et al.* 2011). The metal membrane has high strength but with much larger pore sizes, usually over 20 μm (Aryanti *et al.*

2006, Holdich *et al.* 2013, Vladisavljevic and Williams 2006). Therefore, development of a new technology for making membranes which bear high pressure meanwhile with small pore size and low cost was the second motivation of this dissertation.

In short, the overall objective of this dissertation study was to improve the understanding of the modified T-junction and optimize the microsphere generation process with it, and to advance the technology for making a new membrane emulsification device.

1.2 Objectives and scope

To achieve the foregoing overall objective, the following specific objectives were defined.

Objective 1: Build both a computational model and experimental test-bed to examine the flow pattern of the microsphere generation process with the modified T-junction device to characterize the flow pattern and find the mechanism of the microsphere generation process with the modified T-junction device.

Objective 2: Investigate the methodology for optimizing the performance in terms of the size and uniformity of microspheres generated with any micro-fluidic device and then demonstrate its effectiveness on the modified T-junction device.

Objective 3: To explore the structure of the membrane emulsification device that can be made by the current micro-fabrication technology such that the performance of the device for microsphere generation can be improved in terms of the size and uniformity of microspheres.

1.3 The organization of dissertation

Chapter 2 presents a comprehensive literature review on microsphere generation by fluid-fluid interaction techniques, including the review of the force balance model of a microsphere during its formation and three operating principles for this model. Many micro-fluidic devices were discussed, and modeling of fluidic devices was also reviewed.

Chapter 3 presents a study on developing a mathematical model based on the fundamental governing principle of flows and computational fluid dynamics. The model was realized with the software tool called COMSOL. The model was verified by the experiment. The model was then used as a simulator (i.e., simulation test-bed) to understand the mechanism of microsphere generation with respect to Objective 1 of the dissertation and to optimize the performance of micro-fluidic devices, the modified T-junction device in particular.

Chapter 4 presents a study on understanding the fundamental mechanism of the microsphere generation process with the modified T-junction device with the help of the simulator developed in Chapter 3. The study also involved the experimental observation with a physical test-bed built along with this study. The outcome of the study was very useful to the optimization of the performance of the modified T-junction device, presented in Chapter 5.

Chapter 5 presents a new design methodology for optimizing the so-called process system such as the microsphere generation process with micro-fluidic devices (e.g., the modified T-junction device). Both the simulator (in Chapter 3) and physical test-bed (in Chapter 4) were employed in this methodology. This chapter then describes the optimization of the microsphere generation process with the modified T-junction device by applying this methodology.

Chapter 6 presents the design and fabrication of a new membrane emulsification device based on a rational analysis of problems with this device, which led to some new findings. This chapter subsequently presents an experimental study of the performance of this device to confirm the findings.

Chapter 7 presents the conclusions and future work.

CHAPTER 2. MICROSPHERE GENERATION BY FLUID-FLUID INTERACTION TECHNIQUE: REVIEW AND FUTURE DIRECTIONS

2.1 Introduction

This chapter presents a review of the literature in relation to the proposed objectives in Chapter 1. The scope of the review is the micro-fluidic approach to generate microspheres. The review also covers the modeling of the microsphere generation process, as this is an important tool in this field. Section 2.2 provides a background on fundamental mechanics of the microsphere generation. Section 2.3 discusses three well known operating principles of various micro-fluidic devices in the literature, including their configuration and how microspheres are formed. Section 2.4 provides a review of the existing micro-fluidic devices. Section 2.5 presents a discussion on the modeling of the microsphere generation process. Finally, there is a revisit of the objectives as proposed in Chapter 1 and discusses the need and urgency of this dissertation research. A part of the content presented in this chapter was written into a paper submitted to *Recent Patents on Nanotechnology*.

2.2 The fluid mechanics of microsphere generation

Microspheres are formed from the main body of one fluid say A by a cutting force or pressure which induces an internal stress in the fluid A. One of the means to generate the stress in the fluid is to subject it to the flow of another fluid say B. The flow from which a microsphere is formed is called the dispersed flow while the other fluid is called the continuous flow. Note that generation of the stress is not always induced by mechanical interaction with another flow, but other approaches such as the optical-electric effect may also be possible. Although this dissertation study only considered the mechanism of flow interaction, sometimes referred to as the fluid-cut-fluid paradigm, the discussion of the fundamental mechanics that governs drop formation remains generally applicable.

During the process of two fluids interacting, there are two opposing forces exerted on the dispersed flow: (1) holding force and (2) detaching force. The holding force tends to maintain the integrity of the dispersed fluid, and therefore can be considered to hinder the formation of the microsphere. The

detaching force tends to separate the tip region of the dispersed fluid, which subsequently forms into a microsphere. Their relationship accounts for how a microsphere is formed.

Figure 2.1 illustrates the microsphere formation process for four different scenarios. Note that the holding force and detaching force must balance each other when the microsphere just starts to detach, and the mechanical equilibrium is broken to initiate the detaching process. The principle of the microsphere generation based on the notion of a holding force and a detaching force is discussed in detail in the following.

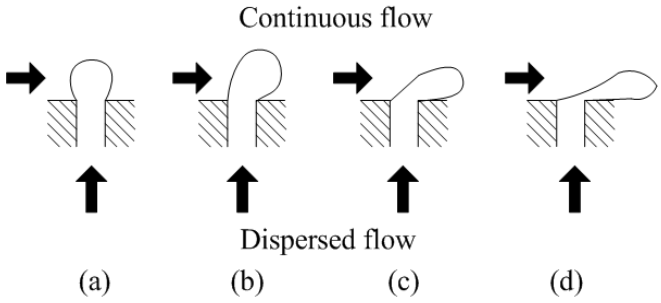

Figure 2.1. Illustration of the droplet formation under different conditions: (a) low detaching force, (b) high detaching force compared to the interfacial tension, (c) very small contact angle or extremely high detaching force, (d) membrane surface wetted by dispersed flow. Reprinted with kind permission from Peng and Williams (1998).

In a typical microsphere formation process, the detaching forces are hydrodynamic forces which arise from the pressure and stress fields in the continuous flow, while the holding force is primarily caused by interfacial tension. The discussion of the forces below is presented in the context of two different assumptions about the rigidity of the microsphere being formed, and mostly follows from "Experimental and theoretical approaches on microsphere formation from a micrometer screen hole" by Xu et al. (2005) and "Microsphere detachment in cross-flow membrane emulsification: comparison among torque-based and force-based models" by De Luca et al. (2008).

2.2.1 Rigid microsphere model

Peng and Williams (1998) presented a torque-based balance model of microsphere formation by assuming the microsphere to be non-deformable or rigid. Under this assumption, the center of the

microsphere and the contact line will always be perpendicular to the membrane.

2.2.1.1 Hydrodynamic forces

The hydrodynamic forces can be conveniently resolved into the drag ($\boldsymbol{F}_D$) and lift ($\boldsymbol{F}_L$) components on the microsphere. By definition, the drag and lift force components exerted on the microsphere by the continuous flow act parallel and normal, respectively, to the relative approach velocity of the continuous flow（Streeter *et al.* 1998）. For micro-fluidic devices, the velocity profile very close to the microsphere is treated as parallel to the microsphere surface, since the Reynolds number of the continuous flow $Re = \frac{UD}{\mu}$ is typically less than 1, where U is the continuous flow velocity, D is the dimension of the channel, and μ is the viscosity of the continuous flow. The net force due to the shear stress acting on the microsphere can include both lift and drag components, although the drag component will be dominant. The lift force component acting on the microsphere is contributed primarily by the pressure field acting on the microsphere. Note that there is also a pressure difference ($\mathrm{P}_1 - \mathrm{P}_2$) across the surface of the microsphere, which is called the Laplace pressure（Butt *et al.* 2006）. It is proportional to the interfacial tension of the two phases, and inversely proportional to the radius of the microsphere, which is a measure of the curvature of the local surface. The net force due to this pressure difference $\boldsymbol{F}_P$ acts in the direction of the lift force and tends to induce the detachment.

The net drag force exerted on the microsphere is contributed by both the shear stress and pressure fields around the microsphere. The component due to the shear stress is called the skin friction drag, while the component due to the difference in pressure between the upstream and downstream of the microsphere is called the form drag. The ratio of the skin friction and form drag depends on the geometry of the microsphere and the Reynolds number of the continuous flow（Streeter *et al.* 1998）. The total drag will increase with an increase in the microsphere diameter for a constant continuous flow rate.

2.2.1.2 Interfacial tension force $\boldsymbol{F}_\gamma$

The interfacial tension force is caused by the interfacial tension associated with the surface between the microsphere and the continuous flow. In the rigid microsphere model, the contact angle θ is constant along the contact line of the microsphere and membrane wall, as shown in Figure 2.2. As a result, the

interfacial tension force $\boldsymbol{F}_\gamma = \pi\gamma D_p$ is constant, and the direction is perpendicular to the membrane, i.e. in the negative lift direction.

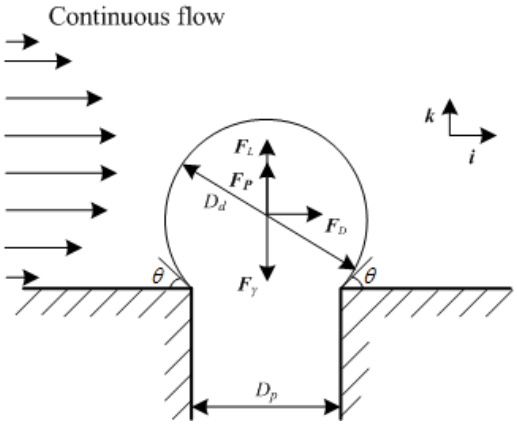

Figure 2.2. Forces acting on the rigid droplet. $\boldsymbol{F}_p$: the pressure difference force; $\boldsymbol{F}_L$: the lift force; $\boldsymbol{F}_d$: the drag force; $\boldsymbol{F}_\gamma$: the interfacial tension force; $\boldsymbol{D}_d$ is the diameter of the droplet. $\boldsymbol{D}_p$ is the diameter of the pore. θ is the contact angle along the contact line. $\boldsymbol{i}$ and $\boldsymbol{k}$ are the unit vectors parallel and perpendicular to the wall, respectively. Reproduced from De Luca et al. (2008).

2.2.2 Deformable droplet model

When the size of the microsphere is significantly larger than the size of pore, the rigid microsphere model does not apply. De Luca and his group (2008) proposed a different model, called the deformable microsphere model, to analyze the forces exerted on the microsphere. In their model, the contact angle is no longer constant when the microsphere grows. It represents an advancing contact angle when it is located on the upstream side of the microsphere, and a receding contact angle when it is located downstream, as shown in Figure 2.3.

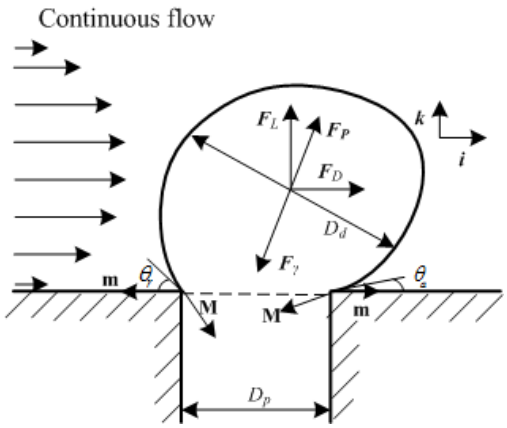

Figure 2.3. Forces acting on the deformable droplet. $\boldsymbol{M}$ and $\boldsymbol{m}$ are the unit vectors. $\boldsymbol{i}$ and $\boldsymbol{k}$ are the unit vectors parallel and perpendicular to the wall, respectively. Reproduced from De Luca et al. (2008).

2.2.2.1 Hydrodynamic forces

For the deformable microsphere, the generation of the hydrodynamic force components becomes more complicated. For the lift component, the shear stress around the microsphere contributes a small part of the total lift due to the unsymmetrical geometry of the microsphere. Similar to the rigid microsphere model, the drag component is contributed by both the pressure and shear stress fields. The drag force component can be calculated once the flow pattern and associated pressure field are known using the following equation:

$$\text{Drag} = \int (\text{p}\, sin\, \alpha + \tau_0\, cos\, \alpha) dA \tag{2.1}$$

where τ_0 is the surface shear stress; p is the local pressure; dA is a differential surface area; α is the angle between the tangent line of the surface and the direction of the continuous flow, see Figure 2.3.

2.2.2.2 Interfacial tension force F_γ

In the deformable microsphere model, the interfacial tension force is not constant along the contact line since the contact angle varies. Therefore, the relation used to compute the interfacial tension needs to account for the variation in the contact angle, i.e.

$$\begin{cases} F_{\gamma i} = \int_{\Gamma} \gamma(\boldsymbol{M}\cdot\boldsymbol{m})\,\boldsymbol{m}\cdot\boldsymbol{i}\,d\Gamma & (parallel\ to\ the\ membrane) \\ F_{\gamma k} = \int_{\Gamma} \gamma(\boldsymbol{M}\cdot\boldsymbol{k})\,\boldsymbol{k}\cdot\boldsymbol{k}\,d\Gamma & (perpendicular\ to\ the\ membrane) \end{cases} \tag{2.2}$$

where Γ refers to the contact line, $\boldsymbol{M}$ and $\boldsymbol{m}$ are unit vectors, and $cos\,\theta = \boldsymbol{M}\cdot\boldsymbol{m}$; see Figure 2.3.

It is clear that the balance between the hydrodynamic forces and interfacial tension force affects the microsphere formation process. Normally, a dimensionless number called the capillary number (Ca) is introduced to indicate whether a microsphere will be formed. From its definition, $Ca = \frac{\mu u}{\gamma}$ represents the magnitude of the viscous force relative to the interfacial tension force, where μ and u are the viscosity and a relevant velocity scale of the continuous phase, respectively, and γ is the interfacial tension of the two phases. The threshold value of Ca above which a microsphere will be formed is called the critical value of the capillary number, and is denoted as Ca_{cr}. Specifically, if Ca is greater than Ca_{cr}, the physical meaning is that the dominating effect is that of the viscous force, and as such, microspheres can be formed from a disperse phase. However, this critical value depends on the underlying fluid system（De Menech *et al.* 2008, Tice *et al.* 2003, Van der Graaf *et al.* 2005）. For instance, based on the different flow configurations they considered, De Menech et al. (2008) found a critical value of $Ca_{cr} = 0.01$, while Tice et al. (2003) suggested that this critical number be $Ca_{cr} = 1$, and Van der Graaf et al. (2005) suggested that the critical number be $Ca_{cr} = 0.1$.

2.3 Three basic operating principles

In Section 2.2, the fundamental fluid mechanics of the microsphere formation process based on the interaction of two fluids was discussed. The nature of this hydrodynamic process can be succinctly described by the phrase “fluid-cut-fluid”, and can also be referred to as a micro-fluidic approach. There are three basic operating principles used to configure the two fluids: T-junction, flow focusing, and membrane emulsification, which are described in details below. These principles can be used as building blocks to construct various devices to optimize the microsphere formation and also to form microspheres that have more sophisticated structures, such as multi-shell encapsulation; see a detailed discussion in Section 2.4.

2.3.1 T-junction

The T-junction principle was first developed by Bragg and Nye (1947). For reference in subsequent discussions, a schematic diagram giving the generic configuration of the T-junction principle is shown in Figure 2.4 The dispersed fluid and continuous fluid flow through the vertical channel and the horizontal channel, respectively. According to（Glawdel *et al.* 2012）, the dispersed flow undergoes two periods. In the first period, the microsphere grows (see the previous discussion of Figure 2.2). In the second period, the pressure in the upper stream increases due to the growth of the microsphere of the dispersed flow and the confinement of the channel, and the pressure in the upper stream of the continuous flow builds up to squeeze the neck part between the microsphere of the dispersed flow and the main body of the dispersed flow in the vertical channel to cut the neck eventually. By changing the flow parameters, such as the ratio of the flow rates of the two fluids, physical properties, and the channel geometry, one can alter the capillary number, Ca, of the continuous flow to achieve optimal performance of microsphere formation in terms of the microsphere size, uniformity and production rate（Arias *et al.* 2012, Chen *et al.* 2012, De Menech *et al.* 2008, Li *et al.* 2012, Sivasamy *et al.* 2011, Song and Zhang 2013, Song 2011, Yeom and Lee 2011）.

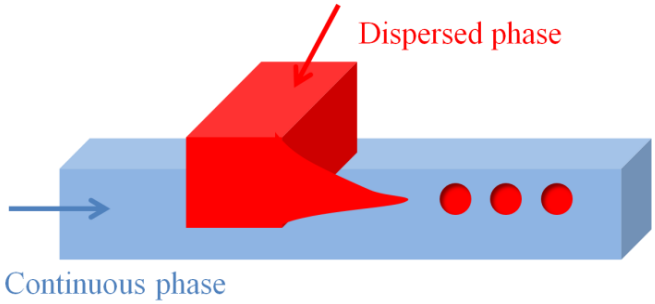

Figure 2.4. Schematic diagram of the T-junction device.

2.3.2 Flow focusing

The flow focusing operating principle was first introduced by Anna et al.（2003）. It was developed to overcome the limitations of the T-junction device with respect to uniformity, controllability, and microsphere size dependency on the channel size（Song 2011）. Figure 2.5 is a schematic diagram of the generic configuration of the flow focusing principle. There are two periods of flow with respect to the dispersed flow according to（Anna *et al.* 2003）. In the first period, the dispersed fluid flows to the

junction, and the flow grows. In the second period, the continuous flow gives pressure to squeeze the disperse flow in the neck until the neck is broken. In comparison with the T-junction approach, the flow focusing approach tends to create a shear force in the dispersed flow in a more symmetrical and thus uniform way（Dupin *et al.* 2006, Li and Wang 2013）. The microsphere formation process is affected by various parameters including the ratio of the two flow rates, Ca of the continuous flow, and properties of the fluids（De Luca and Drioli 2006, De Luca *et al.* 2004, Holgado *et al.* 2008, Liu and Zhang 2011, Meyer *et al.* 2010, Schneider *et al.* 2011, Timgren *et al.* 2010, Wu *et al.* 2008, Zhang *et al.* 2011）.

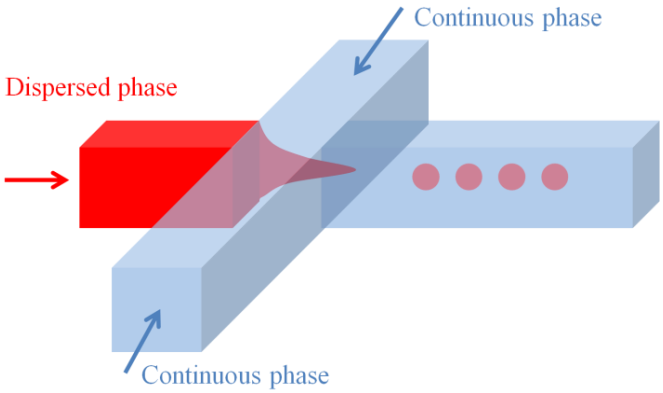

Figure 2.5. Schematic diagram of the flow focusing device.

2.3.3 Membrane emulsification

The membrane emulsification operating principle was first introduced by Kawakatsu and his group（1996）. An advantage of the device based on this principle is a higher production rate compared to devices based on the other two operating principles. Figure 2.6 shows a schematic diagram of the generic configuration of the membrane emulsification operating principle. Similarly, there are also two periods in the microsphere generation process according to（De Luca and Drioli 2006）: filling period and necking period. In the filling period, the dispersed flow is pressed through the polypore array in the membrane and at the exit of each sub-channel forms a sphere due to interfacial tension. The sphere grows until it reaches a specific depth. Then, the necking period begins. A neck is formed and squeezed due to the drag force from the continuous phase. During this time the dispersed phase flows into the microsphere continuously until the neck is broken.

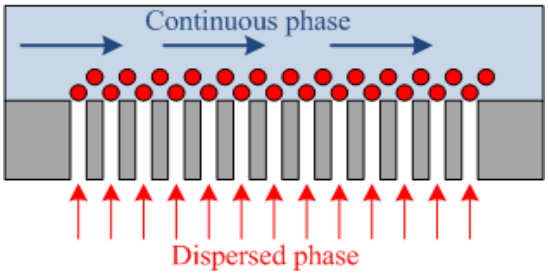

Figure 2.6. A side view of the membrane emulsification device.

The microsphere formation process is affected by various parameters including the wetting properties, the size and spacing of the pores in the membrane, Ca of the continuous flow, and trans-membrane pressure（Gasparini *et al.* 2008, Hancocks *et al.* 2013, Joscelyne and Trägårdh 2000, Krause *et al.* 2011, Meyer *et al.* 2010, Pathak 2011）.

2.4 Microsphere generation devices

Various devices have been developed and reported in the literature based on the aforementioned three operating principles. Table 2.1 shows some of these devices. The following discussion identifies what these devices have achieved and also comments on their limitations.

Table 2.1. Microsphere generation using micro-fluidic devices.

Micro-device	Dimensions of the device	Product	Diameter of microspheres	Reference
T-junction	Dispersed phase width: 20 μm Continuous phase width: 100 μm	Silicon oil	34 μm	Tarchichi et al.（2013）
	Width: 35 μm Height: 6.5 μm	Span 80	12 μm	Thorsen et al.（2001）
	Width = Height: 100 μm	Silicon oil	119 μm	Nisisako et al.（2010）

Table 2.1. Continued.

T-junction	Dispersed phase diameter: 150 μm Continuous phase diameter: 400 μm	TiO_2 suspension	150 μm ~ 400 μm	Schunk et al. (2012)
	Width: 200 μm Height: 100 μm	Poly(lactic-co-glycolic acid) (PLGA)	50 μm	Samimi et al. (2014)
	Width: 120 μm Height: 100 μm	Sodium poly(styrenesulfonate) (NaPSS)	50 μm	Watanabe et al. (2014)
	Width: 126 μm Height: 75 μm	Perfluorooctyl bromide (PFOB) + Polylactic acid (PLA)	20.8 μm	Watanabe et al. (2013)
	T-shaped: 200 μm Y-shaped: 250 μm	Hexadecane/soybean oil	266 μm	Ushikubo et al. (2014)
	Width = Height: 50 μm	Distilled water	65 μm	Ding et al. (2015)
Flow focusing	Width: 50 μm Height: 5 μm	Soybean oil	9 μm	Xu and Nakajima (2004)
	Width: 50 μm Height: 80 μm	Chitosan	44 μm ~ 83 μm	Yeh and Lin (2013)
	Width: 70 μm Height: 50 μm	PLGA	24 μm	Perez et al. (2015)
	Width: 70 μm Height: 50 μm	Chitosan/agarose	18 μm	Zamora-Mora et al. (2014)
	Diameter:1.58 mm	Gelatin	around 50 μm	Moon et al. (2014)

Table 2.1. Continued.

Flow focusing	Width: 20 μm Height: 25 μm	Alginate	26 μm	Akbari and Pirbodaghi (2014)
	Diameter:1 mm	PLA	18 μm ~ 150 μm	Vladisavljević et al. (2014)
Flow focusing	Width = Height: 100 μm	PLA and PLGA	25 μm ~ 60 μm	Yang et al. (2014)
	Width: 150 μm Height: 20 μm	Mineral oil, silicon oil, and distilled water	20 μm ~ 300 μm	Wu et al. (2014)
	Width: 35 μm Height: 75 μm	Alginate	40 μm ~ 60 μm	Chen et al. (2013)
Membrane emulsification	1.4 μm	Rape seed oil	4.6 μm	Vladisavljevic and Schubert (2002)
	2.5 μm	Sunflower oil	40 μm	Piacentini et al. (2013)
	10 μm	Sunflower oil	30 μm	Holdich et al. (2010)
	6.1 μm	Sunflower oil/Silicon oil	23.4 μm	Lloyd et al. (2014)
	4.7 μm	Agarose dissolved in water	15 μm	Zhou et al. (2007)
	5 μm	Sunflower oil	33 μm	Wagdare et al. (2010)

Table 2.1. Continued.

Membrane emulsification	10 μm	N,N-dimethyldecanamide (AMD-10TM) and d-limonene containing 0–35 wt% AMD-10TM	6 μm	Santos et al. (2015)
	1.1 μm	Chitosan	10 μm	Akamatsu et al. (2010)
Modified T-junction	Width: 38 μm Height: 5 μm	Distilled water	16 μm ~ 35 μm	Song (2011)
Multiple emulsifications	Inner diameter: 100 μm Outer diameter: 150 mm Collection diameter: 150 μm	PEG6000 and PVA (1:4) in ethyl acetate	23 μm ~ 47 μm	Pessi et al. (2014)
	Inner diameter: 80 μm Outer diameter: 1 mm Collection diameter: 120 μm	Hydrocarbonized PSi microparticles (THCPSiMPs) encapsulated within the aqueous cores of lipid vesicles	114 μm	Herranz-Blanco et al. (2014)
	Inner: 25 μm (width)× 25 μm (height) Middle: 25 μm (width)× 25 μm (height) Outer: 50 μm (width)× 200 μm (height)	Water in ethoxylated trimethylolpropane triacrylate (ETPTA)	30 μm	Wu et al. (2013)

Table 2.1. Continued.

Multiple emulsifications	First: 60 μm (width)× 25 μm (height); 40 μm (width)× 10 μm (height); 85 μm (width)× 35 μm (height) Second: 130 μm (width)× 65 μm (height); 180 μm (width)× 75 μm (height); 225 μm (width)× 100 μm (height)	Water in corn oil	106 μm	Okushima et al.（2004）

2.4.1 T-junction

Tarchichi et al.（2013）discovered a new regime during the microsphere generation called the balloon regime. In the balloon regime, microspheres are circular in shape before they detach from the dispersed phase. The velocities of each flow and dimensions of the device were identified as key variables for the microsphere formation. Note that during the detachment process, there is no further deformation of the spheres. A schematic diagram for the microsphere formation in the balloon regime is shown in Figure 2.7. Nisisako and Hatsuzawa（2010）developed a new T-junction device to produce biphasic microspheres, see Figure 2.8. The shape of microspheres could be controlled by adjusting the flow rates.

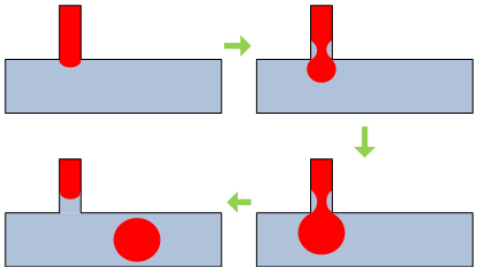

Figure 2.7. Schematic diagram for the droplet formation in the balloon regime. Reproduced from Tarchichi et al. (2013).

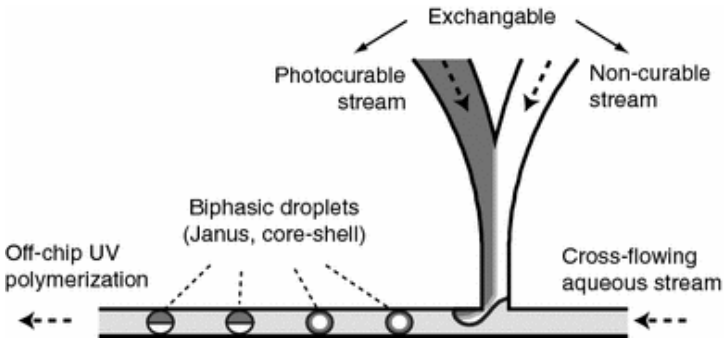

Figure 2.8. Schematic diagram of a micro-fluidic system for producing two-phase droplets. Reprinted with kind permission from Nisisako and Hatsuzawa (2010).

Schunk et al.（2012）encapsulated TiO_2 particles into uniform microspheres ranging from 150 μm to 400 μm in diameter. Samimi et al.（2014）encapsulated Acetyl Ginsenoside Rb_1 as a drug into microspheres. Watanabe et al.（2014）produced microspheres with a polymer shell and internal porous structure by adding an extraction process, see Figure 2.9. They also obtained PFOB microspheres encapsulated by PLA without any special extraction process（Watanabe *et al.* 2013）. The process for producing this particle is illustrated in Figure 2.10.

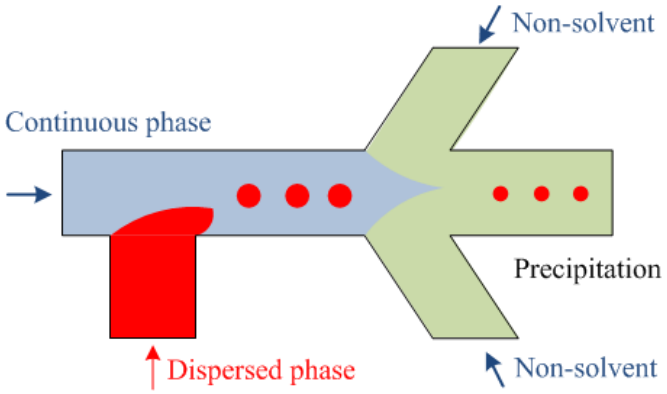

Figure 2.9. Schematic diagram of the NaPSS particles formation process via the micro-fluidic emulsification and the solvent extraction. Reproduced from Watanabe et al. (2014).

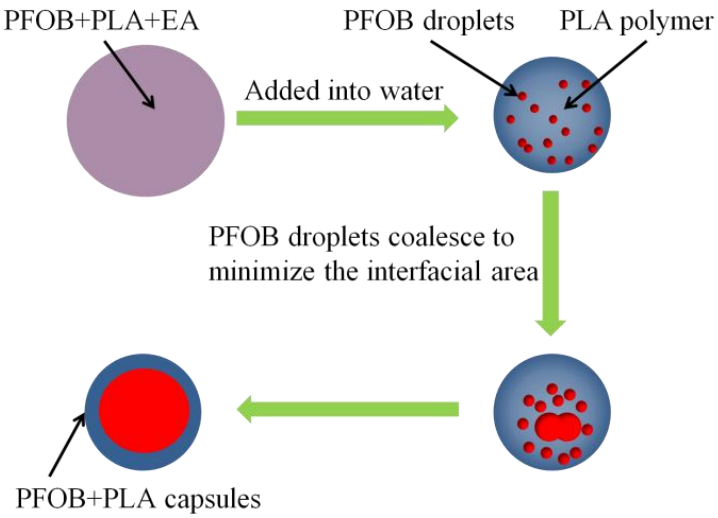

Figure 2.10. Schematic diagram of the mechanism of the PLA microcapsules formation. Reproduced from Watanabe et al. (2013).

Ding et al.（2015）proposed a special “V-junction” to make microspheres. A schematic of the structure of the device is shown in Figure 2.11. The control channel is connected to a suction pump. Once impurities have been completely removed from the control channel, it will be blocked so that water enters the main channel to produce microspheres. Ushikubo and Birribilli（2014）compared two different T-junction geometries: one is a normal T-junction, the other is Y-shaped T-junction, which is shown in Figure 2.12. They studied the effects of flow rates and fluid properties on the microsphere size. According to their result, with the Y-shaped T-junction, microspheres produced were non-uniform, and microspheres could not be formed at low velocity ratios between the continuous and dispersed phase. In contrast, the T-shaped T-junction was able to produce uniform microspheres and to form microspheres for a relatively low velocity ratio between the continuous and dispersed phase.

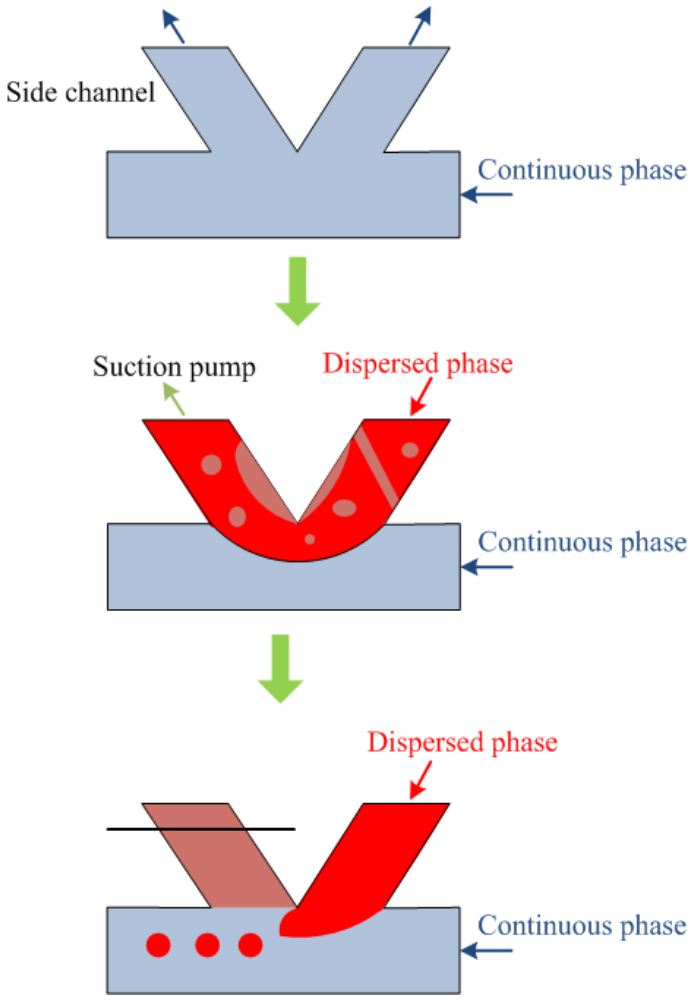

Figure 2.11. Schematic diagram of the V-junction structure. A side channel was used for control. The angle between the two side channels was 60°. Reproduced from Ding et al. (2015).

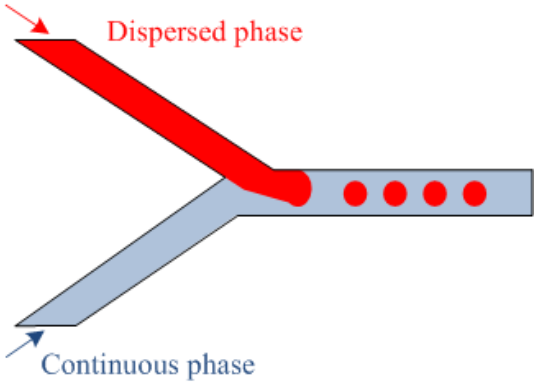

Figure 2.12. Schematic diagram of the Y-shaped T-junction. Reproduced from Ushikubo et al. (2014).

In summary, the T-junction device has some advantages for microsphere formation. The structure is simple, and it is easy to alter the size of microspheres. Its main limitation is that it is not suitable for mass production, which restricts its application in industry.

2.4.2 Flow focusing

Using devices based on the flow focusing principle, Yeh and Lin（2013）produced chitosan microspheres encapsulating metal (Fe_3O_4) nanoparticles with the standard deviation of 4.4 μm, while Perez et al.（2015）generated microspheres of high uniformity with the standard deviation less than 0.4 μm. Perez et al.（2015）further compared microspheres generated by the flow-focusing device and a conventional emulsification process: they found that although the size of microspheres produced by these two methods is similar, microspheres made by the flow focusing device are more uniform. Zamora-Mora et al.（2014）used chitosan and agarose to make composite microspheres with different concentrations of agarose in the dispersed phase.

They also investigated the release rate of microspheres under different pH values, and found that high pH value have high release rate. Moon et al.（2014）studied the effects that influence the microsphere generation process. They found that the flow rate of the continuous phase and the viscosity of the dispersed phase were key factors to determine the formation regime, e.g. jetting or dripping. They also suggested that the critical value of Ca was 0.0136 for successfully generating microspheres. Akbari and Pirbodaghi（2014）encapsulated mammalian cells and $CaCO_3$ into alginate microspheres. Their research contributed to the improvement of the viability of cells in gelled alginate particles. Vladisavljević et al.（2014）used a special flow-focusing device to produce microspheres with different composition, and also studied the process numerically. Figure 2.13 shows a schematic diagram of their device. They also investigated the dispersed flow rate and found the We number of the dispersed phase to have a significant effect on the flow regime. Yang et al.（2014）tested multiple materials for the flow focusing device fabrication, and concluded that Phenol formaldehyde resin (PFA) was low-cost, can be easily cleaned and reused compared to a more conventional material like Polydimethylsiloxane (PDMS). Wu et al.（2014）proposed a new flow focusing device which was readily assembled, circumvented the issue of hydrophilicity and hydrophobicity, and produced microspheres with a larger production rate than PDMS. A schematic diagram of their device is shown in Figure 2.14. Chen et al.（2013）used the micro-

fluidic device in a biological application. They made alginate microspheres encapsulating a specific antibody, so that the concentration of antibody could be easily controlled.

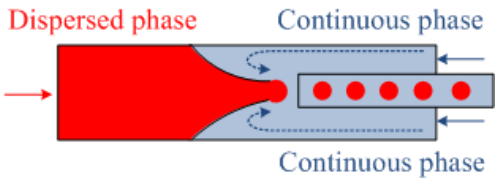

Figure 2.13. Schematic diagram of the micro-fluidic device. Reproduced from Vladisavljević et al. (2014).

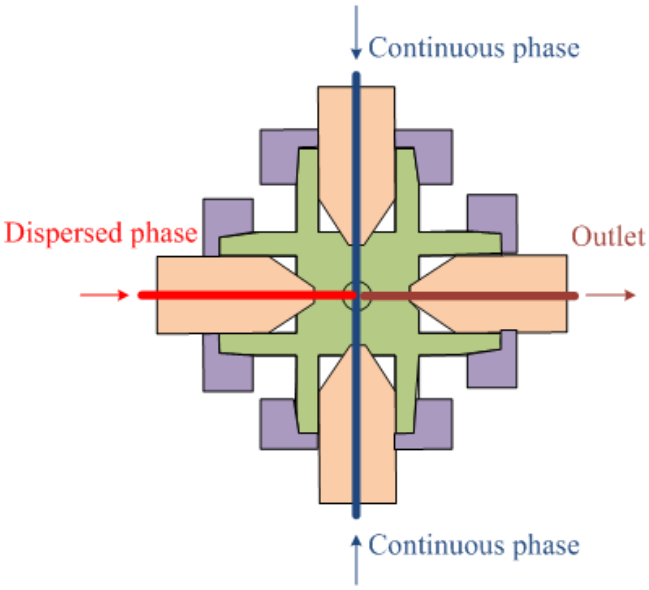

Figure 2.14. A top view of the Micro-Cross. Reproduced from Wu et al. (2014).

Overall, the flow focusing device is a promising approach for making microspheres. Flow focusing devices can readily make smaller microspheres than the T-junction device. The flow-focusing device is well suited to make microspheres due to its symmetric structure. However, this method is not suitable for mass production.

2.4.3 Membrane emulsification

Vladisavljevic and Schubert（2002）produced microspheres using Shirasu Porous Glass (SPG)

membrane. According to their study, the microsphere size was 3.5 times larger than the pore size under the pressure which was slightly larger than the trans-membrane pressure. One issue of their study was that only 20% pores were active, which may be caused by this low pressure. However, the broader size distribution was found if they increased the pressure. Piacentini et al.（2013）investigated the influence of the parameters (i.e., pH value, biopolymer (fish gelatine and gum arabic) ratio and concentration, surfactant, and dispersed phase concentration) on the diameter of microspheres and the thickness of the shell around the microsphere. Lloyd et al. (2014) studied the effects of the trans-membrane pressure, rotational speeds, annular gap width (between the membrane surface and the outer vessel wall), dispersed and continuous phase viscosity on the diameter of microspheres. Zhou et al. (2007) studied the effect of the oil phase, surfactant, and temperature on the uniformity of microspheres. The uniformity of microspheres (SD) could be under 2.2 μm by optimising the experiment condition. They also found that there was a linear relationship between the diameter of microspheres and the pore size of the membranes. Wagdare et al.（2010）found that by adding a surfactant into the dispersed phase (normally the surfactants were added into the continuous phase), the coalescence of microspheres and wetting of the silicon nitride membrane by the dispersed phase was prevented. This phenomenon was explained by the faster adsorption dynamics due to the surfactant in the dispersed phase. Thus, they suggested that the combination of surfactants in both the dispersed and continuous phases led to more effective microspheres generation process. Santos et al.（2015）found that by premix the dispersed phase by agitation, the microsphere diameter (6 μm) could be smaller than the pore size (10 μm and 20 μm). Although the diameter distribution of microsphere produced with the premix process was broader than microspheres produced without the premix process, this issue could be overcame by making microspheres passing through the membrane two or three times.

The efficiency of production of the membrane emulsification method is much improved over the other two methods due to its porous structure. However, to generate small microspheres, the pores on the membrane need to be very small. As the size of the pores decreases while the thickness of the membrane is keeping unchanged (in order to ensure an adequate strength in the membrane), the aspect ratio of each pore increases. The aspect ratio, in turn, is limited by the present micro-fabrication techniques, so the size of pores in the membrane is limited. Currently, the size of pores in the membrane could be less than 1 μm.

2.4.4 Modified T-junction device

Song（2011）proposed a modified T-junction operating principle so that the size of the microsphere can be adjusted without a need to change the channel size. The idea was to have a sheath flow surrounding the dispersed flow. Figure 2.15 is a schematic diagram of this device, which shows the configuration of the three flows: the middle flow or dispersed flow, the sheath flow which squeezes the middle flow, and the continuous flow. By adjusting the sheath flow, the width of the dispersed phase flow can be modified, which further changes the size of microspheres formed from the middle flow. In this configuration, the sheath flow also plays the role of focusing the middle flow, i.e. which is the flow focusing operating principle. However, since the design is novel and relatively new, the performance of the modified T-junction device is not yet fully understood.

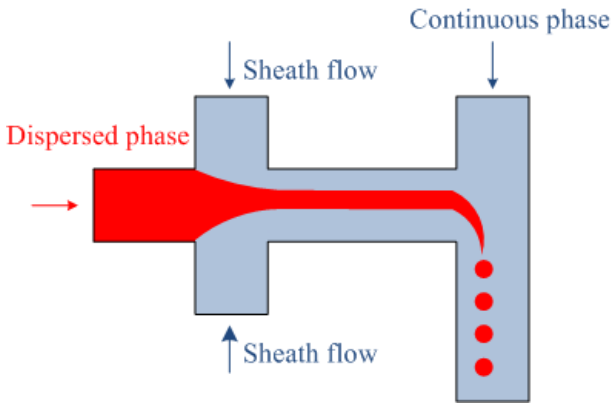

Figure 2.15. A top view of the integrated flow focusing and T-junction device. Reproduced from Song（2011）.

2.4.5 Combined devices for multiple emulsification

Combined devices are those based on more than one operating principle and they are intended for the purpose of multiple emulsifications. Multiple emulsifications refer to the process which consists of more than one emulsification step. Possible combinations include: double T-junction（Okushima *et al.* 2004）, double flow focusing（Chu *et al.* 2007, Herranz-Blanco *et al.* 2014, Nie *et al.* 2005, Pessi *et al.* 2014, Vilanova *et al.* 2013）, and integrated flow focusing and T-junction（Wan *et al.* 2008）. Figure 2.16, Figure 2.17, and Figure 2.18 provide schematics of double T-junction, double flow focusing, and integrated flow-focusing and T-junction devices, respectively. For double emulsion devices, which

represent the combination of two single microsphere generation devices, the integrated operating principle is a combination of two basic operating principles. Using the integrated flow focusing and T-junction device as an example, there are three different phases involved in the process: phase I, phase II, and phase III. Phase I and III are hydrophilic, while phase II is hydrophobic, as shown in Figure 2.16.

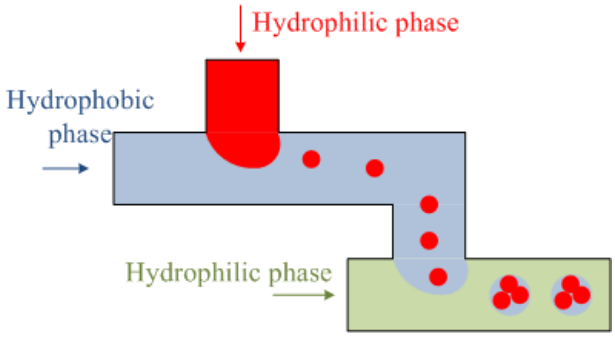

Figure 2.16. Schematic diagram of the double T-junction device.

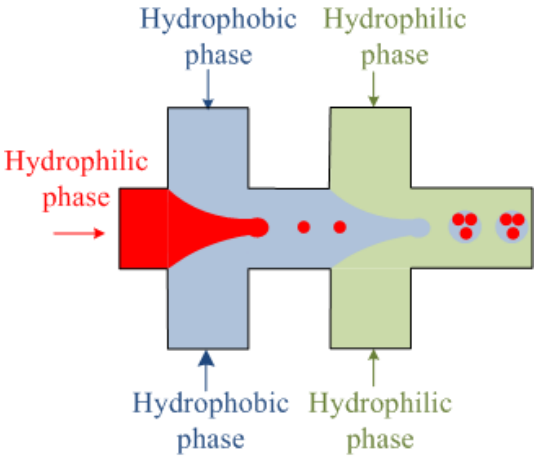

Figure 2.17. Schematic diagram of the double flow focusing device.

The operation principles for the T-junction and the flow focusing geometry are same as described in Section 2.2. By use of multiple emulsification devices, the dose of functional agents such as protein can be more effectively controlled. In addition, the technique allows the functional agents to be contained in a protective shell in order to facilitate a controlled release. Thus, the multiple emulsification method has far reaching implications in mechanical, biomedical and other applications.

Okushima et al.（2004）obtained water-in-oil-in-water (W/O/W) and oil-in-water-in-oil (O/W/O) microspheres using a double T-junction micro-fluidic device as shown Figure 2.16. They successfully controlled the size and number of microspheres in one shell by controlling the flow rates.

Wan et al.（2008）produced gas-in-water-in-oil microspheres by using an integrated flow focusing and T-junction device as shown in Figure 2.18. The size and number of microspheres inside microspheres could be tuned by controlling the flow rates.

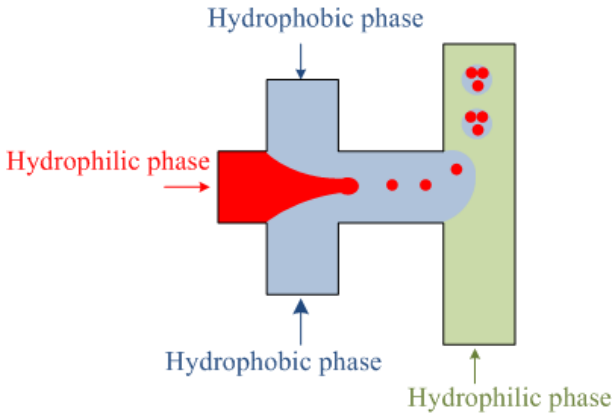

Figure 2.18. Schematic diagram of the integrated flow focusing and T-junction device.

Herranz-Blanco et al.（2014）used a double flow focusing device to produce uniform and stable THCPSiMP microspheres encapsulated by a thin lipid shell. They investigated the release rate of the drug loaded with and without the lipid shell at different pH values, and found that the lipid shell improved the sustained release effect, especially at pH 7.4. Similarly, Vilanova et al.（2013）also used a double flow focusing device to generate particles. They focused on controlling the thickness of the shell of the particles, and the release rate of the drug. Chu et al.（2007）produced W/O/W/O microspheres by the introduction of a triple flow focusing device. Pessi et al.（2014）produced W/O/W microspheres which could be stable for up to 4 weeks. Microspheres they obtained had a good sustained release property: the microsphere released 30% of the drug within 168 h.

2.5 Modeling the microsphere generation process

The flow behavior in the micro-channel is complex and the governing equations are a set of partial differential equations. An analytical solution is generally impossible. Therefore, the modeling of the microsphere generation process typically considers numerical approaches. The basic idea of any numerical approach is first of all to discretize the whole domain into a set of simple elements, where simple means that on these elements the differential equation can be replaced by an algebraic equation with acceptable accuracy. As such, the problem on the whole domain can be obtained by solving a set of algebraic equations. These numerical approaches are called Computational Fluid Dynamics (CFD) approaches. In general, CFD approaches can be categorized into three groups based on the characteristic length scale adopted（Yan 2007）: (1) the micro-level, where the fluid is modeled by atoms, whose behavior obeys statistical laws; (2) the meso-level, where the fluid is modeled in terms of a set of atomic groups; (3) the macro-level, where the fluid is considered to be a continuum. In this review, we shall only briefly discuss the micro-scale methods, and instead focus on the meso-scale and macro-scale methods.

2.5.1 Micro-scale method: Molecular Dynamics

The molecular dynamics (MD) method is based on the molecular dynamic process, Newton's Law, and statistical methods. Theoretically, the MD method could model any fluid dynamic system with high accuracy. However, the method requires large computational resources and is difficult to apply to flows with an irregular area. These two limitations of the MD method restrict its application（Wörner 2012）.

2.5.2 Macro-scale method: Navier-Stokes equation

The Navies-Stokes (N-S) equations arise from Newton's second Law. This equation describes the fluid stress as the sum of a viscous term plus the pressure term. The expression for the Navier-Stokes equation is as follows:

$$\rho\left(\frac{\partial \boldsymbol{u}}{\partial t}+\boldsymbol{u}\cdot\nabla\boldsymbol{u}\right)=\nabla\cdot\left[-p\boldsymbol{I}+\eta(\nabla\boldsymbol{u}+(\nabla\boldsymbol{u})^{T})-\frac{2}{3}\eta(\nabla\cdot\boldsymbol{u})\boldsymbol{I}\right]+\boldsymbol{F}_{st} \tag{2.3}$$

where $\boldsymbol{u}$: velocity, ρ: fluid density, p: pressure, t: time, η: dynamic viscosity, and $\boldsymbol{F}_{st}$: surface tension

force.

For incompressible flow, the N-S equation can be simplified as follows:

$$\rho\left(\frac{\partial \boldsymbol{u}}{\partial t}+\boldsymbol{u}\cdot\nabla\boldsymbol{u}\right)=-\nabla p+\eta\nabla^2\boldsymbol{u}+\boldsymbol{F}_{st} \tag{2.4}$$

The N-S equation above can be applied to any incompressible flow of a Newtonian flow. For micro-fluidic flows, the flow regime is typically laminar. Typically, the macro-scale properties, such as the velocity, pressure and density, are of interest, instead of the behavior of each individual molecule.

The N-S equation applies to a single fluid; when two or more immiscible fluids are present, then some additional equation or technique is required to model the interaction of the different flows. Two possible approaches are the level set equation and the fraction function. Accordingly, the Level Set (LS) method and Volume of Fluid (VOF) method are introduced below.

2.5.2.1 Level set method

The drawbacks of the conventional interface tracking method are their difficulty to track sharp corners, the overlap of separate edges, and a high dimensional interfacial flow（Osher and Sethian 1988）. Osher and Sethian（1988）developed a new algorithm for interface tracking, i.e., the level set method. The key idea associated with this method is the introduction of an additional dimension. The principle of this method is discussed below.

For the LS method, the level set function φ is defined as a function of x and y. The contour of the fluid particle is given by the condition $\varphi = 0$, that is,

$$\varphi(x(t), y(t), t) = 0 \tag{2.5}$$

Taking the time derivative of Eqn. (2.5) leads to

$$\frac{\partial \varphi}{\partial t} + \frac{\partial \varphi}{\partial x}\frac{dx}{dt} + \frac{\partial \varphi}{\partial y}\frac{dy}{dt} = 0 \Rightarrow \frac{\partial \varphi}{\partial t} + \varphi_x \frac{dx}{dt} + \varphi_y \frac{dy}{dt} = 0 \Rightarrow \frac{\partial \varphi}{\partial t} + \varphi_x u_x + \varphi_y u_y = 0 \Rightarrow \frac{\partial \varphi}{\partial t} + \boldsymbol{u} \cdot \nabla \varphi = 0 \tag{2.6}$$

If the curve Γ moves with velocity $\boldsymbol{u}$, then the level set function will satisfy the level set equation $\frac{\partial \varphi}{\partial t} + \boldsymbol{u} \cdot \nabla \varphi = 0$.

The governing equations for the interface tracking using the LS method are the N-S equation, LS equation, and continuity equation, which can be written as follows:

$$\rho\left(\frac{\partial \boldsymbol{u}}{\partial t} + \boldsymbol{u} \cdot \nabla \boldsymbol{u}\right) = \nabla \cdot [-\mathrm{p}\mathbf{I} + \eta(\nabla \boldsymbol{u} + (\nabla \boldsymbol{u})^{\mathrm{T}})] + \boldsymbol{F}_{st} \tag{2.7}$$

$$\frac{\partial \phi}{\partial t} + \boldsymbol{u} \cdot \nabla \phi = \gamma \nabla \cdot \left[\varepsilon \nabla \phi - \phi(1-\phi)\frac{\nabla \phi}{|\nabla \phi|}\right] \tag{2.8}$$

$$\nabla \cdot \boldsymbol{u} = 0 \tag{2.9}$$

In the equations above, ρ denotes density ($\mathrm{kg} \cdot \mathrm{m}^{-3}$), $\boldsymbol{u}$ velocity ($\mathrm{m} \cdot \mathrm{s}^{-1}$), t time (s), η dynamic viscosity ($\mathrm{Pa} \cdot \mathrm{s}$), p pressure (Pa), and $\boldsymbol{F}_{st}$ the surface tension force ($\mathrm{N} \cdot \mathrm{m}^{-3}$) acting on the interface between two fluids, which can be written as $\sigma\kappa\delta\mathbf{n}$, where σ is the surface tension coefficient and δ is the delta function concentrated at the interface between the two fluids. The curvature of the interface κ can be defined as $\kappa = -\nabla \cdot \mathbf{n}$, where $\mathbf{n}$ can be written in terms of the level set function as $\mathbf{n} = \frac{\nabla \phi}{|\nabla \phi|}$.

Furthermore, ϕ is the level set function, and γ and ε are numerical stabilization parameters such that ε determines the thickness of the interface, and γ is the re-initialization parameter. The first term on the right side is the divergence of $\varepsilon\nabla\phi$, acting as an artificial diffusivity in order to prevent discontinuities at the interface. The second term on the right side determines the stabilization of the level set function. The two phase interface is modeled where the level set function $\phi = 0$, for the water phase, $\phi = 1$, for the oil phase and $\phi = 0.5$ at the interface.

An important characteristic of the LS model is that the density and viscosity depend on the level set function. The level set function is treated as a "smooth" step function, so that the overall density ρ and viscosity η are calculated from:

$$\left.\begin{aligned}\rho &= \rho_1 + (\rho_2 - \rho_1)\phi \\ \eta &= \eta_1 + (\eta_2 - \eta_1)\phi\end{aligned}\right\} \tag{2.10}$$

where ρ_1, ρ_2, η_1 and η_2 are the densities and viscosities of Fluid 1 and Fluid 2, respectively.

A significant drawback with the LS method is that it does not conserve mass because of the numerical dissipation（Kim and Liou 2011）. To overcome this drawback, two methods were proposed in the literature. The first one is to combine the LS method with the mass conservation principle（Van der Pijl *et al.* 2005, Yokoi 2007）. The second method is to combine the LS method with the Lagrangian method which is based on the mass-free particle（Enright *et al.* 2002）.

Bashir et al.（2011）used a conventional two-phase LS method to study the drop formation in a T-junction. They primarily focused on the effects of wettability of the channel walls on microsphere formation, and their study was validated by a laboratory experiment and other studies in the literature. Balabel（2012）investigated the collision of two equal-sized microspheres numerically by applying the surface tension model and LS method, and the results were found to be consistent with the previous experimental observations（Qian and Law 1997）. Moreover, the numerical model could predict the separation, bouncing and coalescence of two-equal-sized microspheres.

2.5.2.2 Volume of fluid method

The volume of fluid method is a classic interface tracking method which was developed by Hirt and Nichols（1981）. Its fundamental function is the fraction function C, which is the integral of a fluid characteristic function over the control volume. If there is no tracked fluid inside the cell, $C = 0$; if the cell is full of the tracked fluid, $C = 1$; if the interface cuts the cell, $0 < C < 1$. As such, C is a discontinuous variable. When the fluid moves with the velocity $\boldsymbol{u} = (u(x, y, z), v(x, y, z), w(x, y, z))$, the fraction function C satisfies Eqn. (2.11),

$$\frac{\partial C}{\partial t} + \boldsymbol{u} \cdot \nabla C = 0 \tag{2.11}$$

By solving Eqn. (2.11), the fraction function *C* can be obtained. Then the overall density ρ and viscosity η can be written as:

$$\left.\begin{aligned}\rho &= C\rho_1 + (1-C)\rho_2 \\ \eta &= C\eta_1 + (1-C)\eta_2\end{aligned}\right\} \tag{2.12}$$

where ρ_1, ρ_2, η_1 and η_2 are the densities and viscosities of Fluid 1 and Fluid 2, respectively.

By substituting Eqn. (2.12) into the NS and continuity equations, the overall density ρ and viscosity η could be calculated.

The advantage of the VOF method is that it ensures mass conservation of the fluid being tracked and it is more computationally efficient than the LS method. Its limitation is poor accuracy arising from the discontinuity of the fractional function C. This limitation can lead to the discontinuous physical quantities such as the density and viscosity（Sussman and Puckett 2000）.

Sivasamy et al.（2011）investigated the mechanism of microsphere formation in a T-junction device with the VOF method, and their work was validated using experiments. The numerical results showed the change of the pressure profile during the microsphere generation process, and indicated that the minimum pressure difference occurs at the last moment of the microsphere break-up. Timgren et al.（2007）studied the formation of a microsphere from a single capillary tube with the VOF method. They studied the shear stress and the pressure field around the microsphere, and the velocity field inside the microsphere. Li et al.（2012）also investigated the mechanism of the microsphere formation based on the VOF model. Their research showed that the fluctuations of the local velocity and pressure decreased as the velocity of the continuous phase grew. The pressure inside a microsphere was found to depend on the viscosity ratio, shear at the interface and the Laplace pressure. Soleymani et al.（2008）proposed four formation periods for microsphere generation, as shown in Figure 2.19. They found that the shape of the hole strongly affects the size of the drops, and they determined the optimal conditions for microsphere formation. Chen et al.（2012）studied the microsphere formation in a wide-type T-junction. They identified two distinct regimes: dripping and jetting. For both regimes, the microsphere size decreases with an increase in the capillary number. They also found that the wettability of the wall and

the dispersed flow rate can significantly affect the process of microsphere detachment from the channel wall and the size of the microsphere. Their finding is in good agreement with theory which indicates that the capillary number is an important indicator for the microsphere formation but is not the only factor.

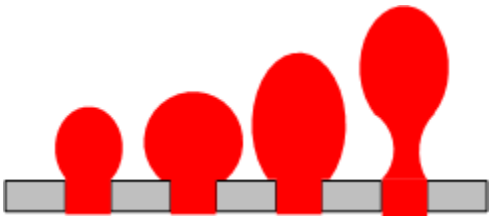

Figure 2.19. Four periods of drop formation. Reproduced from Soleymani et al. (2008).

2.5.3 A meso-scale method: the Lattice Boltzmann method

The idea of the Lattice Boltzmann (LB) method is such that the interface is not tracked directly as for the level set method. The LB method uses a grid to define a matrix of nodes throughout the solution domain and considers the fluid as particles with mass but no volume. The particles stream between nodes on the grid, and they collide with each other at nodes. The simulation is used to determine the distribution functions of these particles in every direction. The macroscopic parameters, such as the density and velocity, can be calculated from these distribution functions. There are four commonly used models for describing intermolecular forces in the LB method: coloring model, Shan-Chen model, free energy model, and He model（Gunstensen *et al.* 1991, Shan and Chen 1993, Zhang 2011）. The coloring model distinguishes the phases by different colors and tracks the interface according to the interaction between adjacent particles. The Shan-Chen model considers the multiphase fluid as a non-ideal fluid. This model can solve the phase transition problem very well, although the local momentum is not conserved. The free energy model uses the total density and density difference to determine the density of the two fluids. The He model replaces the interfacial tension force by molecular interaction and tracks the interface by a main function. It is mostly used for incompressible fluids.

One common limitation for all these models is that they fail to effectively track the interface of two fluids with a high ratio of densities. Various modifications have been proposed to overcome this problem（Amaya bower and Lee 2011, Inamuro *et al.* 2004, Liu and Zhang 2009, Yu 2009, Yuan and Schaefer 2006）. However, these studies only considered 2D models, and other factors, e.g. wettablility

of the wall, have not been taken into consideration. The main advantage of the LB method is that it is simple to implement. The disadvantage of the LB method is that mass conservation cannot be ensured （Bao *et al.* 2008, Rohde *et al.* 2006）. Chao et al.（2011）improved the mass conservation by using a global mass correction procedure, however, the computation time was significantly increased. The typical procedure of the LB method is presented below.

The LB method has two steps: a collision step and streaming step. The governing equations for these two steps are Eqn. (2.13) and Eqn. (2.14), respectively.

$$f_i^{(new)}(\boldsymbol{x}, t) - f_i(\boldsymbol{x}, t) = \Omega_{\mathrm{i}} \tag{2.13}$$

$$f_i(\boldsymbol{x} + \boldsymbol{e}_i, t + 1) = f_i^{(new)}(\boldsymbol{x}, t) \tag{2.14}$$

$$\Omega_{\mathrm{i}} = -\frac{1}{\tau}\left(f_i(\boldsymbol{x}, t) - f_i^{(0)}(\rho, \boldsymbol{v})\right) \tag{2.15}$$

$$\tau_\nu = \frac{1}{2} + \frac{3\Delta t}{\Delta x^2}\nu \tag{2.16}$$

where f_i is the distribution function value for each iteration, Ω_{i} is the collision operator, Δt is the time needed for a particle traverse a lattice length, Δx refers to the lattice length, and ν is the kinematic viscosity.

The equilibrium distribution function can be obtained by solving the following equation

$$f_i^{(0)}(\rho, \boldsymbol{v}) = \rho(A^{\mathrm{q}} + B^{\mathrm{q}}\langle \boldsymbol{e}_i, \boldsymbol{v}\rangle + C^{\mathrm{q}}\langle \boldsymbol{e}_i, \boldsymbol{v}\rangle^2 + D^{\mathrm{q}}\langle \boldsymbol{v}, \boldsymbol{v}\rangle) \tag{2.17}$$

where $f_i^{(0)}$ is the value of the equilibrium distribution function at the equilibrium state, $\langle \boldsymbol{x}, \boldsymbol{y}\rangle$ denotes the cross product of two vectors, and A^{q}, B^{q}, C^{q}, and D^{q} are constants based on the lattice in which the particle moves. Once the distribution factor is known, then, the macro-scale properties, typically the density and velocity of the fluids, can be calculated as follows:

$$\rho = \sum_{i=0}^{n} f_i \tag{2.18}$$

$$\boldsymbol{v} = \frac{1}{\rho}\sum_{i=0}^{n} f_i\, \boldsymbol{e}_i \tag{2.19}$$

where $\boldsymbol{e}_i$ is a velocity vector corresponding to the direction i on the lattice.

Frisch（1991）has shown that the LB method could be taken as a stable form of Navier-Stokes equations using the finite difference approximation. It is a powerful modeling method with high computational efficiency and relatively high accuracy for complex geometries（Zhang 2011）. Wang et al.（2007）modeled fluid-solid heat transfer using the LB method and then compared their model with the commercial CFD software Fluent. Their study showed that to obtain the same accuracy target, the grid cells with the LB method are much smaller than for macro-scale CFD methods. Additionally, the computational time with the LB method is less than half the time required by the macro-scale CFD methods. Yoshino et al.（2004）obtained the same conclusion that the LB method is more efficient than the macro-scale methods, especially for complex geometries. However, there is a limitation for the LB method: for simple geometries, the macro-scale method is found to be better than the LB method（Geller *et al.* 2006, Lai *et al.* 2001, Zhang 2011）. This is due to the fact that for the LB method, the accuracy may degrade when the bounce back boundary condition is used. To obtain a high accuracy, the half bounce back scheme is usually used, which leads to an increase in the computational time. Thus, to improve the efficiency and still maintain high accuracy with the LB method for simple geometries is a promising future work（Freitas and Schröder 2008, Schulz *et al.* 2002）.

There are many studies on use of the LB method to simulate the microsphere generation process（Kim *et al.* 2008, Kuzmin *et al.* 2011, Liu and Zhang 2009, Mbanjwa *et al.* 2011, Van der Graaf *et al.* 2006, Wang *et al.* 2011）. Yu et al.（2007）performed both experimental and simulation studies on gas-liquid flows in micro-channels. Mbanjwa et al.（2011）generated water in oil microspheres and discussed various flow regimes as a function of the capillary number and the flow rate ratio. Their work was validated by experiments. Wu et al.（2008）discussed how the capillary number affects microsphere formation and the microsphere sizes using 3D models, and validated their results by experiments. Liu and Zhang（2011）found that in both the T-junction and the flow focusing device, the capillary number, the viscosity ratio, the flow rate ratio and the contact angle were important for microsphere formation. They also settled the critical capillary numbers from squeezing to dripping.

Wang et al.（2011）modified the conventional T-junction geometry into Venturi shaped configurations

(see Figure 2.20) and found that the flows in micro-fluidic devices could be very sensitive to any change in the device geometry. Yu et al. (2007) studied the bubble shape, size, and formation mechanism in a gas-liquid system in a flow focusing device. They found that the bubble production was influenced by the capillary number and the geometry of the device, as shown in Figure 2.21. The studies above identify two variables as being important in the microsphere generation process: the geometry of the device, and the capillary number. This finding could be considered during the optimization for the microsphere generation process and the controllability of microspheres.

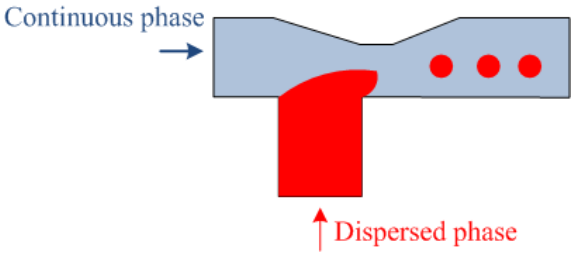

Figure 2.20. A top view of the modified T-channel. Reproduced from Wang et al.（2011）.

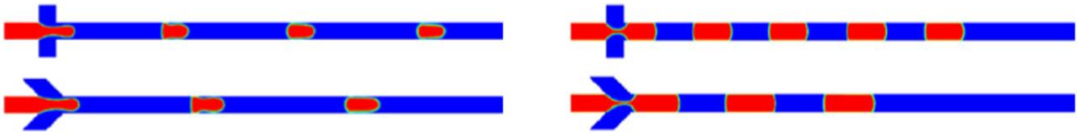

Figure 2.21. Comparison of the simulation results in “cross” and “converging” channels; (a) $Ca = 0.035$, $Q_g : Q_l$ = 1:4, (b) $Ca = 0.006$, $Q_g : Q_l$ = 1:1. Reprinted with kind permission from Yu et al. (2007).

2.6 Concluding remarks

The above review has shown some opportunities for further research on the micro-fluidic approach to generate microspheres. First, the mechanism of the modified T-junction has not been studied, though the initial launch of this new principle is successful and as well its possibility to produce a range of microspheres of different sizes with one device is very promising. Second, the size of microspheres with the modified T-junction may be further reduced by optimization of the process performance (the current smallest size is 16 μm ~ 35 μm with distilled water（Song 2011）). At this point, the literature does not

have any systematic approach to guide into optimizing the performance of the microsphere generation process with micro-fluidic devices in general. Finally, the membrane emulsification is very efficient in mass production of microspheres, but the size and uniformity of microspheres with the membrane emulsification are possibly improved by improved design and fabrication. In short, the finding of the foregoing three opportunities may have sufficiently demonstrated the need of the proposed objectives of this dissertation study in Chapter 1. As far as the urgency of the proposed research, the literature review reveals that the desire to have one device for a range of microspheres in different sizes, which may be called device flexibility, and process optimization (in terms of the size of microspheres and uniformity of microspheres) for micro-fluidic devices are the current interests in the field.

CHAPTER 3. MODELING OF THE MODIFIED T-JUNCTION

3.1 Introduction

In the conventional T-junction approach, the size of the middle flow is mainly determined by the dimensions of the micro-channel, which means the size of microspheres could only be adjusted batch by batch in a small range. To overcome this disadvantage, a novel modified T-junction device was developed by Song（2011）in our group, as shown in Figure 3.1. By introducing the sheath flow, the size of the middle flow is not only determined by the size of micro-channel but also by the sheath flow rate, making the device or device system more flexible. A direct benefit is that a single device (micro-channel in this case) can be used for producing different types of microspheres.

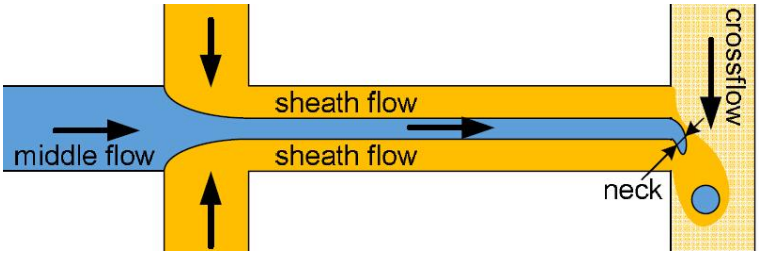

Figure 3.1. Schematic diagram of the modified T-junction device. Three types of flows were involved: middle flow, sheath flow, and cross flow. The fluids of the sheath flow and cross flow were the same, and immiscible with the middle flow. Reprinted with kind permission from Song（2011）.

Uniform microspheres with a size range from 16 μm to 35 μm were produced with the SD of the microsphere sizes being about 0.80 μm to 2.46 μm（Song 2011）. However, how the flow rates, device dimensions and structure (or topology and shape), and fluid properties influence the microsphere generation process has not been investigated for the modified T-junction device. Further, understanding the effects of these parameters could help optimize the device to achieve smaller sizes of microspheres with greater uniformity.

This chapter presents the development of a computational model for the microsphere generation process

with the modified T-junction device, which will then be used to investigate the mechanism of the microsphere generation process in this device (Chapter 4) and to optimize the microsphere generation process (Chapter 5). A part of the content presented in this chapter was published in conference proceedings: Lei L., Zhang H. B., Bergstrom D. J., Zhang B., and Zhang W. J., "Modeling Of Droplet Generation by a Modified T-Junction Device Using COMSOL," in *Applied Mechanics and Materials*, 2015, pp. 112-116, and Lei, L., Zhang, H., Bergstrom, D., Zhang, B., Song, K., Zhang, W. J., "Modeling and Validation of Microspheres Generation in the Modified T-Junction Device," in *Mechanical and Mechatronics Engineering*, 2015, 1(5), 696.

3.2 Model development

3.2.1 Dimensions of the micro-channel

Two configurations of the modified T-Junction were used in this study: straight channel and crooked channel, as shown in Figure 3.2a and Figure 3.2b, respectively. For both of the configurations, the channels were uniform in width and height, and the cross section of the channel was square. The details of the devices are listed in Table 3.1 and the optical images of these four devices are given in Figure 3.3. Details of the design and micro-fabrication of these devices will be discussed later in this chapter.

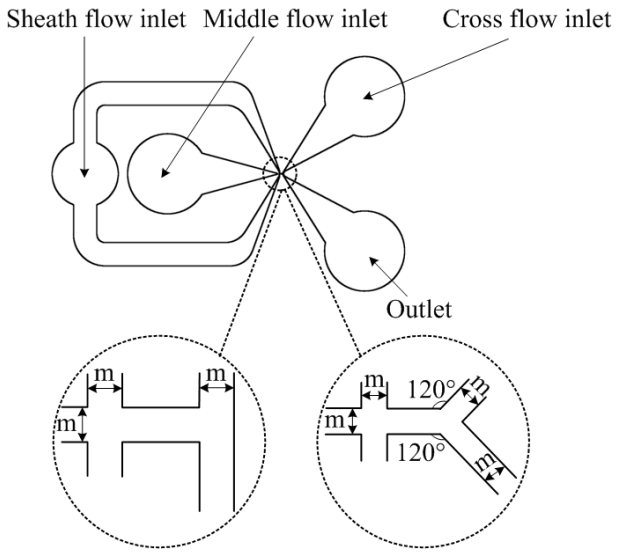

Figure 3.2. Schematic diagram of the modified T-junction device: (a) straight channel, (b) crooked channel. m: the channel width.

Table 3.1. The structure and dimension of the modified T-junction device.

Device	Structure	m (μm)
1	Straight	50
2	Straight	75
3	Crooked	50
4	Crooked	100

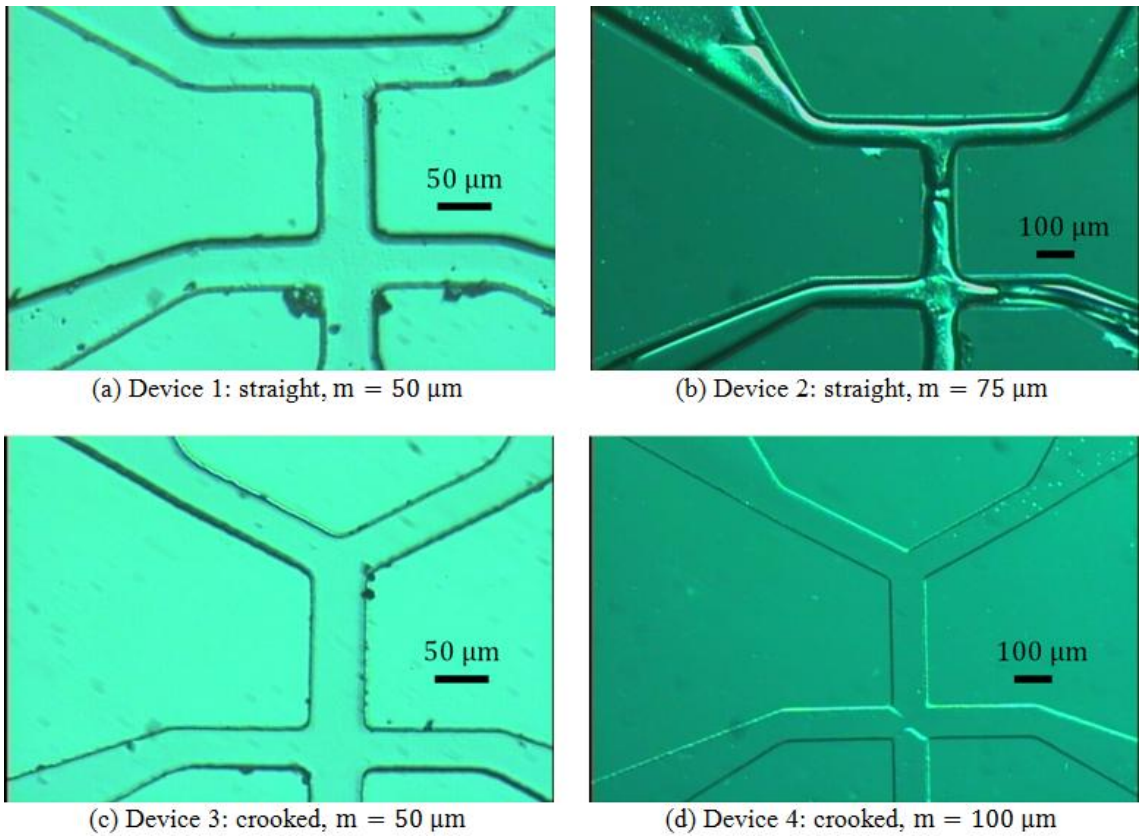

(a) Device 1: straight, m = 50 μm (b) Device 2: straight, m = 75 μm

(c) Device 3: crooked, m = 50 μm (d) Device 4: crooked, m = 100 μm

Figure 3.3. Optical images of four devices.

3.2.2 Governing equation

The behavior to be modeled is the interaction among multiple fluids which are in motion. A challenge in modeling is to track the changing interfaces among multiple flows. In this study, the LS method (reviewed in Chapter 2) was employed because of its ability to deal with the sharp corners of the interface, the overlaps of separate edges of the interface, and high dimensional interfacial flow（Lan *et al.* 2014, Sussman and Puckett 2000, Sussman *et al.* 1994）. The following are the underlying

assumptions of model development,

a. All the flows were assumed to be laminar.
b. There was no pressure acting on the outlet except for the atmospheric pressure.
c. All the solid boundaries were set to be no-slip boundaries.
d. Fluids were incompressible, Newtonian fluids. Further, the flow rates of the three flows were given as initial conditions. The sheath flow rate and middle flow rate were constant and given as $Q_s = Q_m = 0.01\ \text{ml} \cdot \text{min}^{-1}$.

The Navier-Stokes equation and the continuity equation combined with the LS method for the interface tracking are applied to the flow system under the above assumptions, namely:

$$\frac{\partial \phi}{\partial t} + \boldsymbol{u} \cdot \nabla \phi = \gamma \nabla \cdot \left[\varepsilon \nabla \phi - \phi(1-\phi) \frac{\nabla \phi}{|\nabla \phi|} \right] \tag{3.1}$$

$$\rho \left(\frac{\partial \boldsymbol{u}}{\partial t} + \boldsymbol{u} \cdot \nabla \boldsymbol{u} \right) = \nabla \cdot [-\mathrm{p}\boldsymbol{I} + \eta(\nabla \boldsymbol{u} + (\nabla \boldsymbol{u})^T)] + \boldsymbol{F}_{st} \tag{3.2}$$

$$\nabla \cdot \boldsymbol{u} = 0 \tag{3.3}$$

where $\phi(\mathbf{x}, t)$ is the level set function, $\mathbf{x}$ is the coordinate of the system, $\boldsymbol{u}$ is velocity ($\text{m} \cdot \text{s}^{-1}$), t is time (s), ε is the thickness of the interface and γ is the re-initialization parameter, ρ is density ($\text{kg} \cdot \text{m}^{-3}$), η is the dynamic viscosity ($\text{Pa} \cdot \text{s}$), p is the pressure (Pa), and $\boldsymbol{F}_{st}$ is the surface tension force ($\text{N} \cdot \text{m}^{-3}$) acting on the interface between two fluids. In this work, $\boldsymbol{F}_{st} = \sigma \kappa \delta \boldsymbol{n}$, where σ is the surface tension coefficient, δ is the Dirac delta function at the interface between the two fluids, and κ is the curvature of the interface which can be defined as $\kappa = -\nabla \cdot \boldsymbol{n}$, where the normal vector $\boldsymbol{n}$ can be written in terms of the level set function as $\boldsymbol{n} = \frac{\nabla \phi}{|\nabla \phi|}$.

The overall density (ρ) and viscosity (η) are calculated from:

$$\left.\begin{aligned} \rho &= \rho_1 + (\rho_2 - \rho_1)\phi \\ \eta &= \eta_1 + (\eta_2 - \eta_1)\phi \end{aligned}\right\} \tag{3.4}$$

where ρ_1, ρ_2, η_1 and η_2 are the densities and the viscosities of fluid 1 and fluid 2, respectively.

In this study, the interface of the microsphere was represented by the 0.5 contour of the level set function, which meant if the level set function was bigger than 0.5 ($\phi(\mathbf{x},t) > 0.5$), it belonged to fluid 1 (i.e., the continuous flow in this study), and if $\phi(\mathbf{x},t) < 0.5$, it belonged to fluid 2 (i.e., the dispersed flow in this study). The reason for using the 0.5 contour was that it could achieve a good conservation of mass（Olsson and Kreiss 2005）. Commercial software COMSOL Multi-physics (COMSOL Incorporated, USA), which contains the LS method for dealing with a multi-phase flows problem, was employed to assist the modeling and simulation.

3.2.3 Materials and Properties

The fluid of the middle flow was PLGA dissolved in dichloromethane (DCM) solution, and both the fluids of the sheath flow and cross flow were 1% polyvinyl alcohol (PVA) dissolved in distilled water solution. PLGA is a biodegradable and biocompatible material, and is approved by the Food and Drug Administration (FDA) for the use of diagnostics, drug delivery, and other applications of basic science research（Gasparini *et al.* 2008, Holgado *et al.* 2008, Jain 2000, Lü *et al.* 2009, Nie and Wang 2007, Thanh Ha *et al.* 2013, Zabihi *et al.* 2014）. DCM is a commonly used organic solvent due to its relatively low toxicity and low boiling point（Gasparini *et al.* 2008, Jain 2000, Nie and Wang 2007）. PVA was a surfactant which was used to decrease the interfacial tension between two immiscible fluids while enhancing the stability of the microsphere formation. For comparison, three different concentrations of the PLGA solution were used, 1%, 5%, and 15 wt%, respectively.

PLGA (50/50, inherent viscosity $0.16 - 0.24\ \mathrm{dl \cdot g^{-1}}$) was obtained from Jinan Daigang Biomaterial Company (Jinan, China). PVA (Mw $85{,}000 - 124{,}000$, 99+% hydrolyzed) was obtained from Shanghai Lingfeng Chemical Reagent Company (Shanghai, China). DCM was obtained from Shanghai Chemical Reagent Company (Shanghai, China).

The viscosities of the 1%, 5%, 15% PLGA solutions and 1% PVA solution were measured using DV-III Ultra programmable rheometer and DV-I viscometer (Brookfield Engineering Laboratories Incorporated, USA). They were 1.5, 4.3, 15, and 1.7 $\mathrm{mPa \cdot s}$, respectively. These values were consistent with the literature（Ghanbar *et al.* 2013, Song *et al.* 2009, Yoo and Mitragotri 2010）. The densities of the 1%, 5%, 15% PLGA solutions and 1% PVA solution were 1329, 1326, 1315, and 1000 $\mathrm{kg \cdot m^{-3}}$,

respectively. The interfacial tensions between 1%, 5%, 15% PLGA solutions and 1% PVA solution were measured by A. Krüss Optronic GmbH using the tensiometer K100 (A. Krüss Optronic GmbH, Germany). They were 2.19, 2.23, 3.73 $mN \cdot m^{-1}$, respectively.

3.2.4 Meshing and grid dependency study

The mesh of the model consisted of triangular elements for the two structures (Table 3.1). Refined meshes were taken in the regions where the two phases of flows interacted with each other. Mesh dependency studies were performed for each configuration under different meshes. The size of microspheres generated was used as the check point, specifically: varying the mesh until the size became stable (the difference between two meshes is less than 5%). Mesh with 9133 and 7815 grids were chosen for the two structures, as shown in Figure 3.4a and Figure 3.4b, respectively.

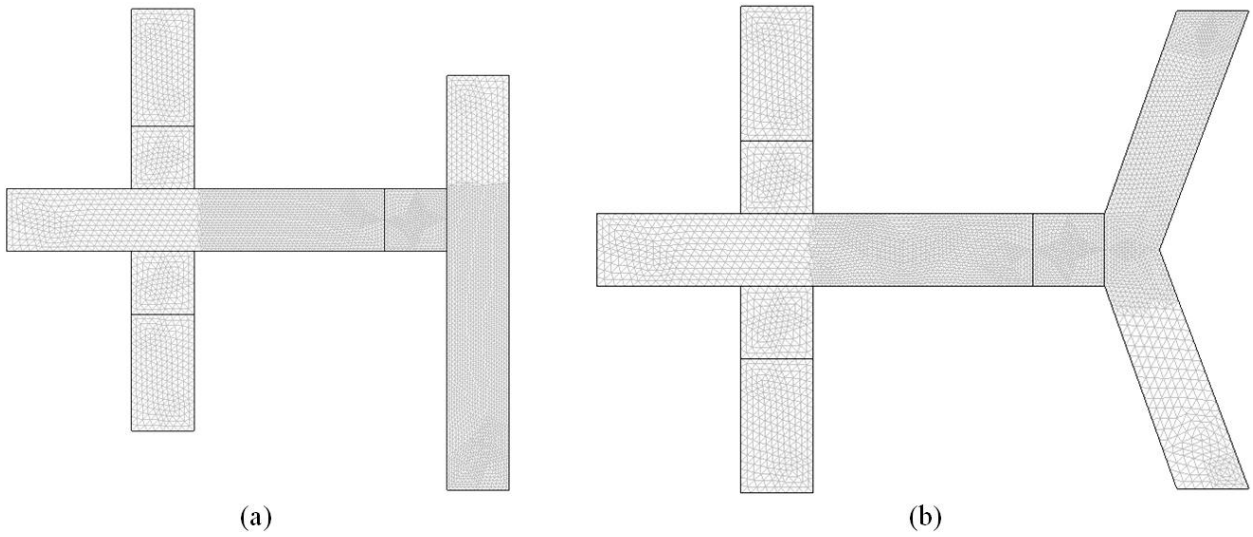

Figure 3.4. Meshed geometric domains for the modified T-junction device: (a) straight channel, (b) crooked channel.

3.3 Model validation

3.3.1 Experimental set-up

Four devices were fabricated and tested, as shown in Figure 3.3. Figure 3.5 shows the experimental set-up. Three syringe pumps (Kent Scientific Corporation, USA) controlling the flow rates of the sheath

flow, middle flow and cross flow were connected to the micro-channel with syringes (6 ml, Covidien Limited, Ireland) and PTFE tubing with inner diameter of 1.34 mm (Adtech Polymer Engineering Limited, United Kingdom). All three syringe pumps were calibrated before the experiments. The optical microscope Sharp-scope SF-1 (Sharp-Scope Precision Industrial Company, China) was connected to a computer and used to observe the microsphere generation. The images of the microspheres were taken by a camera attached to the microscope. The commercial image processing software (ImageJ, National Institutes of Health, USA) with its corresponding data analysis software (especially for the image measurement) was used to measure the size of microspheres using the images. It is noted that although the CCD camera with the microscopy used in the experiment has a resolution of 1 μm, but the image measurement software allows for the measurement resolution down to 0.01 μm through an interpolation technique. The experimental procedure was as follows. The cross flow and sheath flow were pumped into the device in advance to wet the micro-channel. This procedure was expected to form a thin layer to separate the formed microspheres and the wall, and thus obtain a clean transport of the middle flow. Microspheres were collected after the flows were stable. A single microsphere was measured multiple times (> 5 times) and their average value was taken. The experiments were performed in room temperature ($20℃ \pm 2℃$).

Figure 3.5. Experimental set-up for the model validation.

3.3.2 Design and fabrication of the test sample

In order to understand how the structure of the micro-devices may influence the microsphere generation, Device 1 (straight, $m = 50$ μm), Device 2 (straight, $m = 75$ μm), Device 3 (crooked, $m = 50$ μm), and

Device 4 (crooked, m = 100 μm) were tested. The polydimethylsiloxane (PDMS) was used for the four devices due to its chemical inertness, non-toxicity, low cost, and easiness in bonding with glass, silicon and itself（Andersen *et al.* 2015, Lin *et al.* 2010, Volk *et al.* 2015）. The fabrication of the PDMS devices was standard, as shown in Figure 3.6. In Figure 3.6, SU-8 was first spin-coated on the silicon substrate (Figure 3.6a). Then, the mask was aligned (Figure 3.6b) and the device was then exposed under UV light (Figure 3.6c). As SU-8 was a commonly used negative photoresist, the exposed part would become insoluble with the developer (Figure 3.6d). Thus, the part covered by the mask was rinsed off by the developer (ethyl lactate and diacetone alcohol) (Figure 3.6e). PDMS was poured on the SU-8 pattern (Figure 3.6f), and baked on a hotplate at 130°C (Figure 3.6g). Next, the PDMS chip was peeled off the substrate (Figure 3.6h) and bonded with another plain PDMS chip (Figure 3.6i). All the micro-fluidic devices were fabricated by the Shanghai WenChang Chip Technology Company (Shanghai, China).

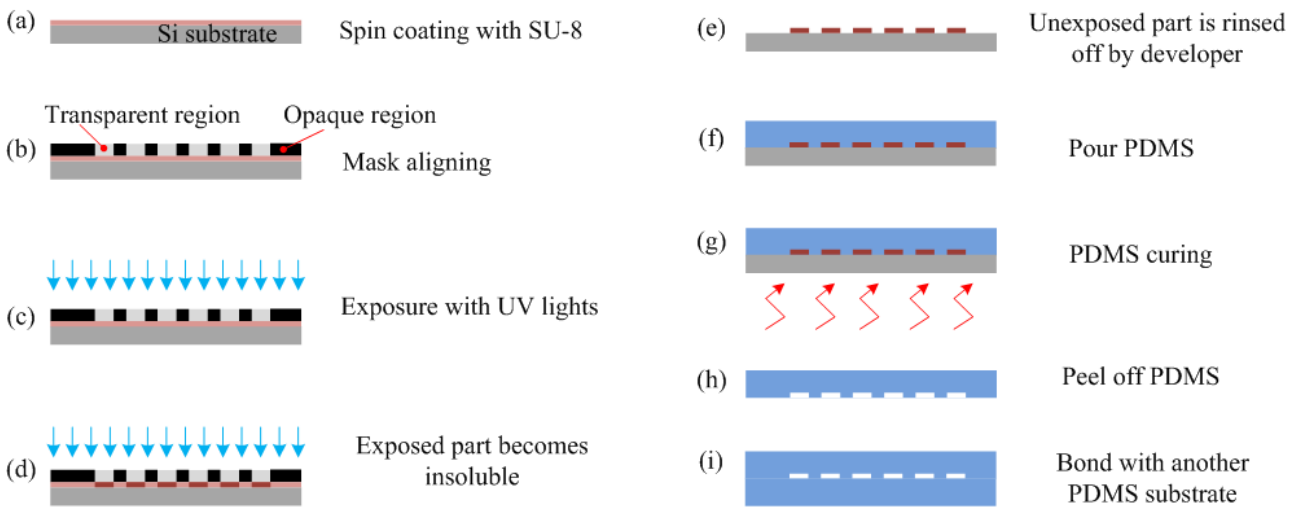

Figure 3.6. The PDMS device fabrication process using photolithography.

3.3.3 Results and discussion

The results for the volume fraction profiles were presented in Table 3.2, in which the snapshots of the flow fields of six groups of situations were shown with their corresponding parameters.

Table 3.2. Volume fraction profiles from the simulation study.

1. m = 50 µm, straight channel, Q_c = 0.02 ml · min^{-1}, PLGA concentration: 1%	2. m = 75 µm, straight channel, Q_c = 0.03 ml · min^{-1}, PLGA concentration: 15%
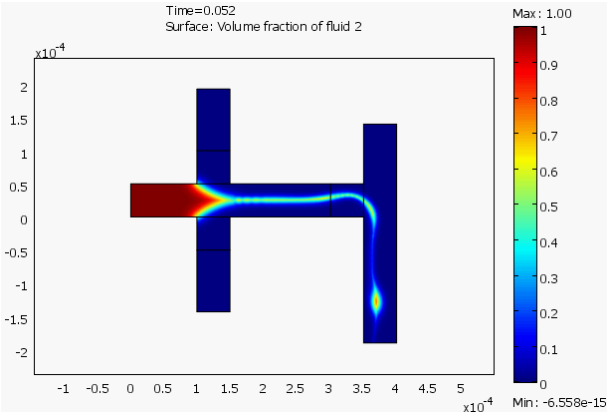	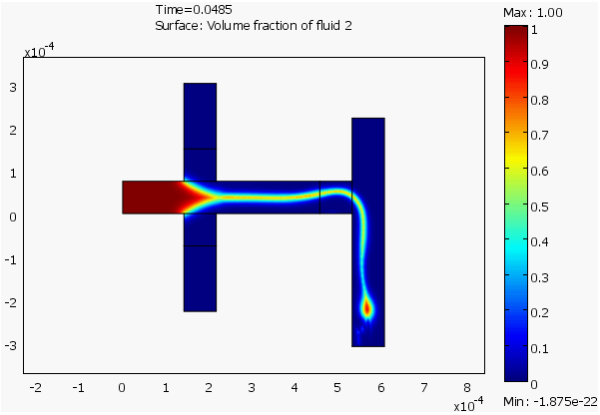
3. m = 50 µm, crooked channel, Q_c = 0.02 ml · min^{-1}, PLGA concentration: 5%	4. m = 100 µm, crooked channel, Q_c = 0.02 ml · min^{-1}, PLGA concentration: 1%
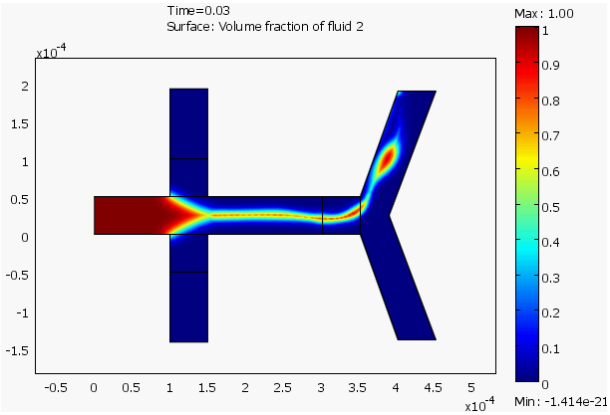	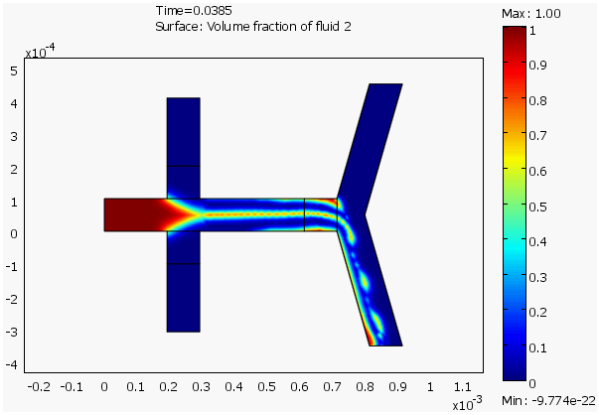
5. m = 100 µm, crooked channel, Q_c = 0.03 ml · min^{-1}, PLGA concentration: 5%	6. m = 50 µm, crooked channel, Q_c = 0.03 ml · min^{-1}, PLGA concentration: 15%
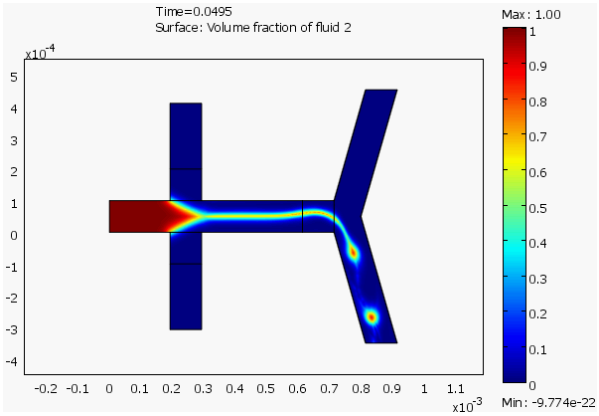	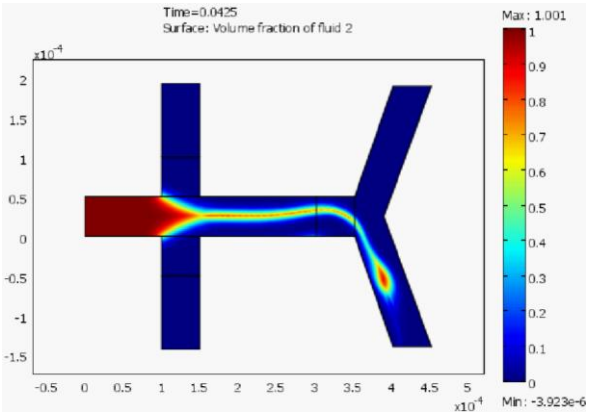

Table 3.3 and Figure 3.7 show the simulated and experimental results for the sizes (mean $\pm$ standard deviation) of microspheres. The PLGA concentration and the cross flow rate Q_c were considered as significant factors that might influence the microsphere generation process together with the channel size and device structure. The red section represents the PLGA solution, while the blue section represents the PVA solution. The size of microspheres was measured based on the level set function with the contour of 0.5. It can be concluded from Table 3.3 that the simulation and experiment results show a good agreement. As shown in Figure 3.7, except for group 1, the diameters of microspheres obtained from the simulation show that they are all located in the corresponding error bars of the diameters obtained from the experiments. For group 1, the diameter of the microspheres in the simulation result is twice that of the experiment. This discrepancy is probably caused by the unsteady environment during the experiments, or the channels in the devices were clogged by PLGA after DCM evaporated (Figure 3.8). It is noted that the clogged channel dramatically reduces the size of the channel and thus the size of microspheres, which is not captured in the model. The reason causing the clog may lie in the small size of the channel ($\mathrm{m} = 50$ μm) and low cross flow rate ($Q_c = 0.02$ ml $\cdot$ min^{-1}).

Table 3.3. Simulation and experimental results.

Experiment	Diameter of microspheres (μm)	
	Simulation	Experiment
1	21.3	11.0 ± 1.8
2	41.6	39.4 ± 4.7
3	23.2	21.0 ± 2.2
4	49.1	48.0 ± 4.7
5	45.8	43.2 ± 3.2
6	34.0	35.6 ± 3.8

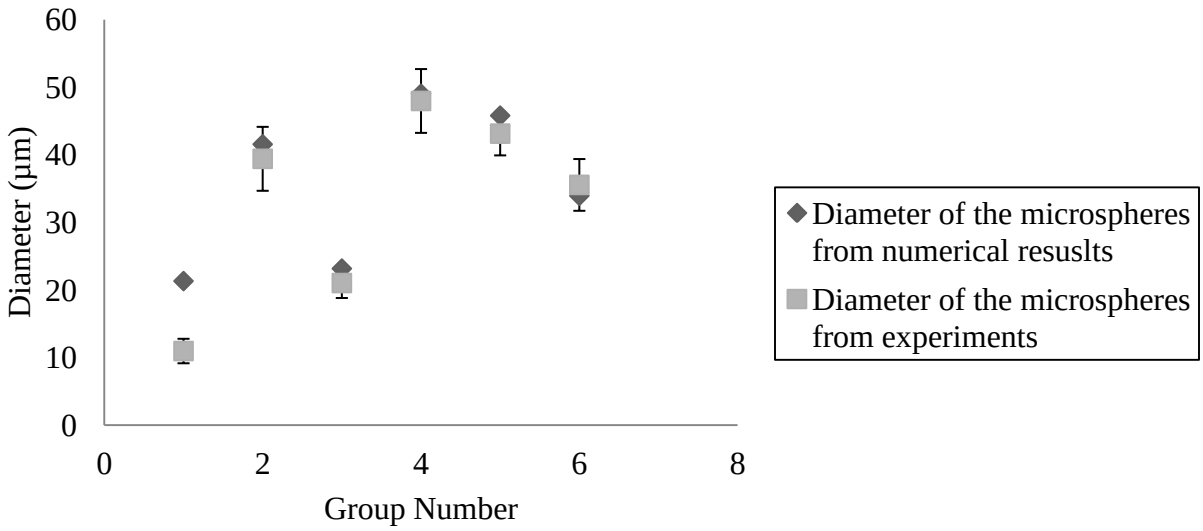

Figure 3.7. Comparison of the simulation and experimental results of the diameter of microspheres.

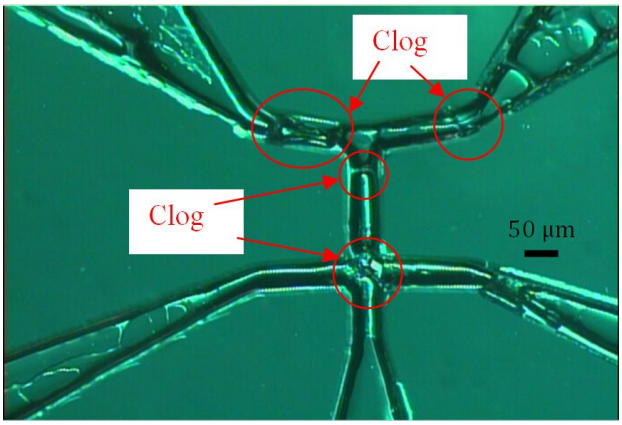

Figure 3.8. An optical image of the clogged micro-channel (m = 50 μm).

3.4 Conclusions

This chapter presented development of a computational model of the microsphere generation process with the modified T-junction device. The test-bed was built, including the design and fabrication of micro-channels and set-up of the micro-fluidic system with the corresponding measurement system. The accuracy of the model was acceptable and confirmed by comparing the simulation results with the experimental results with consideration of measurement uncertainty.

CHAPTER 4. EXPERIMENTAL AND COMPUTATIONAL STUDY OF THE MECHANISM IN THE MODIFIED T-JUNCTION FOR MICROSPHERE GENERATION

4.1 Introduction

This chapter presents a study on the fundamental understanding of the mechanism of microsphere generation with the modified T-junction device. For the conventional T-junction device, the finding in the literature has concluded that there are four possible regimes in the process of microsphere generation: (1) dripping, (2) jetting, (3) squeezing, and (4) continuous（Anna *et al.* 2003, Anna and Mayer 2006, Glawdel and Ren 2012, Moon *et al.* 2014, Ong *et al.* 2007, Ward *et al.* 2005）. In the dripping regime, the microsphere is formed near the junction, as shown in Figure 4.1a. In the jetting regime, there is a distance from the junction to the location where the microsphere is formed, as shown in Figure 4.1b. In the squeezing regime, the microsphere blocks the channel so that the pressure difference is created across the microsphere, as shown in Figure 4.1c (see also the previous discussion in Section 2.3.1). In the continuous regime, the dispersed flow stays continuous and there is no microsphere formed, as shown in Figure 4.1d.

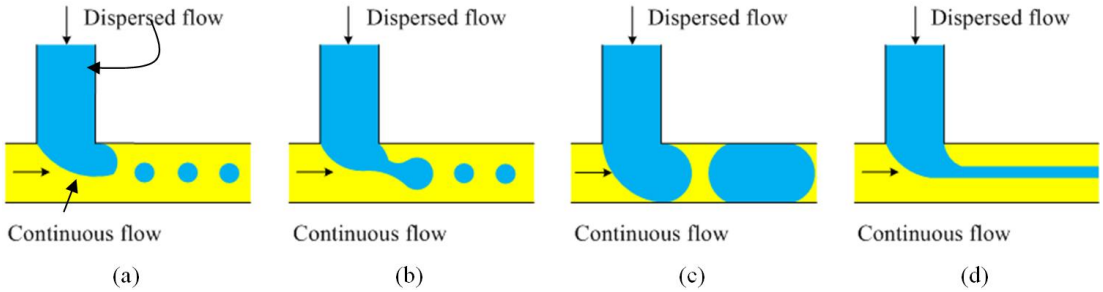

Figure 4.1. Four regimes occur in T-junction (not to scale): (a) dripping regime, (b) jetting regime, (c) squeezing regime, and (d) continuous regime. Reproduced from Nunes et al. (2013).

The reasons behind these different regimes are related to the different flow conditions, and these conditions are further characterized by the capillary number of the continuous flow (Ca). Ca is a

dimensionless number in fluid dynamics, described by

$$Ca = \frac{\mu U}{\gamma} \tag{4.1}$$

where μ is the dynamic viscosity of the fluid; U is the velocity of the fluid; γ is the interfacial tension between the dispersed fluid and the cross flow fluid. A practical meaning in mechanics about Ca is that it represents the ratio of the terms contributing to the viscous force in the dispersed fluid and the interfacial tension force that acts across the interface between two phases. A low Ca suggests that the interfacial tension force is dominant; otherwise the viscous force is dominant. For the conventional T-junction device, Ca is used to predict the flow regimes with the critical values of Ca, denoted as Ca_{cr}, see the work by Nunes et al. (2013).

However, knowledge of the mechanism (i.e., regimes) behind the process of microsphere generation with the modified T-junction device is not yet known. The mechanism valid for the conventional T-junction device may not be valid for the modified T-junction device due to their different architectures. It is thus worthwhile to study the mechanism of microsphere generation with the modified T-junction device, presented in this chapter.

A combined experimental and computational approach is used in this methodology. In particular, the experiment was expected to observe the regimes of multi-phase flows and employed to tune the computational model (finite element model) for improved accuracy. In the remainder of this study, Section 4.2 describes the experimental set-up including the design and micro-fabrication of the devices. Section 4.3 presents the experimental observation of the regimes in the process of microsphere generation with the modified T-junction. Section 4.4 presents a computational model, including the experimental verification. Section 4.5 presents the study of the mechanism as well as the different regimes observed before. Conclusions and further discussions are given in the last section.

4.2 Experimental set-up

The schematic diagram of the micro-fluidic device is shown in Figure 4.2. The dimension of the device was 4×2 cm^2. The inlet of the sheath flow will guide the sheath fluid to flow into the two symmetric

channels so that the flow rates in the two channels are the same. The inlets of the middle flow and the cross flow guide the middle fluid and cross flow fluid to flow into the device, respectively. The zoomed in area in Figure 4.2 shows the structure of the modified T-junction. The width and height of the micro-channel were both 100 μm. The micro-fluidic device was made of PDMS and fabricated in Shanghai Wenchang Chip Technology Company (China) using the photolithography technology. The details of the fabrication process were given in Chapter 3, where the same device was used.

Figure 4.3 shows the experimental set-up. The three syringe pumps (Harvard Apparatus and Stoelting Company, USA) were connected to the micro-fluidic device by the syringes (10 ml, Shanghai Kindly Enterprise Development Group Company, China) and the tubing (0.6 mm PTFE, Suzhou Wenhao Chip Technology Company, China) to control the flow rates of the fluids. All three syringe pumps were calibrated before the experiment. The inverted fluorescent microscope (ECLIPSE TS100, Nikon Instruments Incorporated, Japan) equipped with a high speed camera (1547 frames per second) (pco.dimax HD, PCO AG, Germany) was used to observe the experimental process. A single microsphere was measured multiple times (> 5 times) and their average value was taken. The experiments were performed in room temperature ($20℃ \pm 2℃$).

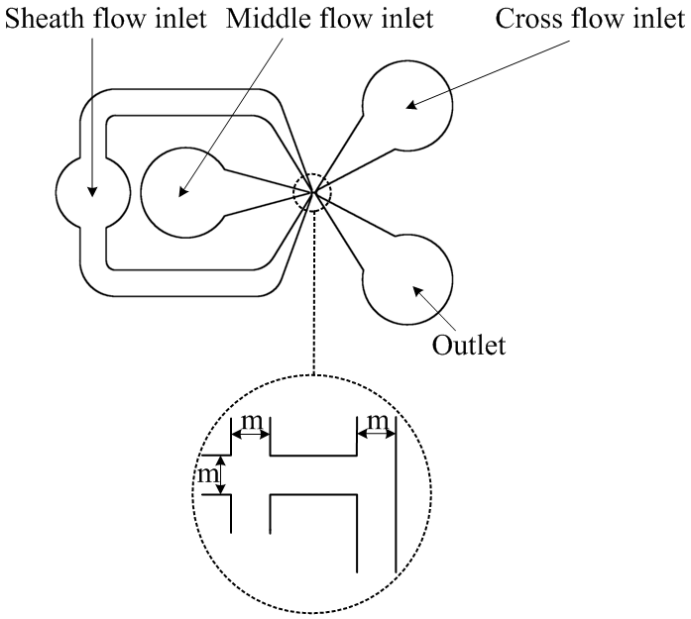

Figure 4.2. A top view of the modified T-junction device, which was molded in PDMS, with a channel width of m = 100 μm.

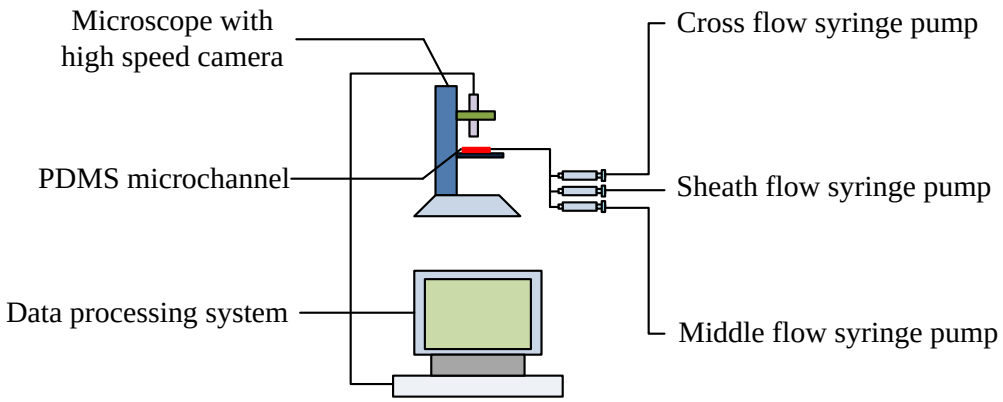

Figure 4.3. Experimental set-up for the investigation of three regimes.

4.3 Experimental observations: three regimes of the multi-phase flows

There are many factors that may influence microsphere generation, such as the flow rates, materials of the fluids, dimensions of the micro-channel device, structure (shape) of the micro-channel device, and so forth. Compared with the conventional T-junction device, the modified T-junction may represent a more complicated situation due to the introduction of the sheath fluid with its flow. The study hypothesized that the sheath fluid with its flow may have a significant influence over microsphere generation. Further, based on our experience, it is the interaction among fluids with their flow rates that should contribute to the microsphere generation. Therefore, the study focused on the examination of the three fluids with their flows, instead of looking at just the Ca of the cross flow as in the conventional T-junction device (see the previous discussion in Section 4.1) on the process of microsphere generation with the modified T-junction device.

Three regimes were found by a trial-and-error procedure for different velocities of the middle flow, sheath flow and the capillary number of the cross flow. The experimental visualization of these three regimes is given in Figure 4.4.

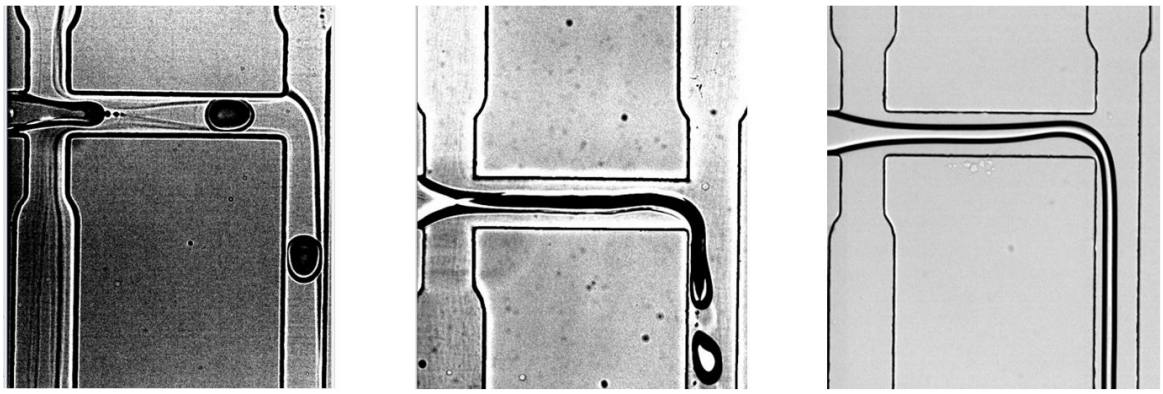

(a) (b) (c)

Figure 4.4. The experimental observation of regimes with the modified T-junction device: (a) detached regime, $U_m = 0.01\ \mathrm{m \cdot s^{-1}}$, $U_s = 0.01\ \mathrm{m \cdot s^{-1}}$, $Ca = 0.010$, (b) successful microsphere formation, $U_m = 0.015\ \mathrm{m \cdot s^{-1}}$, $U_s = 0.01\ \mathrm{m \cdot s^{-1}}$, $Ca = 0.293$, (c) continuous regime, $U_m = 0.02\ \mathrm{m \cdot s^{-1}}$, $U_s = 0.01\ \mathrm{m \cdot s^{-1}}$, $Ca = 0.293$.

Figure 4.4a shows the detached regime. Microspheres were formed primarily by the pressure from the sheath flow. The cross flow made no contributions to the microsphere formation. Figure 4.4b shows the successful microspheres formation. Microspheres were formed mainly by the shear stress from the cross flow, and the sheath flow was acting as a width controller for the middle flow. Figure 4.4c shows the continuous regime, in which the middle flow did not form microspheres.

4.4 The computational model of the modified T-junction

4.4.1 Dimensions of the micro-channel

Figure 4.5a shows the schematic diagram of the 2-D modified T-junction. The dimension of the micro-channel was 100 μm. The following are the underlying assumptions of model development,

a. All the flows were assumed to be laminar.
b. There was no pressure acting on the outlet except for the atmospheric pressure.
c. All the solid boundaries were set to be no-slip boundaries.
d. Fluids were incompressible, Newtonian fluids. Further, the flow rates of the three flows were given as initial conditions.

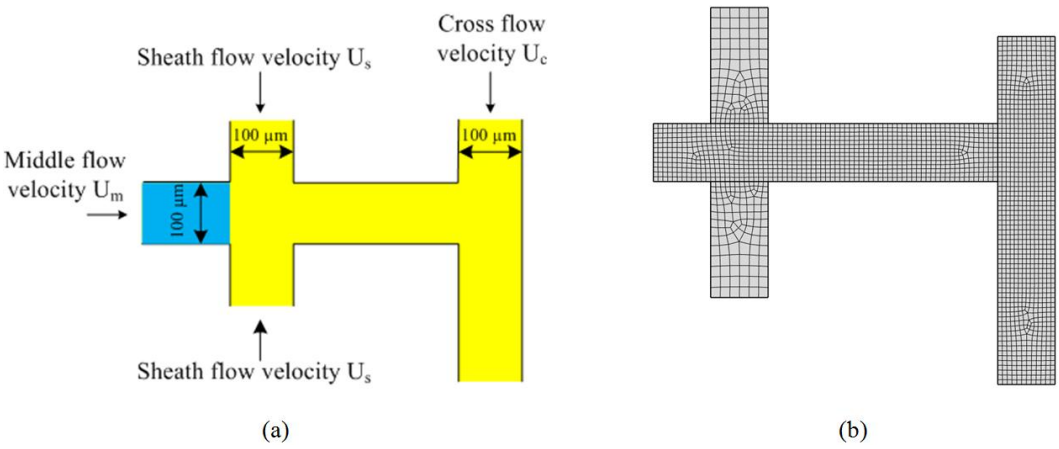

Figure 4.5. Schematic diagram (a) and meshing (b) of the modified T-junction device used in this study.

4.4.2 Governing equations

Computational fluid dynamics (CFD) and the level set (LS) method were employed to model the microsphere formation process. Commercial software COMSOL Multiphysics (COMSOL Incorporated, USA), was used to simulate the model. Please refer to Chapter 3 for the details of the governing equations.

4.4.3 Materials

The cross flow and sheath flow were paraffin oil (Shanghai Ling Feng Chemical Reagent Company, China) with 2% Span 80 surfactant (Sigma-Aldrich Corporation, USA). The middle flow was distilled (DI) water. The viscosities of DI water and mineral oil were 1 and 23.8 mPa · s, respectively（Sivasamy *et al.* 2011）. The densities of DI water and mineral oil were 1000 and 800, $kg \cdot m^{-3}$ respectively. The interfacial tension between water and mineral oil was 3.65 $mN \cdot m^{-1}$（Sivasamy *et al.* 2011）.

4.4.4 Meshing and grid dependency study

The mesh was basically composed of quadrangular elements, while triangles were also included as needed. To increase the accuracy and resolution, a finer mesh was adopted in channels where there are two fluids. A grid dependency study was performed with different grid solutions. The error of the microsphere diameters was calculated for these solutions. Refinement was stopped when the error between two grids was less than 5%. Based on the above analysis a numerical grid with 2166 elements was chosen, as shown in Figure 4.5b.

4.4.5 Validation of the simulator with experiments

Simulation results were compared with experiments using the same geometry and structure of the modified T-junction device. Figure 4.6 shows the comparison of a microsphere evolution visualized in experiments (top) and simulation (bottom) in the detached regime.

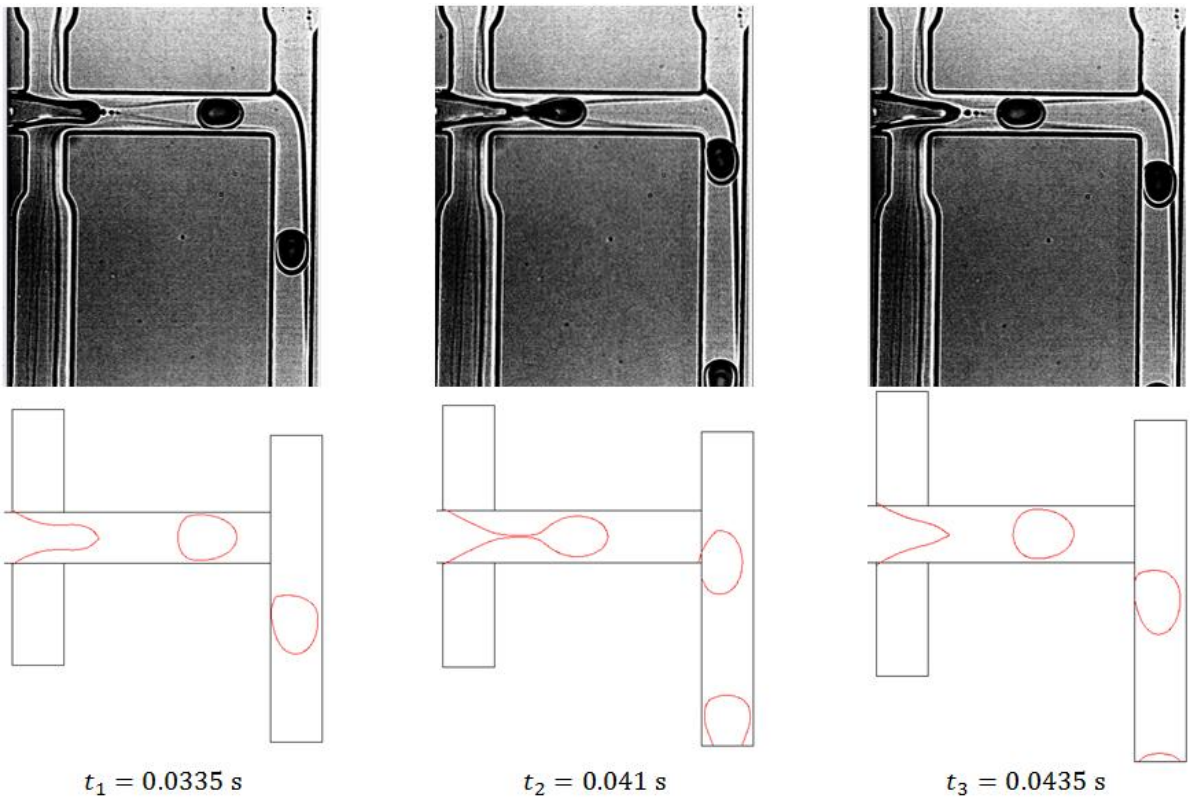

Figure 4.6. Comparison of a microsphere evolution visualized in experiments (top) and simulation (bottom) in the detached regime ($U_m = 0.01$ m $\cdot$ s $^{-1}$, $U_s = 0.01$ m $\cdot$ s $^{-1}$, $Ca = 0.065$).

The microsphere formation process shown in Figure 4.6 can be described as follows. The high pressure from the sheath flow acted on the middle flow, which induces the formation of a neck in the middle flow. This neck was getting thinner and thinner, and finally detachment happened and a microsphere was formed. As the pressure downstream was lower than the pressure upstream, this microsphere was moving towards the T-junction. When it arrived at the T-junction, it flowed to the outlet due to the higher pressure from the continuous flow. Although microspheres can be generated in this regime, the size of microspheres is only dependent on the dimension of the micro-channel, and this does not make sense for the presence of the sheath flow in the modified T-junction device. Further, the different shapes

the microsphere at the upstream and the downstream are due to different contact angles between the microsphere and the channel and different pressures in the flow in the two regions (particularly the pressure in the upstream flow is higher than the pressure in the downstream flow).

Figure 4.7 shows the experimental observation (top row) and numerical visualization (bottom row) of the microsphere evolution in the successful microsphere formation regime. It can be seen that a good agreement was achieved between the experimental and simulation results.

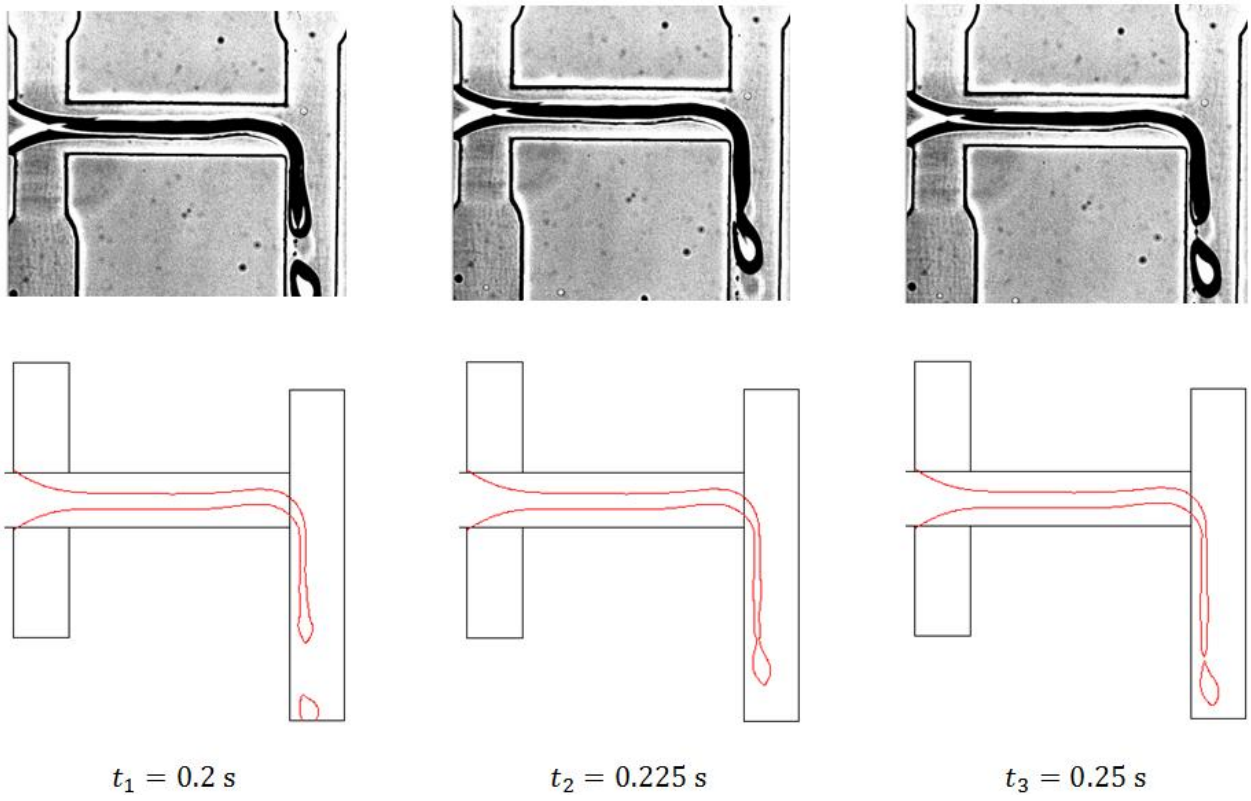

Figure 4.7. Comparison of a microsphere evolution visualized in experiments (top) and simulation (bottom) in the successful microsphere formation regime ($U_m = 0.015$ m · s $^{-1}$, $U_s = 0.01$ m · s $^{-1}$, $Ca = 0.293$).

Figure 4.7 can be explained as follows. The middle flow was squeezed by two symmetrical sheath flows at the cross junction. Then the two phases flowed into the main channel, and a microsphere began to grow. Due to hydrodynamic forces (i.e., lift and drag forces from the cross flow), the microsphere flow was downstream. When the lift and drag forces conquered the interfacial tension force, a microsphere

started to detach. During this process, the neck of the microsphere was getting thinner and thinner, and then the microsphere was eventually fully detached from the dispersed phase. After detachment, the microsphere flows downstream due to the drag force from the continuous phase. A new microsphere began to grow and the process of detachment repeats.

Figure 4.8 compares experimental (left) and simulation (right) observation of the continuous regime. In this regime, no microsphere was formed. The reason was that the pressure gradient and the shear stress cannot overcome the interfacial tension.

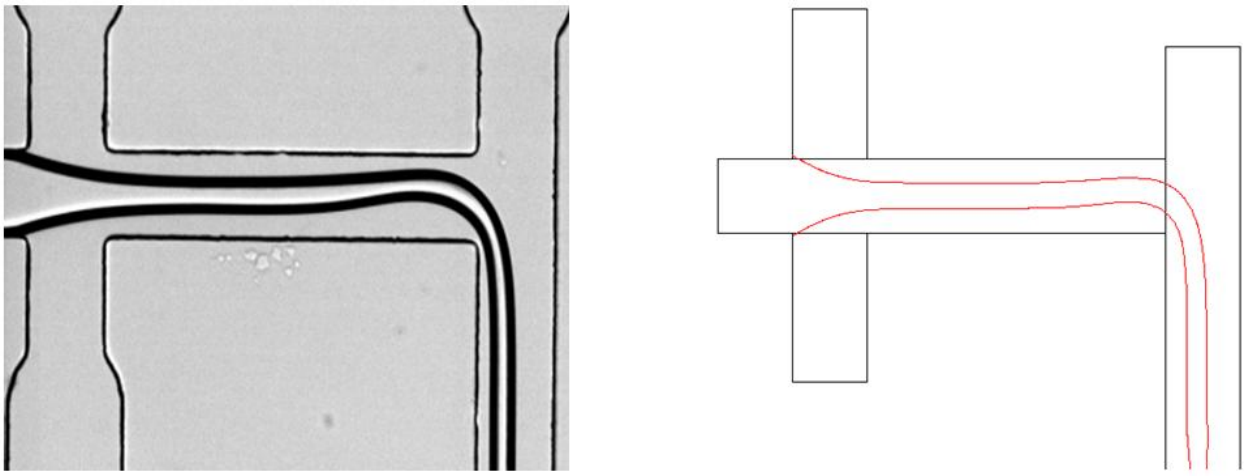

Figure 4.8. Comparison of experiment (left) and simulation (right) images in the continuous regime ($U_m = 0.02$ m · s $^{-1}$, $U_s = 0.01$ m · s $^{-1}$, $Ca = 0.293$).

4.5 Results and discussion

4.5.1 Effect of the velocity of the middle flow on the regime

The velocity of the sheath flow and middle flow, along with the capillary number of the cross flow were studied in this work, as summarized in Table 4.1. The diameter of the microsphere was measured when the flows were fully developed. The parameter $R_{m/s} = \frac{U_m}{U_s}$ was the velocity ratio of the middle flow to the sheath flow. In contract to the conventional T-junction, there were three regimes observed in the modified T-junction, namely detached (called the squeezing regime in the literature), successful (called the jetting regime in the literature) and continuous regimes (called the continuous regime in the

literature). The key factor leading to the occurrence of each regime was found to be the velocity of the middle flow. In the present study, the successful regime appeared when the velocity of the middle flow was $0.015\ \mathrm{m \cdot s^{-1}}$. When the velocity of middle flow was $0.01\ \mathrm{m \cdot s^{-1}}$, the detached regime appeared, and when the velocity of middle flow was $0.02\ \mathrm{m \cdot s^{-1}}$, the continuous regime appeared. All the flow scenarios are listed in Table 4.1.

Table 4.1. Summary of the investigated velocities.

Velocity of the sheath flow ($\mathrm{m \cdot s^{-1}}$)	Velocity of the middle flow ($\mathrm{m \cdot s^{-1}}$)	Capillary number of the cross flow	Regime	Microsphere diameter (μm)
0.005	0.01 ($R_{m/s} = 2$)	0.065	detached	-
		0.293	detached	-
	0.015 ($R_{m/s} = 3$)	0.065	successful	90.5
		0.196	successful	67.9
		0.293	successful	59.6
	0.02 ($R_{m/s} = 4$)	0.065	continuous	-
		0.293	continuous	-
0.01	0.01 ($R_{m/s} = 1$)	0.065	detached	-
		0.293	detached	-
	0.015 ($R_{m/s} = 1.5$)	0.065	successful	83.9
		0.196	successful	48.4
		0.293	successful	41.9
	0.02 ($R_{m/s} = 2$)	0.065	continuous	-
		0.293	continuous	-
0.02	0.01 ($R_{m/s} = 0.5$)	0.065	detached	-
		0.293	detached	-
	0.015 ($R_{m/s} = 0.75$)	0.065	successful	43.2
		0.196	successful	25.5
		0.293	successful	20.9
	0.02 ($R_{m/s} = 1$)	0.065	continuous	-
		0.293	continuous	-

In order to analyze the foregoing phenomena more accurately, two critical values of the velocity of the middle flow (i.e., U_{m1} and U_{m2}) were introduced and defined: U_{m1} (between 0.01 and 0.015 $\mathrm{m \cdot s^{-1}}$ in this study) was the lower threshold velocity (which distinguished the detached regime from the successful regime). U_{m2} (between 0.015 and 0.012 $\mathrm{m \cdot s^{-1}}$ in this study) was the upper threshold velocity (which distinguished the successful regime from the continuous regime). As such, the above three situations (corresponding to the three regimes) can be predicted in the process of microspheres generation with the modified T-junction. Note that there is no dripping regime (found in the conventional T-junction device) in the modified T-junction device. This absence could be due to the introduction of the sheath flow. In the modified T-junction, the sheath flow acts as a "buffer", which reduces the shear force from the continuous flow. Thus, the detachment of the microsphere delays until the shear force dominates.

Situation 1: $U_m < U_{m1}$,

The forces acting on the middle flow were hydrodynamic forces (lift and drag) and the interfacial tension force. Hydrodynamic force was associated with the pressure gradient across the interface and the shear stress along the interface. The interfacial tension force was associated with the interfacial tension between the two immiscible phases. When $U_m < U_{m1}$, the pressure force acting on the top of the middle flow dominated the interfacial tension force, and a microsphere was thus formed. In this situation, the device could be viewed as a typical flow focusing device, in which the minimum size of microspheres was on the order of the dimensions of the micro-channel（Ward *et al.* 2005）.

The same situation happened under other velocities of the sheath flow (i.e., $U_s = 0.01$ and 0.02 $\mathrm{m \cdot s^{-1}}$). More interestingly, for different velocities of the sheath flow, the two critical values for the velocity of the middle flow, U_{m1} and U_{m2} barely changed. Thus, it could be concluded that the velocity of the middle flow determined the regime (the velocity of the sheath flow: from 0.005 to 0.02 $\mathrm{m \cdot s^{-1}}$).

Situation 2: $U_{m1} \leq U_m < U_{m2}$,

If the velocity of the middle flow was larger than U_{m1}, the interfacial tension force could conquer the hydrodynamic forces from the sheath flow. The middle flow could stay continuous before it arrives at the junction, as $U_m < U_{m2}$, and the interfacial tension force cannot conquer the hydrodynamic force from the cross flow.

Situation 3: $U_m \geq U_{m2}$,

When the velocity of the middle flow was larger than U_{m2}, the interfacial tension force was dominant to the hydrodynamic force from the sheath flow. The interfacial tension force held the top of the middle flow with no breakup happening. As such, no microspheres can be successfully formed in this situation. It was found that if Ca of the cross flow was increased further, the middle flow was pushed to the junction section, as shown in Figure 4.9.

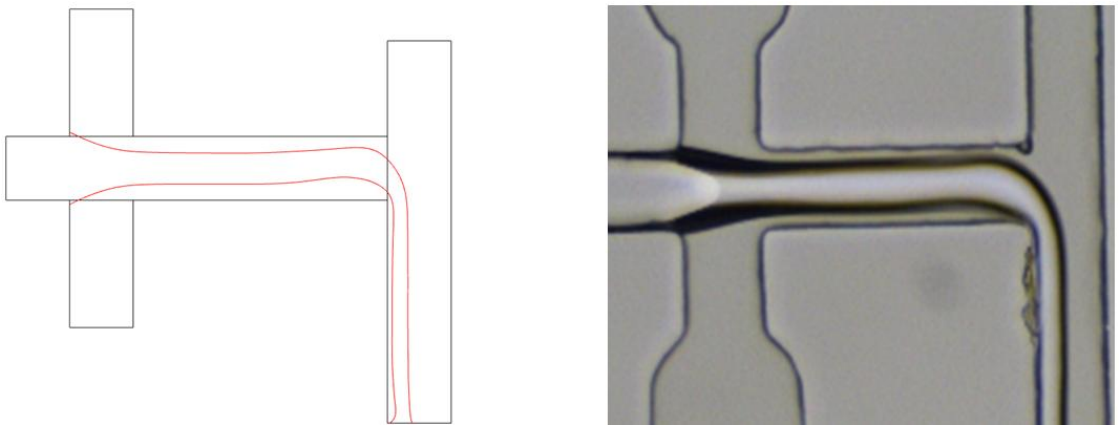

Figure 4.9. Comparison of the experiment (left) and simulation (right) images in continuous regime ($U_m = 0.02$ m · s $^{-1}$, $U_s = 0.005$ m · s $^{-1}$, $Ca = 0.293$).

4.5.2 Effects of $R_{m/s}$ and the capillary number of the cross flow on the microsphere diameter

Figure 4.10 shows the diameter of microspheres for different values of $R_{m/s}$ and the capillary number of the cross flow. It can be seen that higher Ca of the cross flow leads to smaller microspheres. This phenomenon can be explained as follows. As a microsphere started to grow, the interfacial tension force acts as a holding force, which would be dominant before the detachment. Meanwhile, the shear stress from the cross flow acts as a detaching force, which induced the neck formation from the top of the middle flow. With a higher Ca of the cross flow, the shear stress was higher. The neck was formed earlier, which means the volume of the top of the middle flow was smaller. Thus, the microsphere volume was smaller. On the contrary, a lower Ca of the cross flow led to a lower shear stress. The neck was formed with a larger volume of the middle flow, which led to a larger microsphere.

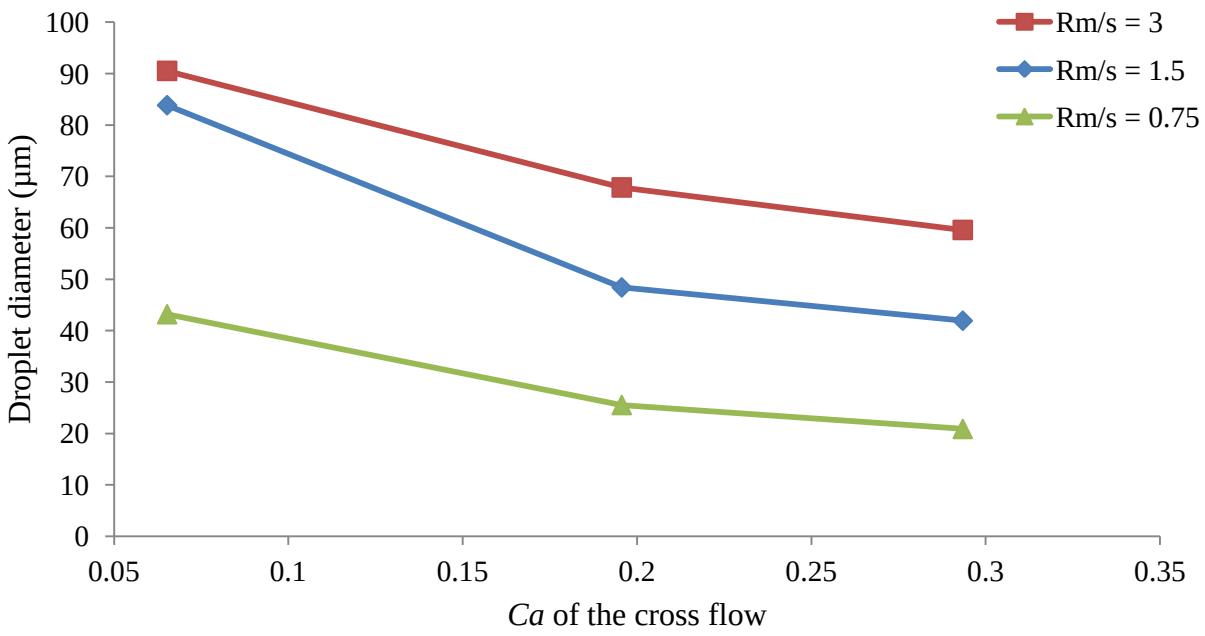

Figure 4.10. Effects of Ca of the cross flow, and the velocity ratio of the middle flow to the sheath flow on the microsphere diameter.

Figure 4.10 also shows that larger microspheres can be generated with a higher $R_{m/s}$ for the same Ca of cross flow. The reason could be as follows. At the junction where the sheath flow and middle flow met, if $R_{m/s}$ was increased, the width of the middle flow was increased. Thus the interfacial tension around the top of the middle flow was increased. With the same Ca of the cross flow, the size of microsphere was increased until the drag and lift force from the cross flow overcame the interfacial tension force. Thus, with the introduction of the sheath flow, microspheres with a different diameter of microspheres can be achieved.

4.6 Conclusions

This chapter reported a study on the fundamental understanding of the mechanism of microsphere generation with the modified T-junction device. Both the simulation and experimental test-bed were employed for this purpose. Specifically, three regimes in the modified T-junction were discovered, namely detached regime, successful regime, and continuous regime. In conclusion, in a range of the velocity of the sheath flow (i.e., $U_s = 0.005\ \mathrm{m \cdot s^{-1}}$ to $U_s = 0.02\ \mathrm{m \cdot s^{-1}}$), the velocity of the middle

flow is mostly responsible for the three regimes in the flow. If the velocity of the middle flow U_m was smaller than a critical value of U_{m1}, the detached regime occurred; if $U_{m1} \leq U_m < U_{m2}$, the successful regime occurred; if $U_m \geq U_{m2}$, the continuous regime occurred. Additionally, the diameter of the microspheres increased with the decrease of the capillary number of the cross flow and with an increase in $R_{m/s}$. The capillary number of the cross flow Ca, and the ratio of the velocity of the middle flow to the velocity of the sheath flow $R_{m/s}$ were found to have significant effects on the diameter of microspheres.

CHAPTER 5. OPTIMIZATION OF THE MICROSPHERE GENERATION PROCESS WITH THE MODIFIED T-JUNCTION DEVICE

5.1 Introduction

There are three basic requirements for the successful generation of microspheres: size (or diameter), uniformity, and size adjustability. The size of microspheres refers to the diameter of microspheres. From the point of view of the micro-fluidic device, the diameter of microspheres should be made as small as possible. Uniformity means that the diameters of the microspheres in one batch of the process are as identical as possible. The standard deviation (SD) of the size distribution of microspheres is used to measure the uniformity of microspheres; the smaller the SD, the more uniform the microspheres. The size adjustability means that the diameter of microspheres can be changed batch by batch using one device; the larger the size range, the better the device.

The micro-fluidic technique is the most popular method to make micro/nano-spheres（Ding *et al.* 2015, Jung and Oh 2014, Peng *et al.* 2015, Perez *et al.* 2015, Song 2011, Xue *et al.* 2015）. Among many devices, the modified T-junction device has been shown to be a promising technique to make microspheres in terms of the three requirements mentioned above, since it was first developed by Song in our group（2011）. The schematic diagram of the modified T-junction is shown in Figure 5.1, where three flows are involved in the microsphere generation process: middle flow, sheath flow, and cross flow. The sheath flow and cross flow are the same type of fluid, and they are immiscible with the middle flow. The role of the sheath flow is primarily to squeeze the middle flow to produce microspheres with varying sizes. The sheath flow and middle flow move co-axially to meet the cross flow in the junction, producing microspheres from the middle flow (Figure 5.1).

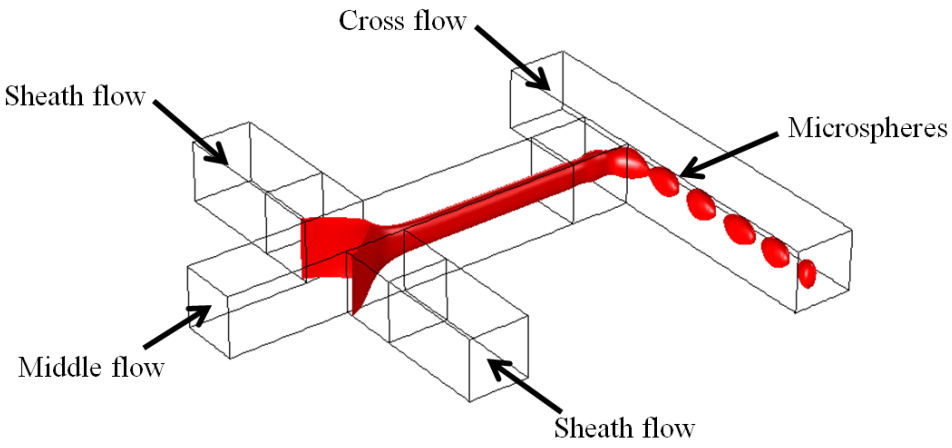

Figure 5.1. A three-dimensional model of the microsphere generation with the modified T-junction device.

In Chapter 4, the mechanism behind how the modified T-junction device works was discussed. This chapter will present the optimal design of the modified T-junction device as well as its microsphere generation process. The foregoing three response variables, namely the size, uniformity, and size range were considered in the study, however, the optimization was only meant for the size (i.e., minimization of the diameter of the microspheres) and uniformity (i.e., minimization of the standard deviation of the diameter of microspheres). The remainder of the chapter is organized as follows. In Section 5.2 a new approach to the optimal design of such process systems is introduced, which combines (1) the discrete variable optimization for the device and (2) the optimization for the process variable (the process is operated upon the device). Section 5.3 shows the application of the new approach to the microsphere generation process with the modified T-junction device. Section 5.4 presents the work for (1) and Section 5.5 presents the work for (2). Some concluding remarks and further discussion are presented in the last section.

5.2 A new approach to the optimization of a process system

A process system consists of two sub-systems: infrastructure and substance（Zhang and Van Luttervelt 2011）. A process results from an external driver on a substance to change the state of the substance over the infrastructure which may also actively change the infrastructure. For the microsphere generation

process with the modified T-junction device, the channel, sheath flow fluid, and cross flow fluid are part of the infrastructure, and the middle flow fluid is part of the substance. The microsphere generation process changes the state of the middle flow fluid (cutting into droplets), driven by the external pressure on the middle fluid and interacted by the cross flow fluid with all these flows confined by the channel.

A process is described by parameters. With the above understanding of the process system, parameters are categorized into the following kinds: (infrastructure) **system parameter**, (infrastructure) **operating parameter**, (substance) **product parameter**. For the microsphere generation process with the modified T-junction device, the system parameter describes the channel configuration and geometry, property of the sheath flow fluid, property of the cross flow fluid; the operating parameter describes the flow rate of the cross flow fluid, flow rate of the sheath flow fluid; the product parameter describes the size of the middle flow fluid, flow rate of the middle flow fluid, diameter of the droplet formed out of the middle flow fluid, and property of the middle flow fluid.

The parameters are expected to be determined in an optimal fashion such that certain objectives can be achieved, for example (in the case of the modified T-junction device along with its process) the smallest diameter of droplets, the smallest variation of the size of droplets, and the largest range of size of droplets. The design optimization refers to a method to determine the parameters to achieve the objectives. The basic challenge in design optimization is to build a test-bed on which parameters can be changed, a corresponding process can be executed, and objectives can be measured. By the nature of design optimization, the number of changes on parameters is very large and further the cost of changes especially those that demand physical changes is very high, and this straightforwardly invalidates the idea of building any physical type of test-bed for optimization. Therefore, building of a simulation type of test-bed (or simulator for simplicity) is a more practical approach. However, a simulator usually has a serious shortcoming that is the inaccurate exhibition of process behaviors owning to its difficulty to represent the effects originated from various noises and/or disturbances in a process system (e.g., changes of the viscosity in non-Newtonian fluids)（Chen *et al.* 2003）.

Various methods or techniques are available in the literature to cope with the above dilemma, notably the Taguchi method for the optimization of parameters for improving the robustness of a process（Jamil and Ng 2013）. The Taguchi method makes the use of two core ideas. The first one is use of the physical

type of test-bed (or prototype for simplicity). The second one is discretization of continuous parameters to the extent that the parameters take two or more levels with the levels being surrogates of the range of values of the parameters. The discredited parameter is called the factor. The Taguchi method is very effective in optimizing parameters that do not require changes on the physical device, such that the cost of changes is thus acceptable in practice. The underlying principle that accounts for the effectiveness of the Taguchi method has two parts: the first enabler for examining the effect of noises and/or disturbances and the second enabler for the feedback adjustment.

A new approach to design optimization for manufacturing processes was proposed in the study presented in this chapter. The approach involves the following steps. Step 1: define the objective (O) or objectives say O_1, O_2 (for example), where O is a set. Step 2: identify the parameter (P) or parameters say P_1, P_2, P_3 (for example), where P is a set. Step 3: analyze the dependency between the parameter set and objective set, O-P relation for short. Step 4: optimize the system parameter (P_s) and product parameter (P_p) in P for the corresponding objectives say $O_{s,p}$ in O with the simulator. Step 5: optimize the operating parameter (P_o) in P for the corresponding objectives say O_o in O with the prototype.

There are several remarks regarding the proposed approach to design optimization. Remark 1: In Step 4 above, the optimization problem may be a multi-objective optimization, and in such a case, the multi-objective optimization technique should be applied（Han *et al.* 2015）. Remark 2: If P and O are coupled, an optimization of P for O should be applied; see the similar observation in Bi et al.（2002）and Zhang et al.（1999）with the notion called “integrated design”. Remark 3: The operating parameter may describe planning, scheduling, coordinating and controlling, so the proposed approach is general and applicable to problems that involve engineering of both the structure and operation of a complex system（Zhang 2010）.

5.3 Optimization of the microsphere generation process with the modified T-junction device

The proposed approach was followed for the optimization of the microsphere generation process with the modified T-junction device. This includes the decisions with the steps as described in Section 5.3.

Step 1: The objectives considered in the study were: the size and uniformity of microspheres; particularly microspheres generated should be as small as possible (O_1) and microspheres generated should meet a required accuracy and uniformity in terms of the size of microspheres (O_2). It is noted that the size range was not considered in this study.

Step 2: The parameters considered in this study were: (1) the configuration of the micro-channel (P_{s1}), (2) the dimension of the micro-channel (P_{s2}), (3) the concentration of PLGA (P_p), and (4) the flow rate of the cross flow (P_o).The first parameters (i.e., P_{s1}, P_{s2}, and P_p) are considered as a discrete variable owing to otherwise huge computational and experimental cost. In particular, the present study considered two configurations for (P_{s1}), as shown in Figure 5.2, as they were used in practice. For each configuration, the width of the micro-channel (P_{s2}) took three values: 50 μm, 75 μm, and 100 μm, as they were used in practice. For the concentration of PLGA (P_p), this study considered three values: 1%, 5%, and 15%. For the cross flow ($\mathrm{ml} \cdot \mathrm{min}^{-1}$), three flow rates were considered in Step 4 of the optimization: 0.01, 0.02, and 0.03. This was to see how sensitive this parameter was to O_1, and then it was considered as a continuous variable in Step 5 of the optimization. It is noted that the flow rates of the sheath flow (Q_s) and middle flow (Q_m) were considered to be constant in the present study, because they are mainly responsible for the size range instead of the two objectives considered in the present study. According to the previous discussion in Chapter 4, Q_s and Q_m must fall into an area such that the regime (where microspheres are generated successfully) dominates; as such, the flow rates of the sheath flow and middle flow were set to be: $Q_s = Q_m = 0.01\ \mathrm{ml} \cdot \mathrm{min}^{-1}$.

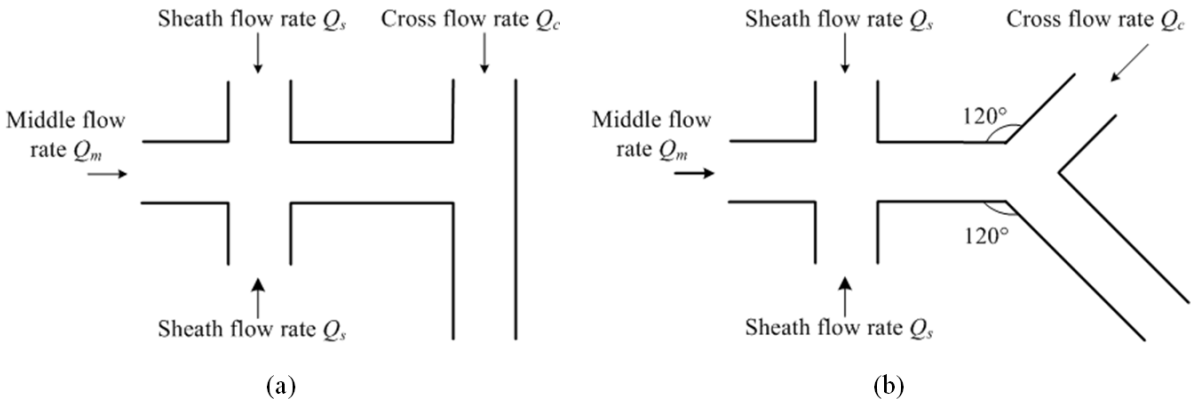

Figure 5.2. Two configurations of the micro-fluidic device; (a) straight channel, (b) crooked channel.

Step 3: The study did some preliminary investigation of the sensitivity of all four factors with respect to the two objectives. The dependency of the parameters on the objectives is shown in Figure 5.3.

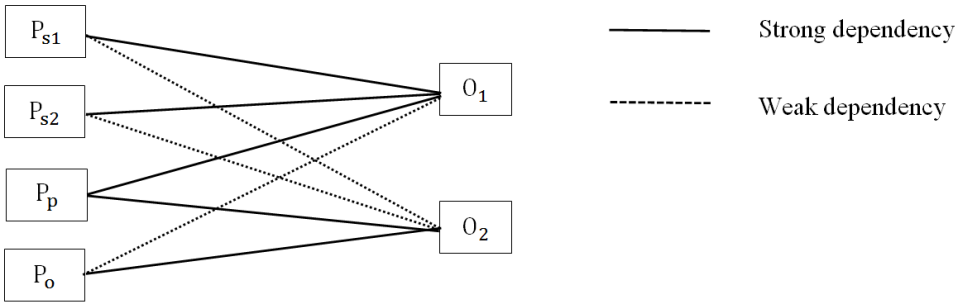

Figure 5.3. D-P dependency relation map.

Step 4: Optimize the parameters or factors for O_1 (see Section 1.4).

Step 5: Optimize the parameter P_o for O_2 (see Section 1.5).

5.4 **Factorial optimization for the smallest size of microspheres**

According to the discussion above, a simulator was employed and a methodology called orthogonal design method (ODM) was employed on the three factors, i.e., the configuration of the micro-channel, the width of micro-channel, and the concentration of PLGA.

5.4.1 Simulator

The computational fluid dynamics (CFD) method was employed to model the microsphere formation process of the modified T-junction, and the details of the model were presented in Chapter 3. Commercial software COMSOL Multi-physics (COMSOL Incorporated, USA), which contains the LS method for dealing with a multi-phase flows problem, was employed to assist the modeling and simulation (see Chapter 3 for details). The following are the underlying assumptions of model development,

a. All the flows were assumed to be laminar.

b. There was no pressure acting on the outlet except for the atmospheric pressure.
c. All the solid boundaries were set to be no-slip boundaries.
d. Fluids were incompressible, Newtonian fluids. Further, the flow rates of the three flows were given as initial conditions.

5.4.2 Orthogonal design method (ODM)

The study considered the three factors plus the factor of the cross flow rate. The purpose of including the cross flow rate was to confirm that indeed it had little influence over the second objective (O_2) in the present study. The levels of the four factors are listed in Table 5.1.

Table 5.1. Parameters or factors with their levels.

Factor	Level 1	Level 2	Level 3
Structure	Straight	Crooked	-
Channel size (μm)	50	75	100
PLGA concentration	1%	5%	15%
Q_c ($\mathrm{ml \cdot min^{-1}}$)	0.01	0.02	0.03

The total number of combinations with the four factors is: $3^3 \times 2 = 54$. By applying the technique called orthogonal L-18 array Minitab (Software, Minitab Incorporated, USA), a reduced number of combinations is 18, as listed in Table 5.2.

Table 5.2. L-18 orthogonal array of four parameters.

Experiment	Structure	Q_c ($\mathrm{ml \cdot min^{-1}}$)	Channel size (μm)	PLGA concentration
1	Straight	0.01	50	1%
2	Straight	0.01	75	5%
3	Straight	0.01	100	15%
4	Straight	0.02	50	1%
5	Straight	0.02	75	5%
6	Straight	0.02	100	15%
7	Straight	0.03	50	5%

Table 5.2. Continued.

8	Straight	0.03	75	15%
9	Straight	0.03	100	1%
10	Crooked	0.01	50	15%
11	Crooked	0.01	75	1%
12	Crooked	0.01	100	5%
13	Crooked	0.02	50	5%
14	Crooked	0.02	75	15%
15	Crooked	0.02	100	1%
16	Crooked	0.03	50	15%
17	Crooked	0.03	75	1%
18	Crooked	0.03	100	5%

5.4.3 Results and discussion

Table 5.3 shows the diameters of microspheres, achieved by the computer simulation for 18 combinations or experiments of the factors. Analysis of Variance (ANOVA) was employed to analyze the sensitivity of the factors with respect to the response (i.e., the first objective O_1) ($p < 0.05$).

Table 5.3. Microsphere diameters achieved by the L-18 orthogonal array.

Experiment	Structure	Q_c ($\mathrm{ml \cdot min^{-1}}$)	Channel size (μm)	PLGA concentration	Microsphere diameter (μm)
1	Straight	0.01	50	1%	21.5
2	Straight	0.01	75	5%	30.3
3	Straight	0.01	100	15%	54.1
4	Straight	0.02	50	1%	21.3
5	Straight	0.02	75	5%	30.0
6	Straight	0.02	100	15%	54.3
7	Straight	0.03	50	5%	23.5
8	Straight	0.03	75	15%	41.6
9	Straight	0.03	100	1%	47.2

Table 5.3. Continued.

10	Crooked	0.01	50	15%	34.1
11	Crooked	0.01	75	1%	41.9
12	Crooked	0.01	100	5%	56 1
13	Crooked	0.02	50	5%	23.2
14	Crooked	0.02	75	15%	45.3
15	Crooked	0.02	100	1%	49.1
16	Crooked	0.03	50	15%	34.0
17	Crooked	0.03	75	1%	34.3
18	Crooked	0.03	100	5%	45.8

Table 5.4 shows the ANOVA results for the four factors obtained by Minitab. It can be found from this table that the configuration ($p = 0.017$), the channel size ($p < 0.001$), and the PLGA concentration ($p = 0.001$) have significant effects on the response (i.e., the diameter of microspheres), but Q_c ($p = 0.253$) has no significant effect on the response. Contributions from each factor were calculated according to their adjusted mean squares.

Table 5.4. The statistic result for the four parameters.

Factor	Degree of freedom	Sums of squares	Adjusted mean squares	F	p	% Contribution	Ranking
Structure	1	88.58	88.58	8.11	0.017	7.66	3
Q_c	2	34.51	17.26	1.58	0.253	1.49	4
Channel size	2	1763.01	881.50	80.73	<0.001	76.21	1
PLGA concentration	2	338.54	169.27	15.50	0.001	14.64	2
Residual error	10	109.18	10.92				
Total	17	2333.82					

Table 5.4 also shows that the three major factors contribute almost 98% of the effect on the response. Q_c accounts for 1.49% of the total effect, which also suggests that the diameter of microspheres was not significantly influenced by Q_c.

Figure 5.4 shows the main effects on the diameter of the four parameters obtained by Minitab. It suggests that the channel size and PLGA concentration are two major effects on the response. It can be understood that the wider micro-channel would produce larger microspheres. For PLGA concentration, higher PLGA concentration could make larger microspheres, which was consistent with the experimental results obtained by Hung et al. (2010). This phenomenon could be explained by the quantity of PLGA monomers. A higher quantity of PLGA monomers leads to slower solvent diffusion, which produced larger microspheres（Hung *et al.* 2010）. Note that the relation between the PLGA concentration and the microsphere diameter was non-linear, as it could be seen in Figure 5.4 which also shows that different intervals have different slopes. The same situation happened for Q_c, though the difference in the slope observed is very small when Q_c changed from 0.01 $\text{ml} \cdot \text{min}^{-1}$ to 0.02 $\text{ml} \cdot \text{min}^{-1}$ and from 0.02 $\text{ml} \cdot \text{min}^{-1}$ to 0.03 $\text{ml} \cdot \text{min}^{-1}$.

According to Figure 5.4, it can be concluded that for the minimization of the microsphere diameter, the best arrangement for the four parameters listed in Table 5.1 was to keep the straight structure, $Q_c = 0.03\ \text{ml} \cdot \text{min}^{-1}$, the channel size at 50 μm, and the PLGA concentration at 1%. This combination of the factors predicts the diameter of microspheres, which is 19.5 μm. Compared with the data listed in Table 5.3, it is clear that the response with the optimal parameters was the minimal value.

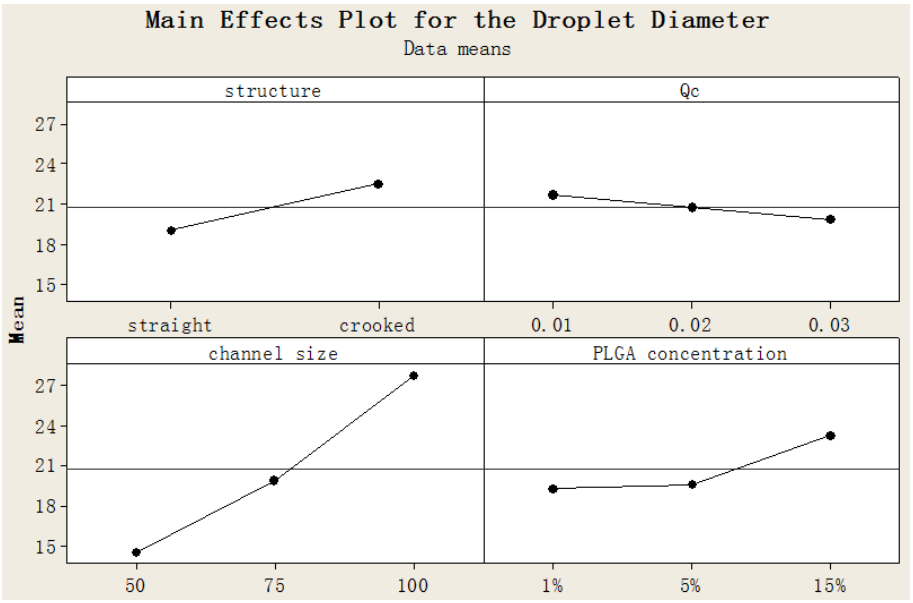

Figure 5.4. Main effects plot for the microsphere diameter.

The experiment with optimized factors was conducted, which showed the diameter of microspheres as 21.4 μm with the standard deviation of 1.3 μm, compared with the theoretically predicted optimal response (i.e., 19.5 μm). Figure 5.5a shows the flow pattern of the middle flow, sheath flow, and cross flow observed during the microsphere generation process. Microspheres were generated in the area of the red circle, as shown in Figure 5.5a. Figure 5.5b shows that microspheres were flowing to the collecting reservoir. Figure 5.5c shows microspheres in the reservoir.

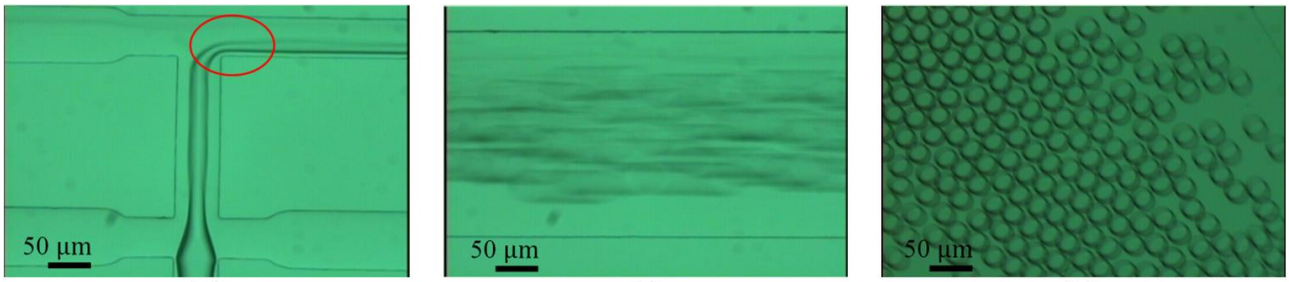

Figure 5.5. Optical microscope images: (a) the flow pattern of the middle flow, sheath flow, and cross flow, (b) microspheres generated under the optimized parameters, (c) microspheres were collected and diameters of microspheres were measured (the diameter $D_o = 21.4 \pm 1.3$ μm).

5.5 Optimization for the highest uniformity of microspheres

In Section 5.4, it is shown that Q_c is not significant to the size of microspheres, which is in agreement with the result shown in Figure 5.3. However, Q_c was chosen for fine tuning or optimization for two objectives (uniformity and desired or optimal size) with three reasons. First, in the ODM optimization procedure, Q_c was there taken as a factor which have three levels while Q_c is a continuous variable. Such discretization of Q_c can introduce some error in the understanding of the influence of Q_c. Second, Q_c may affect the variation of the deviation (i.e., uniformity in this dissertation) with reference to a target diameter of microspheres. Third, Q_c is an operating parameter that can easily be adjusted. The foregoing reasons also led to the idea that the evaluation of the optimal result was performed through the experiment.

The two objective functions are: (1) the error between the actual diameter and required diameter (ϵ) and (2) the uniformity of microspheres (SD). The two objectives are not completely in conflict based on the author's experience and numerical analysis. Therefore, the overall objective function (OF) is defined as OF= $|\epsilon| + |\mathrm{SD}|$. Obviously, the minimal value of OF is zero. In this study, the zero is represented by a small number say 1.5 μm. As such, the optimization problem is to find Q_c* such that the OF is less than 1.5 μm. In the implementation, the algorithm took a simple procedure, namely let Q_c increase in small steps ($0.005\ \mathrm{ml \cdot min^{-1}}$) from $0.005\ \mathrm{ml \cdot min^{-1}}$ to $0.2\ \mathrm{ml \cdot min^{-1}}$ incrementally until the OF < 1.5 μm is satisfied. The next section will describe the experiment test-bed as well as the measurement procedure, followed by results and discussion.

5.5.1 Experimental set-up

The micro-fluidic device was made from PDMS. The size of the device was $3 \times 2\ \mathrm{cm^2}$. The cross section of the device was square (i.e., the width of the channel is the same as the height of the channel). The dimension of the micro-channel was 50 μm. All the micro-fluidic devices were designed by AutoCAD (Autodesk Incorporated, USA), and fabricated using photolithography technology (Shanghai Wenchang Chip Technology Limited, China). The details of the design and fabrication of the devices were given in Chapter 3.

The 1% PLGA solution was used as the middle fluid. The 1% PVA dissolved in distilled water was used

as the middle fluid and cross fluid. PLGA (50/50, inherent viscosity 0.16-0.24 $\mathrm{dl \cdot g^{-1}}$) was obtained from Evonik Industries (Essen, Germany). PVA (Mw 85,000-124,000, 99+% hydrolyzed) and DCM were obtained from Sigma-Aldrich Corporation (St. Louis, USA). The physical properties of the materials were the same as those described in Chapter 3.

Figure 5.6 shows the experimental set-up. Three syringe pumps (New Era Pump Systems Incorporated, USA; Kent Scientific Corporation, USA; and GENEQ Incorporated, Canada) controlling the flow rates of the fluids and the PDMS chip were connected with syringes (6 ml, Covidien Limited, Ireland) and the tubing (1.34 mm PTFE, Adtech Polymer Engineering Limited, United Kingdom). All three syringe pumps were calibrated before the experiments. The inverted microscope (Olympus IX70, Olympus Corporation, Japan) was used to observe the experimental process and a computer with image processing software was used for post-processing. A single microsphere was measured multiple times (> 5 times) and their average value was taken. The experiments were performed at Room 2B63, ENG, in the University of Saskatchewan. The experiments were performed in room temperature ($20℃ \pm 2℃$).

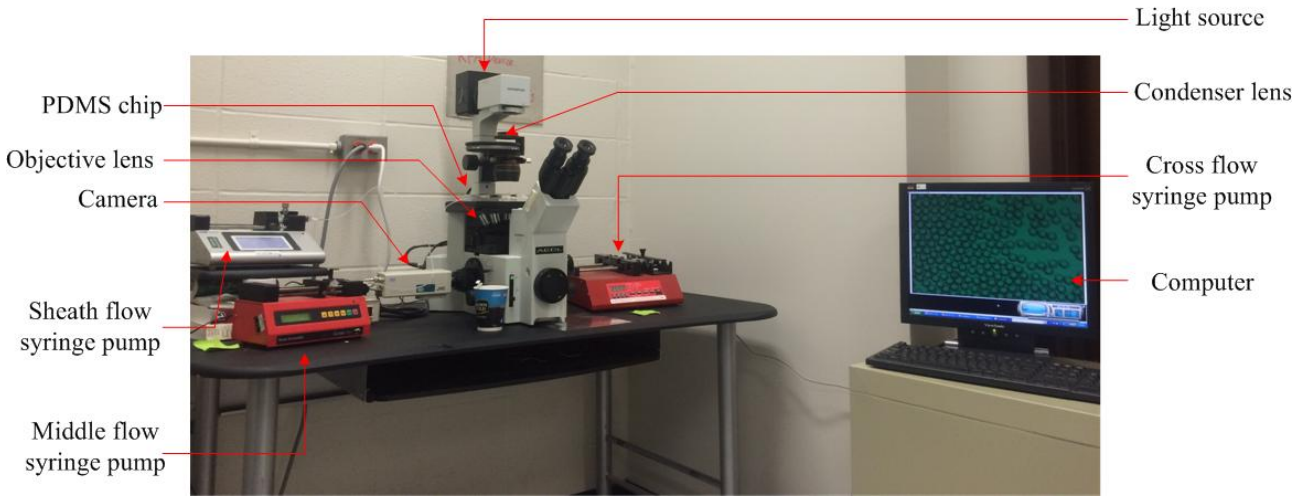

(a)

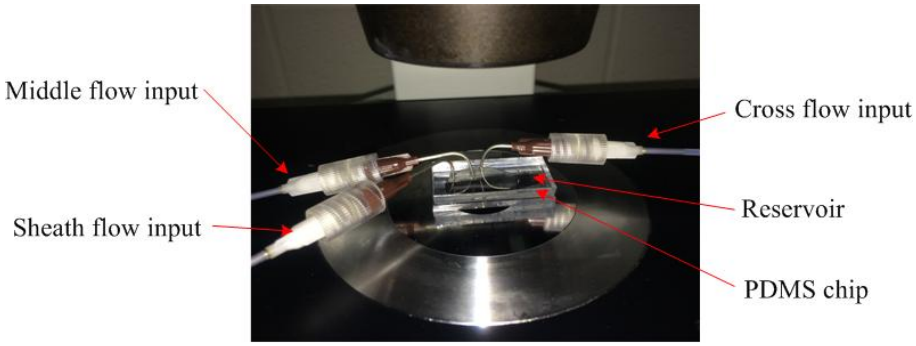

(b)

Figure 5.6. Images of: (a) experimental set-up; and (b) three flows being pumped into the PDMS chip; the microspheres generated were collected in the reservoir.

The optimization process has the following steps: (1) to collect microspheres after the flow pattern was stable; (2) to choose 50 microspheres in an area of $200 \times 200\ \mu m^2$, and measure diameters of microspheres and compare them with the required diameter; (3) to adjust Q_c and proceed the foregoing steps until the condition $OF < 0.15\ \mu m$ is satisfied.

5.5.2 Results and discussion

In this dissertation study, two cases were considered, firstly the case in which the required diameter was smaller than the optimized diameter (*Case 1*) and secondly the case in which the required diameter was larger than the optimized diameter (*Case 2*). The optimal diameter was 19.5 μm (obtained before in Section 5.4).

Case 1: Required diameter of microspheres $(D_r) = 15.0\ \mu m$,

Q_c was increased gradually, while the measurement of the diameters of the microspheres was performed, as shown in Table 5.5. It was found that when $Q_c = 0.11\ ml \cdot min^{-1}$, the actual diameter of the microspheres was 16.1 μm with a standard deviation of 0.23. Though the actual diameter of the microspheres could reach to 14.7 μm when $Q_c = 0.13\ ml \cdot min^{-1}$, the uniformity of microspheres was very poor (which shows the conflicting nature of the two objectives (ϵ, SD). Further, this also shows that the capability of using Q_c to improve the accuracy is quite limited, as Q_c is mainly responsible for the

uniformity of the size of microspheres. Figure 5.7 shows an optical microscope image of microspheres generated after performing the optimization process.

Table 5.5. The mean diameter and standard deviation of microspheres with different Q_c for *Case 1*.

Q_c (ml · min^{-1})	Mean diameter (μm)	SD (μm)
0.03	21.4	1.3
0.05	21.0	2.1
0.07	19.8	0.5
0.09	18.5	1.0
0.11	16.1	0.2
0.13	14.7	1.5

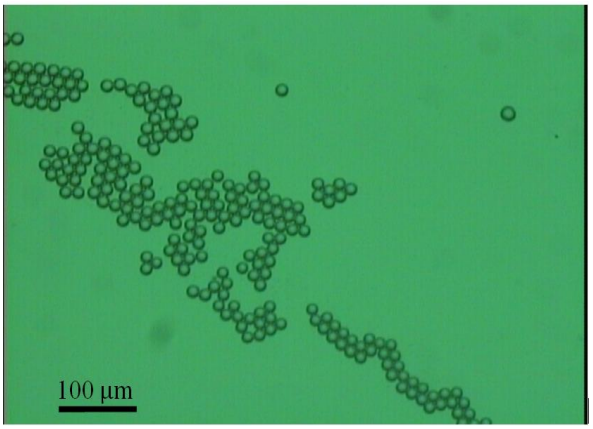

Figure 5.7. An optical microscope image of microspheres generated after performing the optimization process for *Case 1*.

Case 2: Required diameter of microspheres $(D_r) = 25.0$ μm,

By decreasing Q_c gradually from its upper bound, the diameter of the microspheres increased. Table 5.6 shows the diameter of microspheres with the decrease of Q_c. It can be seen that when $Q_c = 0.010$ ml · min^{-1}, the diameter of the microspheres is 24.8 μm with the standard deviation of 0.7 μm. The overall result for the required diameter of 25.0 μm is better than the overall result for the required diameter of 15.0 μm. Figure 5.8 shows an optical microscope image of microspheres generated after performing the

optimization process.

Table 5.6. The mean diameter and standard deviation of microspheres with different Q_c for *Case 2*.

Q_c (ml · min^{-1})	Mean diameter (μm)	SD (μm)
0.030	21.4	1.3
0.025	22.0	1.4
0.020	22.8	0.8
0.015	23.8	1.0
0.010	24.8	0.7
0.005	26.4	0.3

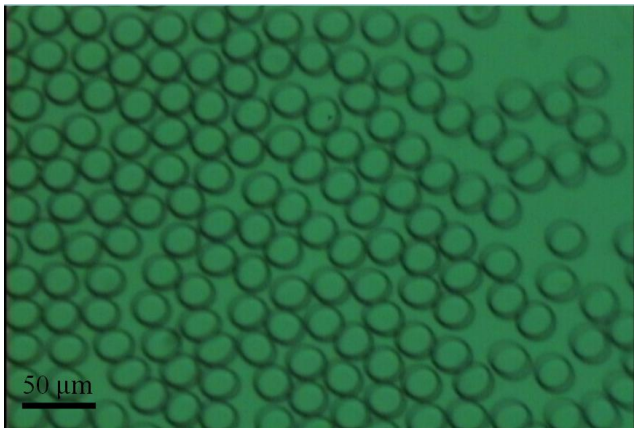

Figure 5.8. An optical microscope image of microspheres generated after performing the optimization process for *Case 2*.

5.6 Conclusions

This chapter discussed the optimization of the microsphere generation process with the modified T-junction device. There was no compelling approach available in the literature about the optimization of this kind of device along with its process. In the area of machine design, e.g., robot design, optimization usually refers to the mechanical structure, though there may be some approach to integrated design of the mechanical structure and design of controllers（Zhang *et al.* 1999）. In the area of chemical process design, the equipment is fixed, and design refers to setting up the process variables such as temperature

and pressure（Fujiu *et al.* 2012）. The modified T-junction device along with its process is different from the foregoing two (for the convenience of discussion, the microsphere generation process was called the process system). Therefore, a new approach was first proposed for the design optimization of complex process systems in this study. Then, the approach was applied to the microsphere generation process with the modified T-junction device.

Several conclusions can be drawn from the study. First, the proposed approach was effective, as the design outcome with this approach indeed improved the performance of the modified T-junction device. Second, for the particular modified T-junction device, the requirement for the diameters of microspheres (i.e., $D_r = 15.0$ μm and $D_r = 25.0$ μm) was satisfied by the result of the optimization, namely the actual diameters were ($D = 16.1 \pm 0.2$ μm and $D = 24.8 \pm 0.7$ μm). Third, the proposed approach is also applicable to the devices built upon the operating principles such as flow focusing and membrane emulsification, as the approach was formulated upon the general process system with the corresponding notions such as infrastructure and substance and system parameter, operating parameter, and product parameter.

CHAPTER 6. A NEW MEMBRANE EMULSIFICATION DEVICE

6.1 Introduction

As one of the methods of microsphere generation, membrane emulsification method has been gathering significant attention due to its high production rate since it was introduced by Nakashima and Shimizu (1986). The schematic diagram of a typical membrane emulsification device is shown in Figure 6.1. Two flows are involved in the process of the microsphere generation (i.e., the continuous flow and the dispersed flow). The dispersed flow is pressed through the pores on the membrane. The dispersed flow is potentially cut off by the shear force from the continuous flow to form microspheres. The continuous phase can be injected by a pump（Laouini *et al.* 2012, Nakashima and Shimizu 1986）, a stirring system（Manga *et al.* 2012, Pawlik and Norton 2012, Silva *et al.* 2015）, an agitator（Dragosavac *et al.* 2012, Fuchigami *et al.* 2000, Kosvintsev *et al.* 2005, Oh *et al.* 2011, Song 2011, Thompson *et al.* 2011）, or both（J.-O. You 2001）, and a vibrating membrane（Holdich *et al.* 2010）.

The diameter of microspheres D_d is highly dependent on the pore size D_p, and normally D_d is 2 to 10 times larger than D_p（Joscelyne and Trägårdh 2000）. Thus, in order to obtain small size microspheres, the pore size has to be very small (nanometer preferably). However, the thickness of the membrane has to be small as well for small pores, as restricted by the fabrication technology for high aspect ratio pores. Consequently, the membrane can become very fragile, as reported by Song (2011). One solution concept is to find a material that has a good strength and ductility even with the very thin structure. The notable material and technology is under the name of Shirasu Porous Glass (SPG) Membrane (SPG Technology Company, Japan). The fabrication of the SPG membrane takes advantages of a characteristic called "phase separation" of the glass, which is the volcanic ash in Japan. Heating of such a glass can form $CaO \cdot B_2O_3$ particles within the glass in a very narrow size distribution. As $CaO \cdot B_2O_3$ is easy to be dissolved in acid, these particles are removed from the glass by acid solutions. Tortuous voids are thus left with the similar narrow size distribution as the $CaO \cdot B_2O_3$ particles（Nakashima *et al.* 1987）. The pore size of a SPG membrane can be in the range of $(0.1 - 20\ \mu m)$. There are two shortcomings with the SPG membrane: (1) easily contaminated by the dispersed fluid because of its tortuous pore structure

and (2) very expensive compared with the silicon membrane which is widely used in micro-systems.

In this dissertation study, the solution concept with a multi-layer architecture was explored for emulsification membrane. The remaining part of this chapter is given as follows. Section 6.2 presents the design and fabrication of a multi-layer membrane. Section 6.3 discusses the experimental result for the new membrane. Finally, Section 6.4 concludes this chapter.

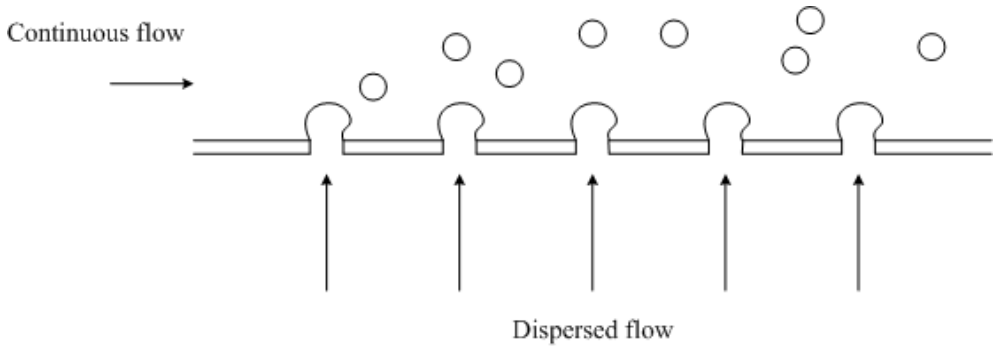

Figure 6.1. A side view of the membrane emulsification device.

6.2 Methods and materials

6.2.1 Design concept

There are two function requirements or constraints: producing microspheres and subjecting to a pressure load which is about 120 kPa according to Song (2011). Design concepts that may fulfill the two constraints are a multi-layer architecture of membrane (see Figure 6.2a). In Figure 6.2a, a membrane has two layers with the upper layer having a 20 μm length of square pore with 20 μm in depth and with the bottom layer having a 1 μm length of square pore with 1 μm in depth. Figure 6.2b shows the cross-section view of the membrane and the dimensions of the pores. It may be clear that the upper layer is to fulfill the constraint of subjecting to a pressure load and the bottom layer is to fulfill the constraint of producing microspheres. The membrane as designed should also have a good manufacturability in terms of the aspect ratio: the upper layer being 20:20 and the bottom layer 1:1. The membrane with this structure (Figure 6.2) can be fabricated with a photolithography technique.

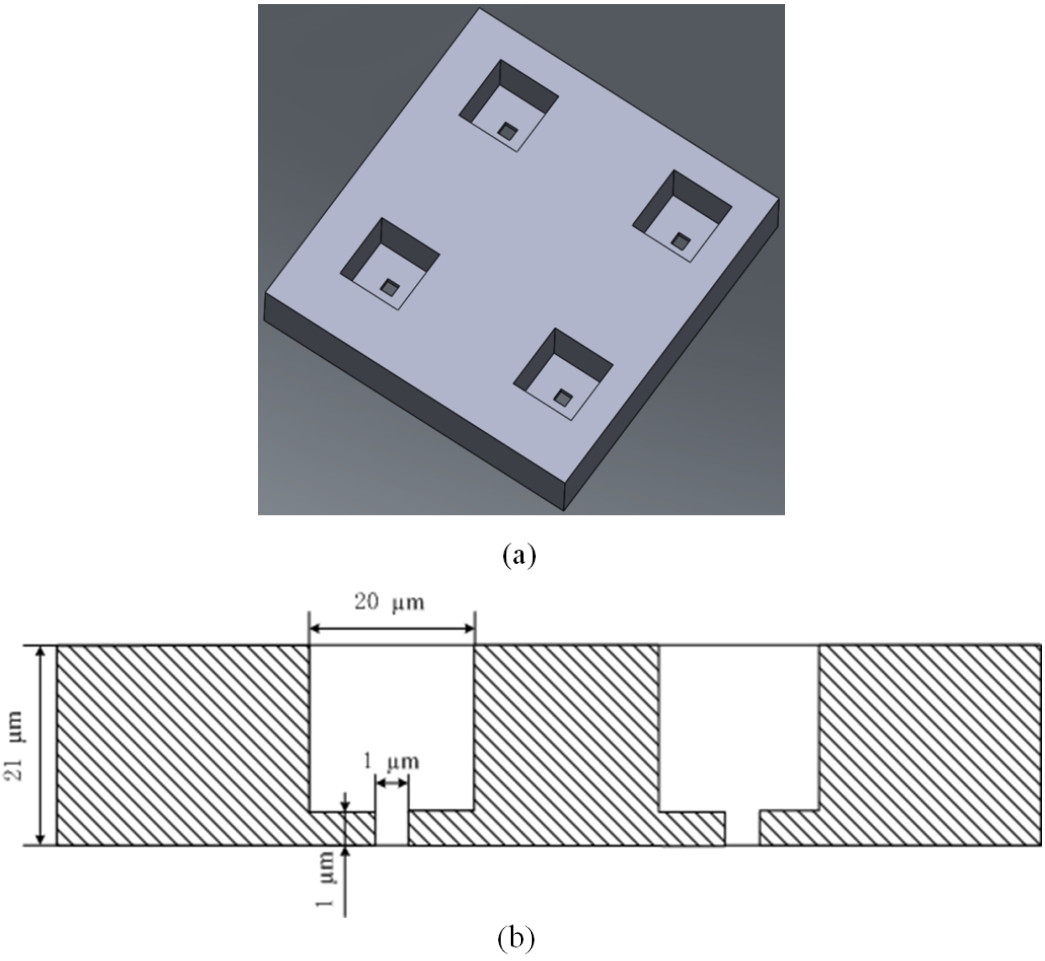

Figure 6.2. (a) Multi-layer structure of the pores on the new membrane emulsification device, and (b) a cross section view of the device (not to scale).

6.2.2 Fabrication

In this study, SU-8 2000 series were used as the photoresist. SU-8 2000 series were improved formulations of SU-8, which were suitable for the thick film (from 0.5 to > 200 μm) and high aspect ratio (> 10∶1) structures（Aktary *et al.* 2003, Bogdanov and Peredkov 2000, Daunton *et al.* 2012, Fan *et al.* 2014, Pierce *et al.* 2014, Vernekar *et al.* 2009）. Details of the fabrication process are given as follows:

(a) Chrome sputtering

Glass substrate with the thickness of 100 μm was sputtered with a layer of chrome with the thickness of

120 nm. The chrome layer was used to help the observation of the pores and the alignment marks because the glass substrate and SU-8 layer were transparent.

(b) SU-8 spin coating (1 μm)

SU-8 2001 was dynamically dispensed on the chrome, 1500 revolutions per minute (rpm) for 3 seconds (s), and then 4000 rpm for 30 s. The membrane was then soft-baked on CEE hotplate (Brewer Science Incorporated, USA) at 95 ℃ for 1 minute.

(c) Mark alignment

Two alignment crosses were used as a marker to help the alignment of two layers of SU-8, as shown in Figure 6.3.

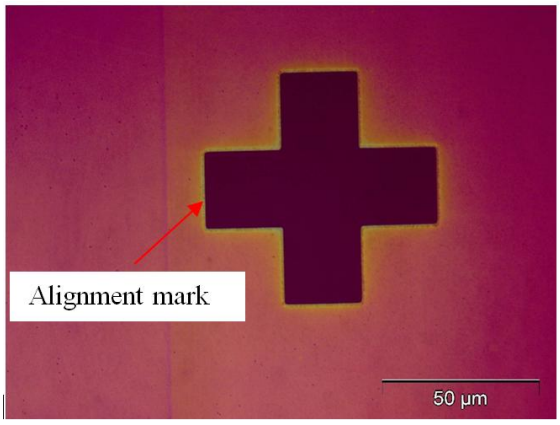

Figure 6.3. An optical image of one alignment cross on the first layer.

(d) Exposure

The membrane was exposed under laser light with 100 mW of laser power and 355 nm of wave length.

(e) Post exposure bake (PEB)

The membrane was baked on the CEE hotplate at 95 ℃ for 1 min.

(f) Development

The membrane was put into Propylene Glycol Methyl Ether Acetate (PGMEA) bath for 1 min, and then

it was rinsed off by Isopropyl alcohol (IPA) for 30 s. At last, the membrane was dried by nitrogen (N_2). Opaque region was removed. Pores with length of $1 \times 1\ \mu m^2$ were obtained, as shown in Figure 6.4.

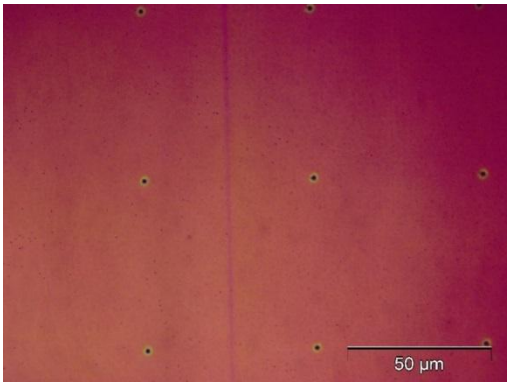

Figure 6.4. An optical image of the pores with $1 \times 1\ \mu m^2$.

(g) Oxygen descum plasma cleaning for 5 min

(h) Chrome Etching

Chrome out of the pores region was etched off by Cr-etch (MicroChemicals GmbH, Germany) by bathing for 45 s, and then rinsed with distilled (DI) water. The membranes before and after chrome etching were shown in Figure 6.5.

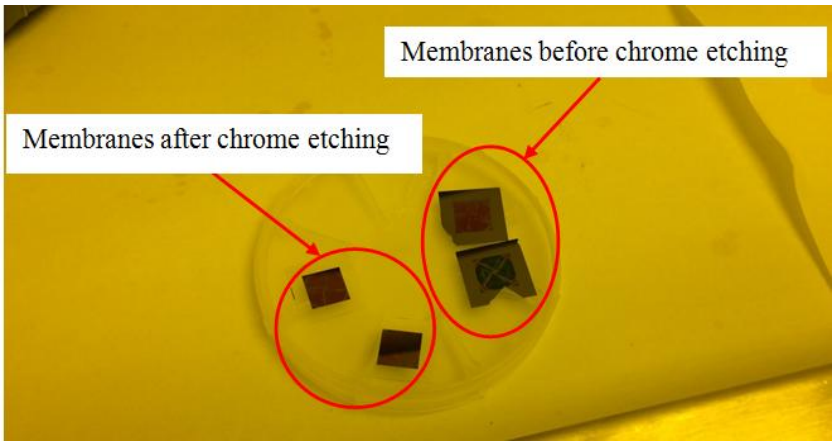

Figure 6.5. Membranes before and after chrome etching.

(i) SU-8 spin coating (20 μm)

SU-8 2025 was dynamically dispensed on the membrane at 500 rpm for 1 s. Then, the spin speed was manually accelerated to 4000 rpm in 10 s, and kept for 30 s. The membrane was then soft baked on CEE hotplate at 65 ℃ for 1 min. Then the temperature was ramped to 95 ℃, and kept for 5 min.

(j) Mark alignment

Two alignment crosses were used as a mark to help the alignment of two layers of SU-8. As shown in Figure 6.6, the alignment mark of the first layer has been covered by the alignment mark of the second layer perfectly.

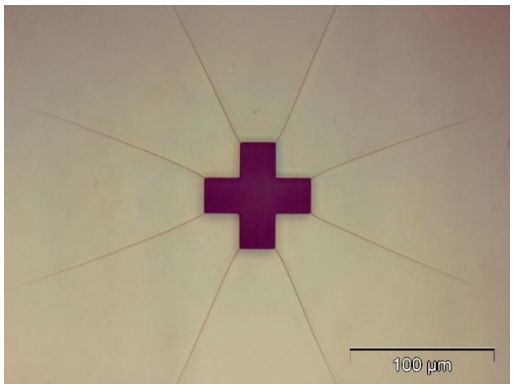

Figure 6.6. An optical image of one alignment cross on the second layer.

(k) Exposure

The membrane was exposed under laser light with 100 mW laser power, 355 nm wave length.

(l) Post exposure bake (PEB)

The membrane was baked on the Torrey hotplate (Torrey Pines Scientific Incorporated, USA) at 65 ℃ for 1 min. Then the temperature was ramped to 95 ℃ and kept for 5 min at 95 ℃.

(m) Development

The membrane had a PGMEA bath for 4 min, and then rinsed with IPA for 30 s. At last, the membrane was dried by N_2. Opaque region was removed. Pores with $20 \times 20\ \mu m^2$ were obtained. The optical images of the top view and bottom view of the pores with $20 \times 20\ \mu m^2$ were presented in Figure 6.7.

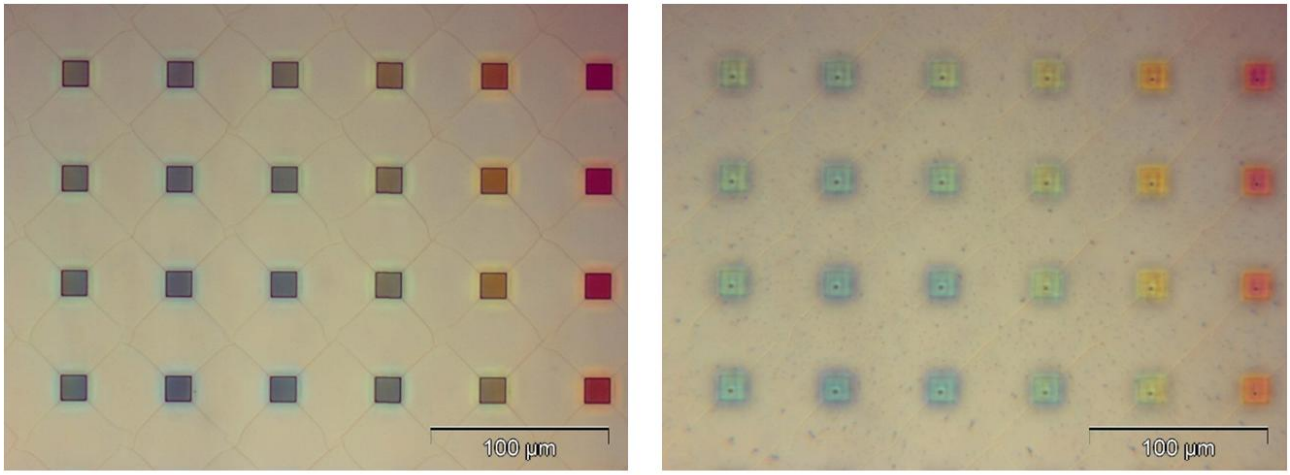

(a) (b)

Figure 6.7. Optical images of (a) the top view and (b) bottom view of the pores with 20×20 µm^2.

(n) Glued to an acrylonitrile butadiene styrene (ABS) tube

Epoxy 907 AB glues (Miller-Stephenson Chemical Incorporate, USA) were mixed for 3 min, and then left to sit for 30 min. Next, the mixed glue was put around the edge of ABS tubing and then the tubing was placed on the top of sample, as shown in Figure 6.8. Twelve hours was needed to wait for the best adhesive property.

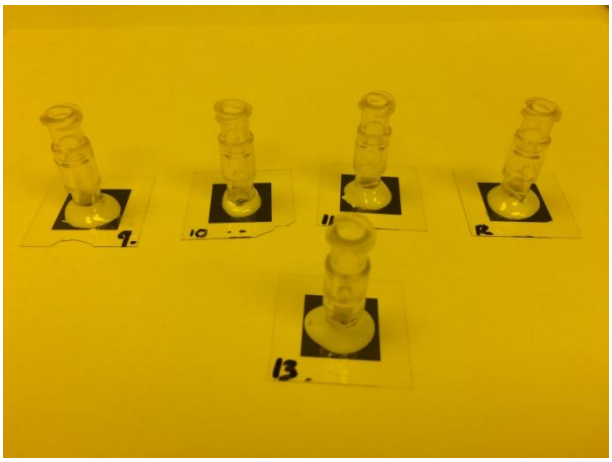

Figure 6.8. The membranes were glued to ABS tubes.

(o) Substrate and chrome removing

On the first day, the membrane was immersed in 5% hydrofluoric (HF) acid for 8 h. On the second day, the membrane was etched by 5% HF acid for another 5 h to fully remove the glass substrate. Then the chrome layer was etched off by taking a Cr-etch bath for 3 to 4 min, and then rinsed with distilled (DI) water and dried by N_2. Three pieces of membranes were obtained for the microsphere generation, as shown in Figure 6.9a. An optical image of one piece of membrane is shown in Figure 6.9b. The diameter of the membrane emulsification device was 0.5 cm.

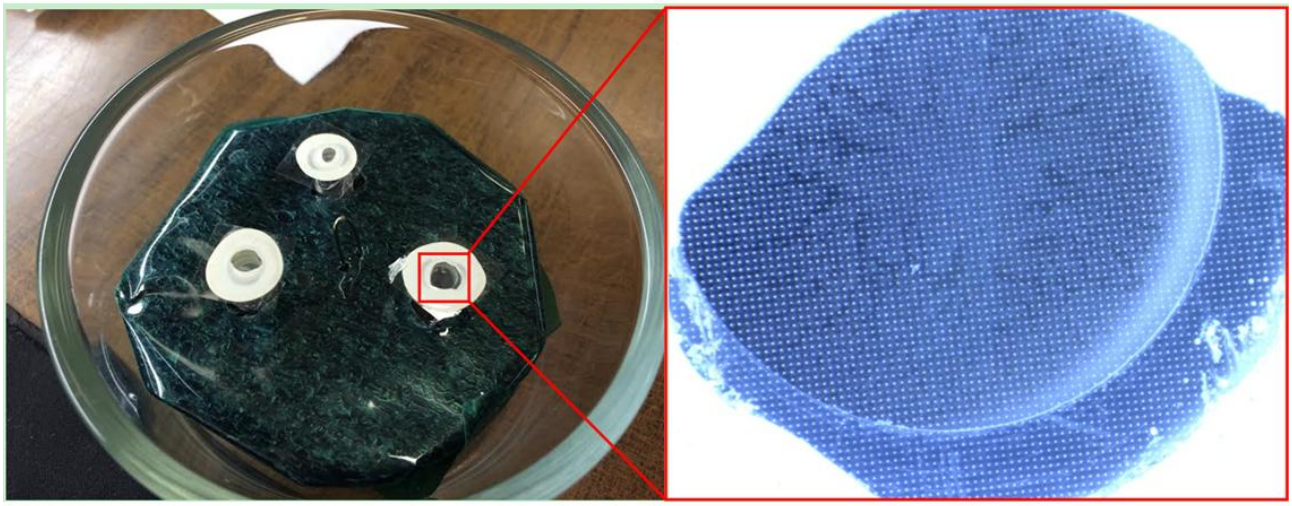

Figure 6.9. (a) Three membranes for the microsphere generation, (b) an optical image of the porous membrane.

To sum up, the fabrication process of the porous membrane is shown in Figure 6.10.

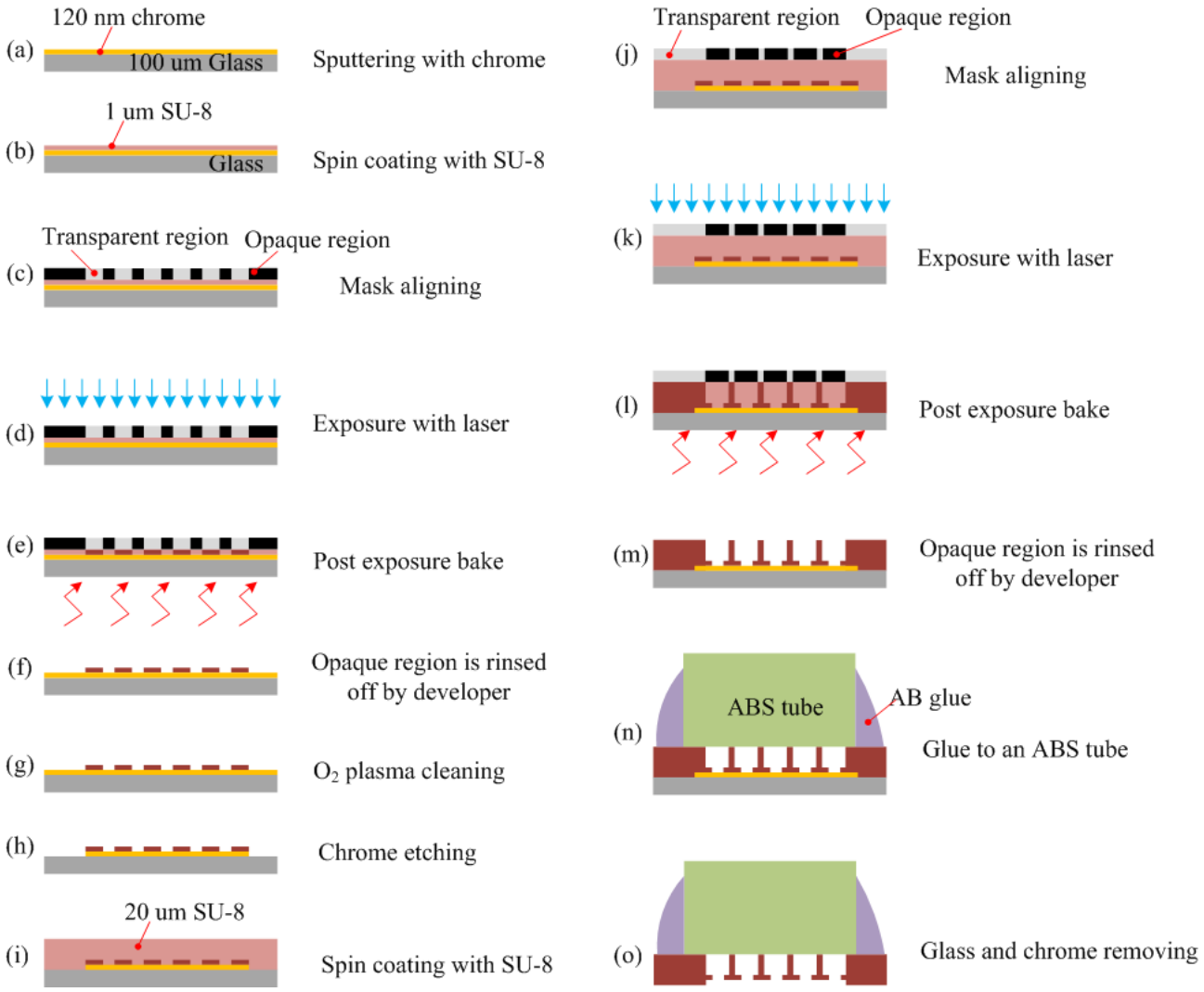

Figure 6.10. Schematic illustration of the fabrication procedure of the membrane with multilayer structure (not drawn to scale).

6.2.3 Materials and preparation

The continuous phase was the paraffin oil (Sigma-Aldrich Corporation, USA) with 2% Span 80 surfactant (Sigma-Aldrich Corporation, USA). The dispersed phase was distilled (DI) water. The membranes were made of SU-8 2000 series. Research described in this chapter was performed in part at the Synchrotron Laboratory for Micro and Nano Devices (SyLMAND) at the Canadian Light Source (CLS). The CLS is supported by the Canada Foundation for Innovation, Natural Sciences and Engineering Research Council of Canada, the University of Saskatchewan, the Government of Saskatchewan, Western Economic Diversification Canada, the National Research Council Canada, and

the Canadian Institutes of Health Research.

6.2.4 Experimental set-up

Figure 6.11 shows the experimental set-up. A magnetic stirrer (Corning PC 210, Corning Incorporated, USA) was used to provided the shear force. A syringe pump (Harvard Apparatus, USA) controlling the flow rate of the dispersed phase was connected to the ABS tube by a syringe (6 ml, Covidien Limited, Ireland) and tubing (1.34 mm PTFE, Adtech Polymer Engineering Limited, United Kingdom). The syringe pump was calibrated before the experiments. The inverted microscope (Olympus IX70, Olympus Corporation, Japan) was used to observe the microsphere generation process, and a computer with image processing software was used for post-processing. A single microsphere was measured multiple times (> 5 times) and their average value was taken. The experiments were performed at the Intelligent Systems Laboratory in the University of Saskatchewan in room temperature (20℃ ± 2℃).

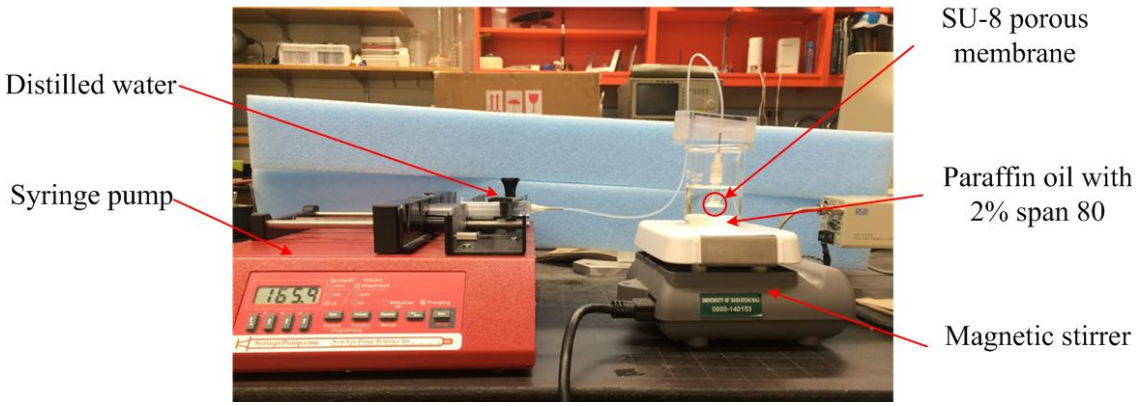

Figure 6.11. Experimental set-up for the membrane emulsification process.

The minimum pressure that ensures the dispersed phase can be pressed through the porous membrane is given by $P_m = \frac{4\gamma \cos\theta}{d_p}$, where γ is the interfacial tension between the continuous and dispersed phase; θ is the contact angle between the dispersed phase and the membrane surface in the continuous phase; d_p is the pore diameter（Vladisavljevic and Williams 2006）. In this work, $\gamma = 3.65 \times 10^{-3}\ \mathrm{N \cdot m^{-1}}$ and the contact angle θ between the dispersed phase and the membrane surface in the continuous phase was assumed to be zero. Therefore, the minimum pressure $P_m = \frac{4\times3.65\times10^{-3}}{1\times10^{-6}} = 1.46\ \mathrm{kPa}$ and the

corresponding flow rate of the dispersed phase is about $5\ \mu l \cdot h^{-1}$. In this work, the flow rate of dispersed phase was set to be ten times larger than the minimum flow rate, namely $50\ \mu l \cdot h^{-1}$. The agitation speeds of the magnetic stirrer were 60, 80, and 100 rpm. The amount of 1 ml continuous fluid with microspheres generated was carefully extracted from the beaker to a clean glass petri dish for observation. The commercial image processing software (ImageJ, National Institutes of Health, USA) with its corresponding data analysis software (especially for the image measurement) was used to measure the size of microspheres using the images. It is noted that although the CCD camera with the microscopy used in the experiment has a resolution of 1 μm, but the image measurement software allows for the measurement resolution down to 0.01 μm through an interpolation technique.

6.3 Results with discussion

In Figure 6.12, it can be seen that there were lots of white dots in the continuous phase, which are microspheres generated and suspended in the continuous phase. Figure 6.13a, b, and c were the optical images of microspheres generated by the SU-8 membrane under the agitation speeds of 60, 80, and 100 rpm, respectively. Figure 6.14 presents the average diameters of microspheres along with the standard deviations for the different agitation speeds. It can be seen from Figure 6.14 that the diameters of the microspheres were 11.0 ± 3.5 μm, 7.4 ± 3.3 μm, and 2.3 ± 0.8 μm at agitation speeds of 60 rpm, 80 rpm, and 100 rpm, respectively. Thus, it can be concluded that the higher agitation speed, the smaller the diameter of microspheres. This phenomenon can be explained by the fact that the higher shear stress produced with the higher agitation speed.

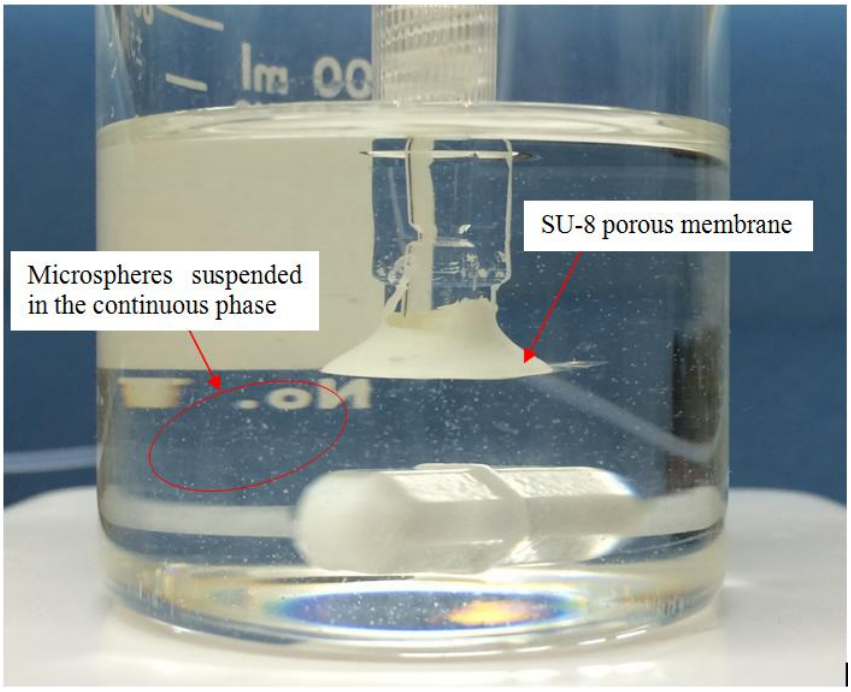

Figure 6.12. White dots were microspheres generated using the SU-8 membrane. Agitation speed: 100 rpm.

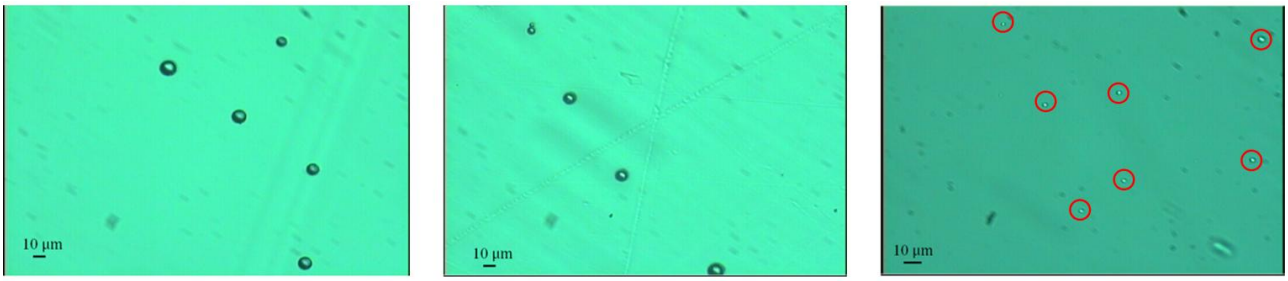

Figure 6.13. Optical images of microspheres generated by the SU-8 membrane regarding agitation speeds of 60 rpm (a), 80 rpm (b), and 100 rpm (c).

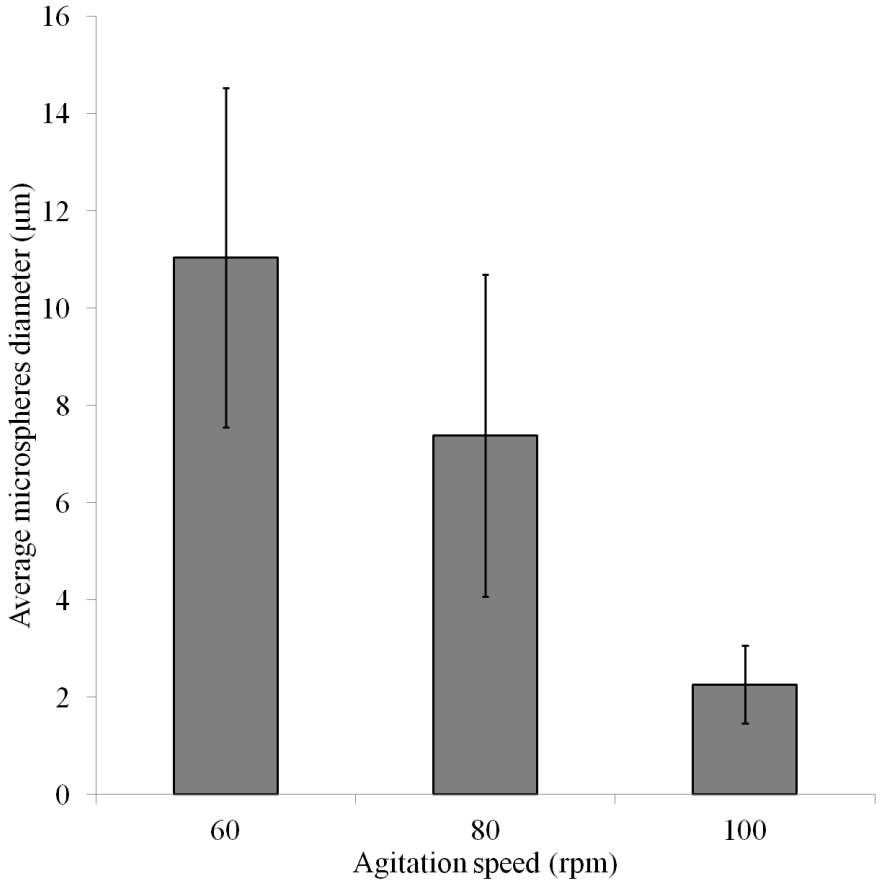

Figure 6.14. Average microsphere diameters with standard deviation for different agitation speeds.

To test the strength of the designed SU-8 porous membrane in this study, the flow rate of the dispersed phase was increased gradually from 50 $\mu l \cdot h^{-1}$ by a step of 100 $\mu l \cdot h^{-1}$. The first membrane failure happened when the flow rate of the dispersed phase was 4500 $\mu l \cdot h^{-1}$ and agitation speed was 100 rpm, as shown in Figure 6.15 (white arrow). It is noted that this flow rate was found comparative to other membranes in the literature by others. For example, Dragosavac et al. (2012) produced microspheres using a nickel membrane with the flow rate of the dispersed flow of 3000 $\mu l \cdot h^{-1}$; the minimum diameter of microspheres was 100 µm. Van der Graaf et al. (2004) produced microspheres using a silicon membrane with the flow rate of the dispersed flow of 1.23 $\mu l \cdot h^{-1}$; the minimum diameter of microspheres was 35 µm. Piacentini et al. (2013) produced microspheres using a nickel membrane with the flow rate of the dispersed flow of 6000 $\mu l \cdot h^{-1}$; the minimum diameter of microspheres was 40 µm. Vladisavljevic and Williams (2006) produced microspheres using a stainless steel membrane with the flow rate of the dispersed flow of 1.2×10^7 $\mu l \cdot h^{-1}$; the minimum diameter of microspheres was

100 μm. Song (2011) produced microspheres using a silicon membrane with the flow rate of the dispersed flow of 1.4×10^6 μl · h^{-1}; the minimum diameter of microspheres was 1.6 μm.

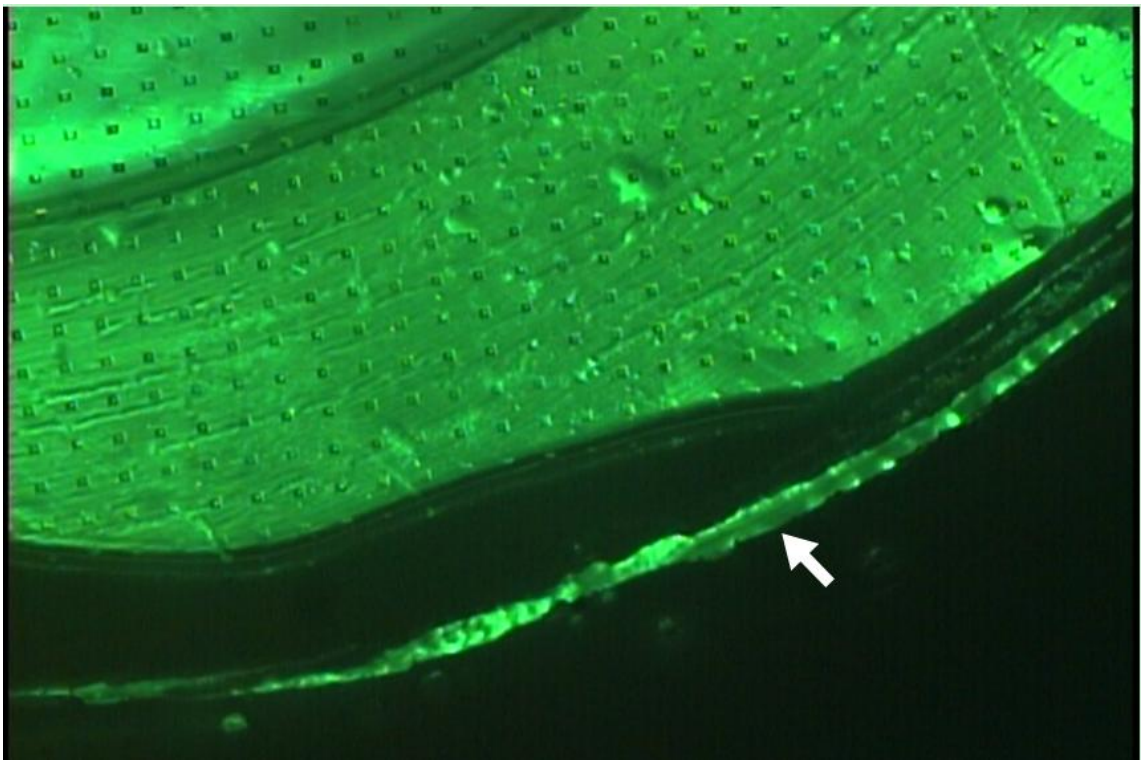

Figure 6.15. An optical image of the failure of the SU-8 membrane.

Thus, compared with the other membranes in the literature as mentioned above, the small diameter of microspheres with a good size uniformity (i.e., 2.3 ± 0.8 μm) was achieved (the flow rate of dispersed flow is 50 μl · h^{-1}, and the agitation speed is 100 rpm) by the developed SU-8 membrane. It is noted that the flow rate of dispersed flow in this experiment can certainly be increased, as the maximal flow rate of the dispersed flow for the developed SU-8 membrane is 4500 μl · h^{-1} under the agitation speed of 100 rpm (notice: the breakage of the membrane is due to the pressure on the membrane, which is further a function of the flow rate of dispersed flow and agitation speed). With the far lower flow rate of dispersed flow and agitation speed of 100 rpm, the agitation speed can definitely be increased, which implies a further improved performance of the microspheres generation process with the SU-8 membrane in terms of the small size and high uniformity of microspheres.

In summary, the membrane proposed in this study was able to generate microspheres with small size and a good uniformity under a relatively low flow rate of dispersed flow and agitation speed. This achievement is due to the multi-layer architecture of membranes with small pores (1 μm in diameter; 20 μm in thickness with 20 μm pores and 1 μm in thickness with 1 μm pores).

6.4 Conclusions

This chapter presented a study on the design, fabrication and testing of a new emulsification membrane. The novelty of this membrane is the multi-layer structure which ensures that the dimension of the pores is small while the strength of the membrane is high. The membrane was made of the SU-8 photoresist and fabricated by the photolithography technique. The result has shown that the new membrane is very promising in terms of the size of microspheres as well as the size uniformity (particularly, the diameter and the uniformity of microspheres were: 11.0 ± 3.5 μm, 7.4 ± 3.3 μm, and 2.3 ± 0.8 μm, under the agitation speeds of 60, 80, and 100 rpm, respectively). The developed membrane is also cost effective because the material of SU-8 photoresist is inexpensive and easy to manufacture with conventional micro-fabrication technique. To the best of my knowledge, it is the first time to use SU-8 photoresist to make the membrane for microsphere generation.

CHAPTER 7. CONCLUSIONS AND FUTURE WORK

7.1 Overview and conclusions

The motivation for this dissertation was the promising perspective of micro-fluidic devices technology for generating microspheres or droplets. The promise lies in the small size (close to 1 μm), the uniformity, the device flexibility (one device can produce a large range of sizes of microspheres), and the mass production. Specifically, opportunities to further advance the technology for two devices, namely the modified T-junction device and emulsification membrane, were observed by the author, and they practically led to this research.

Three specific research objectives were proposed for this dissertation, and they are re-visited herein.

Objective 1: Build both a computational model and experimental test-bed to examine the flow pattern of the microsphere generation process with the modified T-junction device to characterize the flow pattern and find the mechanism of the microsphere generation process with the modified T-junction device.

Objective 2: Investigate the methodology for optimizing the performance in terms of the size and uniformity of microspheres generated with any micro-fluidic device and then demonstrate its effectiveness on the modified T-junction device.

Objective 3: To explore the structure of the membrane emulsification device that can be made by the current micro-fabrication technology such that the performance of the device for microsphere generation can be improved in terms of the size and uniformity of microspheres.

A literature review of the state of the art of the microsphere generation process by the fluid-fluid interaction technology was conducted, which confirms the need and urgency of the above-mentioned objectives in Chapter 2. In Chapter 3, an accurate computational model along with the simulator based on the CFD and LS method was developed. In Chapter 4, with this simulator and the physical test-bed,

three flow patterns or regimes associated with the microsphere were observed, and the mechanisms behind them were discussed. In Chapter 5, a new methodology for optimization of the performance of micro-fluidic systems in general was proposed and the application of this methodology to the modified T-junction device was discussed. The effectiveness of the new methodology was demonstrated in Chapter 5 as well. In Chapter 6, a new design concept called the multi-layer architecture of membrane was presented, and the new design concept was applied to the emulsification membrane for microsphere generation. Several conclusions can be drawn from the study:

With respect to Objective 1, a CFD model for the microsphere generation process with the modified T-junction device was developed and validated. Using this model, three regimes were found in the modified T-junction device, which are: detached regime, microsphere regime, and continuous regime. In comparison with the regimes found in the conventional T-junction device, the jetting regime there corresponds to the microsphere regime here, the continuous regime there corresponds to the continuous regime here, and the squeezing regime there corresponds to the detached regime here. The dripping regime there was absent in the modified T-junction, and this absence is speculated to be related to the presence of the sheath flow in the modified T-junction device. In the range of the velocity of the sheath flow, the velocity of the middle flow was found to play a critical role in the determination of the regimes. Further, it can be concluded that the diameter of microspheres can be controlled by the capillary number of the cross flow and the ratio of middle flow velocity to the sheath flow velocity $R_{m/s}$.

With respect to Objective 2, the proposed methodology for optimizing the microsphere generation process is effective for the modified T-junction device; particularly, the microsphere with its diameter of 16.1 μm and 24.8 μm and their uniformity (SD) of 0.2 μm, 0.7 μm, respectively, can be achieved with the device with the width of 50 μm. The three-step optimization process can be applied to any micro-fluidic systems for generation of microspheres with the optimal objectives of (1) desired size and (2) high uniformity, as the general methodology has been formulated based on a general categorization of the parameters of the device.

With respect to Objective 3, the novel design concept (i.e., the multi-layer architecture for emulsification membranes) was proposed, fabricated and validated. It can be concluded that (1) the new membrane system is cost-effective yet effective to generate small microspheres with high uniformity. In the current

literature (Santos *et al.* 2015), with the membrane technology, microspheres are usually with (1) the size being about 6 μm and (2) the uniformity being 1.37 μm (SD). Finally, it can be concluded that the multi-layer membrane can be fabricated using the popular material of SU-8 with the conventional lithography technology and image-based alignment technique.

7.2 Contributions

In the field of micro-fluidic techniques to generate microspheres, first, the finding that there are three regimes in the microsphere generation process with the modified T-junction is new, which gives evidence that combination of different operating principles for microsphere generation is promising. Second, the methodology for optimizing the microsphere generation process is new, which provides a tool to synthesize microspheres in terms of the size and uniformity, that is, the possibility to design the process to satisfy the required size and uniformity of microspheres is possible. This is opposed to the current situation that such a synthesis process can only be designed in a trial-and-error manner. Third, the multi-layer emulsification membrane with the smallest pore size being 1 μm is new, and its promise to generate very small size microspheres is a breakthrough result (currently the size is 2.3 μm with the acceptable uniformity with the agitation speed of 100 rpm).

In the field of micro-fabrication, the fabrication procedure for the multi-layer membrane on the material of SU-8 with the smallest pore size being 1 μm is new. This is opposed to the current micro-fabrication technology for making membrane with an expensive material and process called SPG technology. Besides the quality improvement with the SU-8 multi-layer membrane, it is believed that the cost of making SU-8 membranes with the multi-layer architecture is about 10% of the cost of making the SPG membrane.

7.3 Limitations and future work

The work presented in this dissertation has some limitations. First, the flow ratio of the middle flow to the sheath flow $R_{m/s}$ was excluded while performing the optimization of the modified T-junction. As presented in Chapter 4, $R_{m/s}$ was one of the factors that influence the diameter of microspheres. It is worth including this factor in optimization. Second, the three regimes were discussed in a specific range

of the flow rate of sheath flow, and a more comprehensive study on the three regimes is warranted. Third, the 2D model of the modified T-junction was used to study the regimes in the device and optimize the microsphere generation process. The 3D model is worth exploring in the future. Fourth, the cost has not been included in the discussion, which is a shortcoming for practical applications. The cost of micro-fluidic systems is mostly reflected by the channel size, and it is known that the smaller the channel size, the higher the cost in manufacturing. Fifth, the loading efficiency of drug was an important performance attribute for the microspheres process in applications (e.g., drug delivery). However, this thesis study only considered the size, uniformity, flexibility and efficacy of the microspheres. Thus, a future work is worthwhile on this attribute.

Besides the further study on overcoming the aforementioned shortcomings, there are several new works that may advance the micro-fluidic device technology for microsphere generation further. The first is to study the critical channel size in terms of whether a sphere can be generated. The author's hypothesis is that the notion of the critical channel size makes sense, as the capillary effect plays an important role in generating microspheres. The second is to study the combination of the principles of emulsification membrane and sheath flow for a new device. The author's hypothesis is that such a device will bring together the benefits of small size of microspheres (membrane approach), device flexibility (sheath flow approach), and efficacy of microsphere generation (membrane approach).

REFERENCES

Akamatsu K., Kaneko D., Sugawara T., Kikuchi R., and Nakao S.-i., "Three Preparation Methods for Monodispersed Chitosan Microspheres Using the Shirasu Porous Glass Membrane Emulsification Technique and Mechanisms of Microsphere Formation," *Industrial and Engineering Chemistry Research,* vol. 49, pp. 3236-3241, 2010.

Akbari S. and Pirbodaghi T., "Microfluidic encapsulation of cells in alginate particles via an improved internal gelation approach," *Microfluidics and Nanofluidics,* vol. 16, pp. 773-777, 2014.

Aktary M., Jensen M. O., Westra K. L., Brett M. J., and Freeman M. R., "High-resolution pattern generation using the epoxy novolak SU-8 2000 resist by electron beam lithography," *Journal of Vacuum Science and Technology B,* vol. 21, pp. L5-L7, 2003.

Amaya bower L. and Lee T., "Lattice Boltzmann simulations of bubble formation in a microfluidic T-junction," *Philosophical Transactions of the Royal Society A: Mathematical, Physical and Engineering Sciences,* vol. 369, pp. 2405-2413, 2011.

Andersen A. S., Zheng W. F., Sutherland D. S., and Jiang X. Y., "Versatile multiple protein nanopatterning within a microfluidic channel for cell recruitment studies," *Lab on a Chip,* vol. 15, pp. 4524-4532, 2015.

Anna S. L., Bontoux N., and Stone H. A., "Formation of dispersions using “flow focusing” in microchannels," *Applied Physics Letters,* vol. 82, pp. 364-366, 2003.

Anna S. L. and Mayer H. C., "Microscale tipstreaming in a microfluidic flow focusing device," *Physics of Fluids,* vol. 18, p. 121512, 2006.

Arias S., Legendre D., and Gonzalez-Cinca R., "Numerical simulation of bubble generation in a T-junction," *Computers and Fluids,* vol. 56, pp. 49-60, 2012.

Aryanti N., Williams R. A., Hou R. Z., and Vladisavljevic G. T., "Performance of rotating membrane emulsification for o/w production," *Desalination,* vol. 200, pp. 572-574, 2006.

Balabel A., "Numerical simulation of two-dimensional binary droplets collision outcomes using the level set method," *International Journal of Computational Fluid Dynamics,* vol. 26, pp. 1-21, 2012.

Bao J., Yuan P., and Schaefer L., "A mass conserving boundary condition for the lattice Boltzmann equation method," *Journal of Computational Physics,* vol. 227, pp. 8472-8487, 2008.

Bashir S., Rees J. M., and Zimmerman W. B., "Simulations of microfluidic droplet formation using the

two-phase level set method," *Chemical Engineering Science,* vol. 66, pp. 4733-4741, 2011.

Bi Z. M., Zhang W. J., and Lang S. Y. T., "Modular robot system architecture," in *Control, Automation, Robotics and Vision, 2002. ICARCV 2002. 7th International Conference on*, 2002, pp. 1054-1059 vol.2.

Bogdanov A. and Peredkov S., "Use of SU-8 photoresist for very high aspect ratio x-ray lithography," *Microelectronic Engineering,* vol. 53, pp. 493-496, 2000.

Bragg L. and Nye J. F., "A Dynamical Model of a Crystal Structure," *Proceedings of the Royal Society of London A: Mathematical, Physical and Engineering Sciences,* vol. 190, pp. 474-481, 1947.

Butt H.-J., Graf K., and Kappl M., *Physics and Chemistry of Interfaces*: John Wiley & Sons, 2006.

Castro-Hernández E., Gundabala V., Fernández-Nieves A., and Gordillo J. M., "Scaling the drop size in coflow experiments," *New Journal of Physics,* vol. 11, p. 075021, 2009.

Chao J., Mei R., Singh R., and Shyy W., "A filter ‐ based, mass ‐ conserving lattice Boltzmann method for immiscible multiphase flows," *International Journal for Numerical Methods in Fluids,* vol. 66, pp. 622-647, 2011.

Chen N. C., Wu J. Z., Jiang H. M., and Dong L. C., "CFD Simulation of Droplet Formation in a Wide-Type Microfluidic T-Junction," *Journal of Dispersion Science and Technology,* vol. 33, pp. 1635-1641, 2012.

Chen W. Y., Kim J. H., Zhang D., Lee K. H., Cangelosi G. A., Soelberg S. D., Furlong C. E., Chung J. H., and Shen A. Q., "Microfluidic one-step synthesis of alginate microspheres immobilized with antibodies," *Journal of the Royal Society Interface,* vol. 10, 2013.

Chen X., Zhang W., Schoenau G., and Surgenor B., "Off-line control of time-pressure dispensing processes for electronics packaging," *Electronics Packaging Manufacturing, IEEE Transactions on,* vol. 26, pp. 286-293, 2003.

Chen X. D., Xue C. D., Zhang L., Hu G. Q., Jiang X. Y., and Sun J. S., "Inertial migration of deformable droplets in a microchannel," *Physics of Fluids,* vol. 26, 2014.

Chiu H. C. and Chen J. M., "Enhancement of Fluid Mixing in a Double T-shaped Micromixer by Periodic Disturbances of Pressure," in *Advanced Manufacturing Systems*. vol. 339, Z. J. Ai, X. D. Zhang, Y. H. Kim, and P. Yarlagadda, Eds., ed, 2011, pp. 118-123.

Chu L. Y., Utada A. S., Shah R. K., Kim J. W., and Weitz D. A., "Controllable monodisperse multiple emulsions," *Angewandte Chemie International Edition,* vol. 46, pp. 8970-8974, 2007.

Cohen C., Giles R., Sergeyeva V., Mittal N., Tabeling P., Zerrouki D., Baudry J., Bibette J., and

Bremond N., "Parallelised production of fine and calibrated emulsions by coupling flow-focusing technique and partial wetting phenomenon," *Microfluidics and Nanofluidics,* vol. 17, pp. 959-966, 2014.

Daunton R., Gallant A., and Wood D., "Manipulation of exposure dose parameters to improve production of high aspect ratio structures using SU-8," *Journal of Micromechanics and Microengineering,* vol. 22, p. 075016, 2012.

De Luca G., Di Maio F. P., Di Renzo A., and Drioli E., "Droplet detachment in cross-flow membrane emulsification: comparison among torque-and force-based models," *Chemical Engineering and Processing: Process Intensification,* vol. 47, pp. 1150-1158, 2008.

De Luca G. and Drioli E., "Force balance conditions for droplet formation in cross-flow membrane emulsifications," *Journal of Colloid and Interface Science,* vol. 294, pp. 436-448, 2006.

De Luca G., Sindona A., Giorno L., and Drioli E., "Quantitative analysis of coupling effects in cross-flow membrane emulsification," *Journal of Membrane Science,* vol. 229, pp. 199-209, 2004.

De Menech M., Garstecki P., Jousse F., and Stone H. A., "Transition from squeezing to dripping in a microfluidic T-shaped junction," *Journal of Fluid Mechanics,* vol. 595, pp. 141-161, 2008.

Ding Y., Solvas X. C. I., and Demello A., ""V-junction": a novel structure for high-speed generation of bespoke droplet flows," *Analyst,* vol. 140, pp. 414-421, 2015.

Dragosavac M. M., Holdich R. G., Vladisavljević G. T., and Sovilj M. N., "Stirred cell membrane emulsification for multiple emulsions containing unrefined pumpkin seed oil with uniform droplet size," *Journal of Membrane Science,* vol. 392–393, pp. 122-129, 2012.

Dupin M. M., Halliday I., and Care C. M., "Simulation of a microfluidic flow-focusing device," *Physical Review E,* vol. 73, 2006.

Enright D., Fedkiw R., Ferziger J., and Mitchell I., "A hybrid particle level set method for improved interface capturing," *Journal of Computational Physics,* vol. 183, pp. 83-116, 2002.

Fan B., Kwon K. Y., Weber A. J., and Li W., "An implantable, miniaturized SU-8 optical probe for optogenetics-based deep brain stimulation," in *Engineering in Medicine and Biology Society (EMBC), 2014 36th Annual International Conference of the IEEE,* 2014, pp. 450-453.

Freitas R. K. and Schröder W., "Numerical investigation of the three-dimensional flow in a human lung model," *Journal of Biomechanics,* vol. 41, pp. 2446-2457, 2008.

Frisch U., "Relation between the lattice Boltzmann equation and the Navier-Stokes equations," *Physica D: Nonlinear Phenomena,* vol. 47, pp. 231-232, 1991.

Fu L. M., Lee C. Y., and Lin C. H., "Computational analysis of double-T-type microfluidic mixer using periodic electrokinetic force," in *Micro Total Analysis Systems 2004, Vol 1*, T. Laurell, J. Nilsson, K. Jensen, D. J. Harrison, and J. P. Kutter, Eds., ed, 2005, pp. 231-233.

Fuchigami T., Toki M., and Nakanishi K., "Membrane Emulsification Using Sol-Gel Derived Macroporous Silica Glass," *Journal of Sol-Gel Science and Technology,* vol. 19, pp. 337-341, 2000.

Fujiu K. B., Kobayashi I., Neves M. A., Uemura K., and Nakajima M., "Influence of temperature on production of water-in-oil emulsions by microchannel emulsification," *Colloids and Surfaces A: Physicochemical and Engineering Aspects,* vol. 411, pp. 50-59, 2012.

Gasparini G., Kosvintsev S., Stillwell M. T., and Holdich R., "Preparation and characterization of PLGA particles for subcutaneous controlled drug release by membrane emulsification," *Colloids and Surfaces B: Biointerfaces,* vol. 61, pp. 199-207, 2008.

Geller S., Krafczyk M., Tölke J., Turek S., and Hron J., "Benchmark computations based on lattice-Boltzmann, finite element and finite volume methods for laminar flows," *Computers and Fluids,* vol. 35, pp. 888-897, 2006.

Ghanbar H., Luo C. J., Bakhshi P., Day R., and Edirisinghe M., "Preparation of porous microsphere-scaffolds by electrohydrodynamic forming and thermally induced phase separation," *Materials Science and Engineering: C,* vol. 33, pp. 2488-2498, 2013.

Glawdel T., Elbuken C., and Ren C. L., "Droplet formation in microfluidic T-junction generators operating in the transitional regime. I. Experimental observations," *Physical Review E,* vol. 85, p. 016322, 2012.

Glawdel T. and Ren C. L., "Droplet formation in microfluidic T-junction generators operating in the transitional regime. III. Dynamic surfactant effects," *Physical Review E,* vol. 86, 2012.

Guillot P., Colin A., and Ajdari A., "Stability of a jet in confined pressure-driven biphasic flows at low Reynolds number in various geometries," *Physical Review E,* vol. 78, p. 016307, 2008.

Gunstensen A. K., Rothman D. H., Zaleski S., and Zanetti G., "Lattice Boltzmann model of immiscible fluids," *Physical Review A,* vol. 43, p. 4320, 1991.

Han B., Zhang W., Lu X., and Lin Y., "On-line supply chain scheduling for single-machine and parallel-machine configurations with a single customer: Minimizing the makespan and delivery cost," *European Journal of Operational Research,* vol. 244, pp. 704-714, 2015.

Hancocks R. D., Spyropoulos F., and Norton I. T., "Comparisons between membranes for use in cross

flow membrane emulsification," *Journal of Food Engineering,* vol. 116, pp. 382-389, 2013.

Herranz-Blanco B., Arriaga L. R., Makila E., Correia A., Shrestha N., Mirza S., Weitz D. A., Salonen J., Hirvonen J., and Santos H. A., "Microfluidic assembly of multistage porous silicon-lipid vesicles for controlled drug release," *Lab on a Chip,* vol. 14, pp. 1083-1086, 2014.

Hirt C. W. and Nichols B. D., "Volume of fluid (VOF) method for the dynamics of free boundaries," *Journal of Computational Physics,* vol. 39, pp. 201-225, 1981.

Holdich R. G., Dragosavac M. M., Vladisavljević G. T., and Kosvintsev S. R., "Membrane Emulsification with Oscillating and Stationary Membranes," *Industrial & Engineering Chemistry Research,* vol. 49, pp. 3810-3817, 2010/04/21 2010.

Holdich R. G., Dragosavac M. M., Vladisavljevic G. T., and Piacentini E., "Continuous Membrane Emulsification with Pulsed (Oscillatory) Flow," *Industrial & Engineering Chemistry Research,* vol. 52, pp. 507-515, Jan 2013.

Holgado M., Arias J., Cózar M., Alvarez-Fuentes J., Ganan-Calvo A., and Fernandez-Arevalo M., "Synthesis of lidocaine-loaded PLGA microparticles by flow focusing: effects on drug loading and release properties," *International Journal of Pharmaceutics,* vol. 358, pp. 27-35, 2008.

Hung L.-H., Teh S.-Y., Jester J., and Lee A. P., "PLGA micro/nanosphere synthesis by droplet microfluidic solvent evaporation and extraction approaches," *Lab chip,* vol. 10, pp. 1820-1825, 2010.

Inamuro T., Ogata T., Tajima S., and Konishi N., "A lattice Boltzmann method for incompressible two-phase flows with large density differences," *Journal of Computational Physics,* vol. 198, pp. 628-644, 2004.

J.-O. You S.-B. P., H.-Y. Park, S. Haam, C.-H. Chung, W.-S. Kim, "Preparation of regular sized Ca-alginate microspheres using membrane emulsification method," *Journal of Microencapsulation,* vol. 18, pp. 521-532, 2001.

Jain R. A., "The manufacturing techniques of various drug loaded biodegradable poly(lactide-co-glycolide) (PLGA) devices," *Biomaterials,* vol. 21, pp. 2475-2490, 2000.

Jamil M. and Ng E. Y. K., "Ranking of parameters in bioheat transfer using Taguchi analysis," *International Journal of Thermal Sciences,* vol. 63, pp. 15-21, 2013.

Joscelyne S. M. and Trägårdh G., "Membrane emulsification — a literature review," *Journal of Membrane Science,* vol. 169, pp. 107-117, 2000.

Jung J. and Oh J., "Cell-induced flow-focusing instability in gelatin methacrylate microdroplet

generation," *Biomicrofluidics,* vol. 8, p. 036503, 2014.

Kawakatsu T., Kikuchi Y., and Nakajima M., "Visualization of microfiltration phenomena using microscope video system and silicon microchannels," *Journal of Chemical Engineering of Japan,* vol. 29, pp. 399-401, 1996.

Kim H. and Liou M.-S., "Accurate adaptive level set method and sharpening technique for three dimensional deforming interfaces," *Computers & Fluids,* vol. 44, pp. 111-129, 2011.

Kim L. S., Jeong H. K., Ha M. Y., and Kim K. C., "Numerical simulation of droplet formation in a micro-channel using the lattice Boltzmann method," *Journal of Mechanical Science and Technology,* vol. 22, pp. 770-779, 2008.

Kosvintsev S. R., Gasparini G., Holdich R. G., Cumming I. W., and Stillwell M. T., "Liquid−Liquid Membrane Dispersion in a Stirred Cell with and without Controlled Shear," *Industrial & Engineering Chemistry Research,* vol. 44, pp. 9323-9330, 2005/11/01 2005.

Krause F., Li X. G., and Fritsching U., "Simulation of droplet-formation and -interaction in emulsification processes," *Engineering Applications of Computational Fluid Mechanics,* vol. 5, pp. 406-415, 2011.

Kuzmin A., Januszewski M., Eskin D., Mostowfi F., and Derksen J. J., "Three-dimensional binary-liquid lattice Boltzmann simulation of microchannels with rectangular cross sections," *Chemical Engineering Journal,* vol. 178, pp. 306-316, 2011.

Lai Y. G., Lin C.-L., and Huang J., "Accuracy and efficiency study of lattice Boltzmann method for steady-state flow simulations," *Numerical Heat Transfer: Part B: Fundamentals,* vol. 39, pp. 21-43, 2001.

Lan W., Li S., Wang Y., and Luo G., "CFD Simulation of Droplet Formation in Microchannels by a Modified Level Set Method," *Industrial & Engineering Chemistry Research,* vol. 53, pp. 4913-4921, 2014.

Laouini A., Fessi H., and Charcosset C., "Membrane emulsification: A promising alternative for vitamin E encapsulation within nano-emulsion," *Journal of Membrane Science,* vol. 423–424, pp. 85-96, 2012.

Li X., Li F., Yang J., Kinoshita H., Oishi M., and Oshima M., "Study on the mechanism of droplet formation in T-junction microchannel," *Chemical Engineering Science,* vol. 69, pp. 340-351, 2012.

Li X. and Wang S., "Flow field and pressure loss analysis of junction and its structure optimization of

aircraft hydraulic pipe system," *Chinese Journal of Aeronautics,* vol. 26, pp. 1080-1092, 2013.

Li Y. H., Reddy R. K., Kumar C., and Nandakumar K., "Computational investigations of the mixing performance inside liquid slugs generated by a microfluidic T-junction," *Biomicrofluidics,* vol. 8, p. 054125, 2014.

Lin H.-H., Chang S.-C., and Su Y.-C., "On-demand double emulsification utilizing pneumatically actuated, selectively surface-modified PDMS micro-devices," *Microfluidics and Nanofluidics,* vol. 9, pp. 1091-1102, 2010.

Liu C., Tanaka H., Ma J., Zhang L., Zhang J., Huang X., and Matsuzawa Y., "Effect of microbubble and its generation process on mixed liquor properties of activated sludge using Shirasu porous glass (SPG) membrane system," *Water research,* vol. 46, pp. 6051-6058, 2012.

Liu C., Tanaka H., Zhang L., Zhang J., Huang X., Ma J., and Matsuzawa Y., "Fouling and structural changes of Shirasu porous glass (SPG) membrane used in aerobic wastewater treatment process for microbubble aeration," *Journal of Membrane Science,* vol. 421, pp. 225-231, 2012.

Liu H. and Zhang Y., "Droplet formation in a T-shaped microfluidic junction," *Journal of Applied Physics,* vol. 106, p. 034906, 2009.

Liu H. and Zhang Y., "Lattice Boltzmann simulation of droplet generation in a microfluidic cross-junction," *Communications in Computational Physics,* vol. 9, pp. 1235-1256, 2011.

Lloyd D. M., Norton I. T., and Spyropoulos F., "Processing effects during rotating membrane emulsification," *Journal of Membrane Science,* vol. 466, pp. 8-17, 2014.

Lü J.-M., Wang X., Marin-Muller C., Wang H., Lin P. H., Yao Q., and Chen C., "Current advances in research and clinical applications of PLGA-based nanotechnology," *Expert review of molecular diagnostics,* vol. 9, pp. 325-341, 2009.

Maan A. A., Nazir A., Khan M. K. I., Boom R., and Schroën K., "Microfluidic emulsification in food processing," *Journal of Food Engineering,* vol. 147, pp. 1-7, 2015.

Manga M. S., Cayre O. J., Williams R. A., Biggs S., and York D. W., "Production of solid-stabilised emulsions through rotational membrane emulsification: influence of particle adsorption kinetics," *Soft Matter,* vol. 8, pp. 1532-1538, 2012.

Mbanjwa M. B., Land K., Jewell L. L., and Gledhill I. M., "Experimental and numerical studies of emulsion formation in a microfluidic T-junction," presented at the AfriCOMP11: Second African Conference on Computational Mechanics, University of Cape Town, Cape Town, 2011.

Meyer R. F., Rogers W. B., McClendon M. T., and Crocker J. C., "Producing monodisperse drug-loaded

polymer microspheres via cross-flow membrane emulsification: The effects of polymers and surfactants," *Langmuir,* vol. 26, pp. 14479-14487, 2010.

Moon S.-K., Cheong I. W., and Choi S.-W., "Effect of flow rates of the continuous phase on droplet size in dripping and jetting regimes in a simple fluidic device for coaxial flow," *Colloids and Surfaces A: Physicochemical and Engineering Aspects,* vol. 454, pp. 84-88, 2014.

Mulligan M. and Rothstein J., "Scale-up and control of droplet production in coupled microfluidic flow-focusing geometries," *Microfluidics and Nanofluidics,* vol. 13, pp. 65-73, 2012.

Nakashima T. and Shimizu M., "Porous glass from calcium alumino boro-silicate glass," *Ceramics,* vol. 21, p. 408, 1986.

Nakashima T., Shimizu M., and Kawano M., "Articles of porous glass and process for preparing the same," 1987.

Nie H. and Wang C.-H., "Fabrication and characterization of PLGA/HAp composite scaffolds for delivery of BMP-2 plasmid DNA," *Journal of Controlled Release,* vol. 120, pp. 111-121, 2007.

Nie Z., Xu S., Seo M., Lewis P. C., and Kumacheva E., "Polymer particles with various shapes and morphologies produced in continuous microfluidic reactors," *Journal of the American Chemical Society,* vol. 127, pp. 8058-8063, 2005.

Nisisako T. and Hatsuzawa T., "A microfluidic cross-flowing emulsion generator for producing biphasic droplets and anisotropically shaped polymer particles," *Microfluidics and Nanofluidics,* vol. 9, pp. 427-437, 2010.

Nunes J. K., Tsai S. S. H., Wan J., and Stone H. A., "Dripping and jetting in microfluidic multiphase flows applied to particle and fibre synthesis," *Journal of Physics D: Applied Physics,* vol. 46, p. 114002, 2013.

Nurumbetov G., Ballard N., and Bon S. A. F., "A simple microfluidic device for fabrication of double emulsion droplets and polymer microcapsules," *Polymer Chemistry,* vol. 3, pp. 1043-1047, 2012.

Oh D. H., Balakrishnan P., Oh Y.-K., Kim D.-D., Yong C. S., and Choi H.-G., "Effect of process parameters on nanoemulsion droplet size and distribution in SPG membrane emulsification," *International Journal of Pharmaceutics,* vol. 404, pp. 191-197, 2011.

Okushima S., Nisisako T., Torii T., and Higuchi T., "Controlled Production of Monodisperse Double Emulsions by Two-Step Droplet Breakup in Microfluidic Devices," *Langmuir,* vol. 20, pp. 9905-9908, 2004.

Olsson E. and Kreiss G., "A conservative level set method for two phase flow," *Journal of*

Computational Physics, vol. 210, pp. 225-246, 2005.

Ong W.-L., Hua J., Zhang B., Teo T.-Y., Zhuo J., Nguyen N.-T., Ranganathan N., and Yobas L., "Experimental and computational analysis of droplet formation in a high-performance flow-focusing geometry," *Sensors and Actuators A: Physical,* vol. 138, pp. 203-212, 2007.

Osher S. and Sethian J. A., "Fronts propagating with curvature-dependent speed-algorithms based on Hamilton-Jacobi formulations," *Journal of Computational Physics,* vol. 79, pp. 12-49, 1988.

Pathak M., "Numerical simulation of membrane emulsification: Effect of flow properties in the transition from dripping to jetting," *Journal of Membrane Science,* vol. 382, pp. 166-176, 2011.

Pawlik A. K. and Norton I. T., "Encapsulation stability of duplex emulsions prepared with SPG cross-flow membrane, SPG rotating membrane and rotor-stator techniques—A comparison," *Journal of Membrane Science,* vol. 415–416, pp. 459-468, 2012.

Peng H., Xu Z., Chen S., Zhang Z., Li B., and Ge L., "An easily assembled double T-shape microfluidic devices for the preparation of submillimeter-sized polyacronitrile (PAN) microbubbles and polystyrene (PS) double emulsions," *Colloids and Surfaces A: Physicochemical and Engineering Aspects,* vol. 468, pp. 271-279, 2015.

Peng S. and Williams R., "Controlled production of emulsions using a crossflow membrane: Part I: Droplet formation from a single pore," *Chemical Engineering Research and Design,* vol. 76, pp. 894-901, 1998.

Perez-Moral N., Watt S., and Wilde P., "Comparative study of the stability of multiple emulsions containing a gelled or aqueous internal phase," *Food Hydrocolloids,* vol. 42, pp. 215-222, 2014.

Perez A., Hernandez R., Velasco D., Voicu D., and Mijangos C., "Poly (lactic-co-glycolic acid) particles prepared by microfluidics and conventional methods. Modulated particle size and rheology," *Journal of Colloid and Interface Science,* vol. 441, pp. 90-97, 2015.

Pessi J., Santos H. A., Miroshnyk I., JoukoYliruusi, Weitz D. A., and Mirza S., "Microfluidics-assisted engineering of polymeric microcapsules with high encapsulation efficiency for protein drug delivery," *International Journal of Pharmaceutics,* vol. 472, pp. 82-87, 2014.

Piacentini E., Giorno L., Dragosavac M. M., Vladisavljević G. T., and Holdich R. G., "Microencapsulation of oil droplets using cold water fish gelatine/gum arabic complex coacervation by membrane emulsification," *Food Research International,* vol. 53, pp. 362-372, 2013.

Pierce R. G., Islam R., Henderson R. M., and Blanchard A., "SU-8 2000 Millimeter Wave Material

Characterization," *Microwave and Wireless Components Letters, IEEE,* vol. 24, pp. 427-429, 2014.

Qian J. and Law C. K., "Regimes of coalescence and separation in droplet collision," *Journal of Fluid Mechanics,* vol. 331, pp. 59-80, 1997.

Raj R., Mathur N., and Buwa V. V., "Numerical Simulations of Liquid-Liquid Flows in Microchannels," *Industrial and Engineering Chemistry Research,* vol. 49, pp. 10606-10614, 2010.

Rohde M., Kandhai D., Derksen J., and Van den Akker H., "A generic, mass conservative local grid refinement technique for lattice‐Boltzmann schemes," *International Journal for Numerical Methods in Fluids,* vol. 51, pp. 439-468, 2006.

Samimi R., Salarian M., Xu W. Z., Lui E. M. K., and Charpentier P. A., "Encapsulation of Acetyl Ginsenoside Rb-1 within Monodisperse Poly(DL-lactide-co-glycolide) Microspheres Using a Microfluidic Device," *Industrial & Engineering Chemistry Research,* vol. 53, pp. 11333-11344, Jul 2014.

Santos J., Vladisavljević G. T., Holdich R. G., Dragosavac M. M., and Muñoz J., "Controlled production of eco-friendly emulsions using direct and premix membrane emulsification," *Chemical Engineering Research and Design,* vol. 98, pp. 59-69, 2015.

Schneider T., Chapman G. H., and Häfeli U. O., "Effects of chemical and physical parameters in the generation of microspheres by hydrodynamic flow focusing," *Colloids and Surfaces B: Biointerfaces,* vol. 87, pp. 361-368, 2011.

Schulz M., Krafczyk M., Tölke J., and Rank E., "Parallelization strategies and efficiency of CFD computations in complex geometries using Lattice Boltzmann methods on high-performance computers," in *High Performance Scientific and Engineering Computing*, ed: Springer, 2002, pp. 115-122.

Schunk D., Hardt S., Wiggers H., and Marlow F., "Monodisperse titania microspheres via controlled nanoparticle aggregation," *Physical Chemistry Chemical Physics*, vol. 14, pp. 7490-7496, 2012.

Shan X. and Chen H., "Lattice Boltzmann model for simulating flows with multiple phases and components," *Physical Review E,* vol. 47, p. 1815, 1993.

Silva P. S., Stillwell M., Williams B., Dragosavac M., Vladisavljević G. T., Bandulasena H., and Holdich R. G., "Azimuthally oscillating membrane emulsification for controlled droplet production," *AIChE Journal,* 2015.

Sivasamy J., Wong T. N., Nguyen N. T., and Kao L. T. H., "An investigation on the mechanism of

droplet formation in a microfluidic T-junction," *Microfluidics and Nanofluidics,* vol. 11, pp. 1-10, 2011.

Soleymani A., Laari A., and Turunen I., "Simulation of drop formation in a single hole in solvent extraction using the volume-of-fluid method," *Chemical Engineering Research and Design,* vol. 86, pp. 731-738, 2008.

Song K.-Y. and Zhang W.-J., "Application of Nanofluids to Microsphere Generation Using MEMS Technology," *Recent Patents on Nanotechnology,* vol. 7, pp. 133-152, 2013.

Song K. Y., "Design and fabrication of novel microfluidic systems for microsphere generation," Doctor of Philosophy, Department of Biomedical Engineering, University of Saskatchewan, 2011.

Song K. Y., Chiao M., Stoeber B., Häfeli U., Gupta M. M., and Zhang W. J., "Formation of Uniform Microspheres Using a Perforated Silicon Membrane: A Preliminary Study," *Journal of Medical Devices,* vol. 3, pp. 034503-034503, 2009.

Sosnik A., "Production of Drug-Loaded Polymeric Nanoparticles by Electrospraying Technology," *Journal of Biomedical Nanotechnology,* vol. 10, pp. 2200-2217, 2014.

Streeter V. L., Wylie E. B., and Bedford K. W., *Fluid Mechanics, WCB*: McGraw-Hill, 1998.

Sussman M. and Puckett E. G., "A coupled level set and volume-of-fluid method for computing 3D and axisymmetric incompressible two-phase flows," *Journal of Computational Physics,* vol. 162, pp. 301-337, 2000.

Sussman M., Smereka P., and Osher S., "A level set approach for computing solutions to incompressible two-phase flow," *Journal of Computational Physics,* vol. 114, pp. 146-159, 1994.

Tarameshlou M., Jafari S. H., Rezaeian I., and Khonakdar H. A., "Synthesis of biocompatible and degradable microspheres based on 2-hydroxyethyl methacrylate via microfluidic method," *Journal of Applied Polymer Science,* vol. 131, 2014.

Tarchichi N., Chollet F., and Manceau J.-F., "New regime of droplet generation in a T-shape microfluidic junction," *Microfluidics and Nanofluidics,* vol. 14, pp. 45-51, 2013.

Thanh Ha H., Thi Phuong Tuyen D., Tuan Anh N., Duy Dam L., and Mau Chien D., "Cross-flow membrane emulsification technique for fabrication of drug-loaded particles," *Advances in Natural Sciences: Nanoscience and Nanotechnology,* vol. 4, p. 045008, 2013.

Thompson K. L., Armes S. P., and York D. W., "Preparation of Pickering Emulsions and Colloidosomes with Relatively Narrow Size Distributions by Stirred Cell Membrane Emulsification," *Langmuir,* vol. 27, pp. 2357-2363, 2011.

Thorsen T., Roberts R. W., Arnold F. H., and Quake S. R., "Dynamic pattern formation in a vesicle-generating microfluidic device," *Physical Review Letters,* vol. 86, pp. 4163-4166, 2001.

Tice J. D., Song H., Lyon A. D., and Ismagilov R. F., "Formation of droplets and mixing in multiphase microfluidics at low values of the Reynolds and the capillary numbers," *Langmuir,* vol. 19, pp. 9127-9133, 2003.

Timgren A., Trägårdh G., and Trägårdh C., "CFD modelling of drop formation in a liquid-liquid system," presented at the 6th International Conference on Multiphase Flow, Leipzig, Germany, 2007.

Timgren A., Trägårdh G., and Trägårdh C., "A model for drop size prediction during cross-flow emulsification," *Chemical Engineering Research and Design,* vol. 88, pp. 229-238, 2010.

Ushikubo F. Y., Birribilli F. S., Oliveira D. R. B., and Cunha R. L., "Y- and T-junction microfluidic devices: effect of fluids and interface properties and operating conditions," *Microfluidics and Nanofluidics,* vol. 17, pp. 711-720, 2014.

Utada A. S., Fernandez-Nieves A., Gordillo J. M., and Weitz D. A., "Absolute Instability of a Liquid Jet in a Coflowing Stream," *Physical Review Letters,* vol. 100, p. 014502, 2008.

Utada A. S., Fernandez-Nieves A., Stone H. A., and Weitz D. A., "Dripping to jetting transitions in coflowing liquid streams," *Physical Review Letters,* vol. 99, p. 094502, 2007.

Van der Graaf S., Nisisako T., Schroen C., Van der Sman R. G. M., and Boom R. M., "Lattice Boltzmann simulations of droplet formation in a T-shaped microchannel," *Langmuir,* vol. 22, pp. 4144-4152, 2006.

Van der Graaf S., Schroën C., Van der Sman R., and Boom R., "Influence of dynamic interfacial tension on droplet formation during membrane emulsification," *Journal of Colloid and Interface Science,* vol. 277, pp. 456-463, 2004.

Van der Graaf S., Steegmans M., Van der Sman R., Schroën C., and Boom R., "Droplet formation in a T-shaped microchannel junction: a model system for membrane emulsification," *Colloids and Surfaces A: Physicochemical and Engineering Aspects,* vol. 266, pp. 106-116, 2005.

Van der Pijl S., Segal A., Vuik C., and Wesseling P., "A mass conserving Level Set method for modelling of multiphase flows," *International Journal for Numerical Methods in Fluids,* vol. 47, pp. 339-361, 2005.

Vernekar V. N., Cullen D. K., Fogleman N., Choi Y., García A. J., Allen M. G., Brewer G. J., and LaPlaca M. C., "SU‐8 2000 rendered cytocompatible for neuronal bioMEMS applications,"

Journal of Biomedical Materials Research Part A, vol. 89, pp. 138-151, 2009.

Vilanova N., Rodríguez-Abreu C., Fernández-Nieves A., and Solans C., "Fabrication of Novel Silicone Capsules with Tunable Mechanical Properties by Microfluidic Techniques," *ACS Applied Materials & Interfaces,* vol. 5, pp. 5247-5252, 2013/06/12 2013.

Vladisavljević G. T., Kobayashi I., and Nakajima M., "Production of uniform droplets using membrane, microchannel and microfluidic emulsification devices," *Microfluidics and Nanofluidics,* vol. 13, pp. 151-178, 2012.

Vladisavljevic G. T. and Schubert H., "Preparation and analysis of oil-in-water emulsions with a narrow droplet size distribution using Shirasu-porous-glass (SPG) membranes," *Desalination,* vol. 144, pp. 167-172, 2002.

Vladisavljević G. T. and Schubert H., "Influence of process parameters on droplet size distribution in SPG membrane emulsification and stability of prepared emulsion droplets," *Journal of Membrane Science,* vol. 225, pp. 15-23, 2003.

Vladisavljević G. T., Shahmohamadi H., Das D. B., Ekanem E. E., Tauanov Z., and Sharma L., "Glass capillary microfluidics for production of monodispersed poly (dl-lactic acid) and polycaprolactone microparticles: Experiments and numerical simulations," *Journal of Colloid and Interface Science,* vol. 418, pp. 163-170, 2014.

Vladisavljevic G. T. and Williams R. A., "Manufacture of large uniform droplets using rotating membrane emulsification," *Journal of Colloid and Interface Science,* vol. 299, pp. 396-402, 2006.

Volk A., Rossi M., Kahler C. J., Hilgenfeldt S., and Marin A., "Growth control of sessile microbubbles in PDMS devices," *Lab on a Chip,* vol. 15, pp. 4607-4613, 2015.

Wagdare N. A., Marcelis A. T. M., Ho O. B., Boom R. M., and van Rijn C. J. M., "High throughput vegetable oil-in-water emulsification with a high porosity micro-engineered membrane," *Journal of Membrane Science,* vol. 347, pp. 1-7, 2010.

Wan J., Bick A., Sullivan M., and Stone H. A., "Controllable microfluidic production of microbubbles in water-in-oil emulsions and the formation of porous microparticles," *Advanced Materials,* vol. 20, p. 3314, 2008.

Wang J., Wang M., and Li Z., "A lattice Boltzmann algorithm for fluid–solid conjugate heat transfer," *International Journal of Thermal Sciences,* vol. 46, pp. 228-234, 2007.

Wang K., Lu Y. C., Tan J., Yang B. D., and Luo G. S., "Generating gas/liquid/liquid three-phase

microdispersed systems in double T-junctions microfluidic device," *Microfluidics and Nanofluidics*, vol. 8, pp. 813-821, 2010.

Wang W., Liu Z., Jin Y., and Cheng Y., "LBM simulation of droplet formation in micro-channels," *Chemical Engineering Journal,* vol. 173, pp. 828-836, 2011.

Ward T., Faivre M., Abkarian M., and Stone H. A., "Microfluidic flow focusing: Drop size and scaling in pressure versus flow-rate-driven pumping," *Electrophoresis,* vol. 26, pp. 3716-3724, 2005.

Watanabe T., G. Lopez C., Douglas J. F., Ono T., and Cabral J. T., "Microfluidic Approach to the Formation of Internally Porous Polymer Particles by Solvent Extraction," *Langmuir,* vol. 30, pp. 2470-2479, 2014.

Watanabe T., Kimura Y., and Ono T., "Microfluidic Fabrication of Monodisperse Polylactide Microcapsules with Tunable Structures through Rapid Precipitation," *Langmuir,* vol. 29, pp. 14082-14088, 2013.

Wörner M., "Numerical modeling of multiphase flows in microfluidics and micro process engineering: a review of methods and applications," *Microfluidics and nanofluidics,* vol. 12, pp. 841-886, 2012.

Wu B. and Gong H.-Q., "Formation of fully closed microcapsules as microsensors by microfluidic double emulsion," *Microfluidics and Nanofluidics,* vol. 14, pp. 637-644, 2013.

Wu L., Tsutahara M., Kim L. S., and Ha M., "Three-dimensional lattice Boltzmann simulations of droplet formation in a cross-junction microchannel," *International Journal of Multiphase Flow,* vol. 34, pp. 852-864, 2008.

Wu P., Wang Y., Luo Z. F., Li Y. T., Li M. F., and He L. Q., "A 3D easily-assembled Micro-Cross for droplet generation," *Lab on a Chip,* vol. 14, pp. 795-798, 2014.

Xu J. H., Luo G. S., Chen G. G., and Wang J. D., "Experimental and theoretical approaches on droplet formation from a micrometer screen hole," *Journal of Membrane Science,* vol. 266, pp. 121-131, 2005.

Xu Q. Y. and Nakajima M., "The generation of highly monodisperse droplets through the breakup of hydrodynamically focused microthread in a microfluidic device," *Applied Physics Letters,* vol. 85, pp. 3726-3728, 2004.

Xue P., Wu Y., Menon N., and Kang Y., "Microfluidic synthesis of monodisperse PEGDA microbeads for sustained release of 5-fluorouracil," *Microfluidics and Nanofluidics,* vol. 18, pp. 333-342, 2015.

Yan Y. Y., "Recent Advances in Computational Simulation of Macro-, Meso-, and Micro-Scale

Biomimetics Related Fluid Flow Problems," *Journal of Bionic Engineering,* vol. 4, pp. 97-107, 2007.

Yang C. H., Huang K. S., Grumezescu A. M., Wang C. Y., Tzeng S. C., Chen S. Y., Lin Y. H., and Lin Y. S., "Synthesis of uniform poly(D,L-lactide) and poly(D,L-lactide-co-glycolide) microspheres using a microfluidic chip for comparison," *Electrophoresis,* vol. 35, pp. 316-322, 2014.

Yeh C. H. and Lin Y. C., "Use of an adjustable microfluidic droplet generator to produce uniform emulsions with different concentrations," *Journal of Micromechanics and Microengineering,* vol. 23, p. 125025, 2013.

Yeom S. and Lee S. Y., "Size prediction of drops formed by dripping at a micro T-junction in liquid-liquid mixing," *Experimental Thermal and Fluid Science,* vol. 35, pp. 387-394, 2011.

Yokoi K., "Efficient implementation of THINC scheme: a simple and practical smoothed VOF algorithm," *Journal of Computational Physics,* vol. 226, pp. 1985-2002, 2007.

Yoo J.-W. and Mitragotri S., "Polymer particles that switch shape in response to a stimulus," *Proceedings of the National Academy of Sciences,* vol. 107, pp. 11205-11210, 2010.

Yoshino M., Matsuda Y., and Shao C., "Comparison of accuracy and efficiency between the lattice Boltzmann method and the finite difference method in viscous/thermal fluid flows," *International Journal of Computational Fluid Dynamics,* vol. 18, pp. 333-345, 2004.

Yu Z., "A novel lattice Boltzmann method for direct numerical simulation of multiphase flows," Doctoral dissertation, The Ohio State University, 2009.

Yu Z., Hemminger O., and Fan L. S., "Experiment and lattice Boltzmann simulation of two-phase gas–liquid flows in microchannels," *Chemical Engineering Science,* vol. 62, pp. 7172-7183, 2007.

Yuan P. and Schaefer L., "Equations of state in a lattice Boltzmann model," *Physics of Fluids,* vol. 18, p. 042101, 2006.

Zabihi F., Xin N., Jia J., Chen T., and Zhao Y., "High Yield and High Loading Preparation of Curcumin–PLGA Nanoparticles Using a Modified Supercritical Antisolvent Technique," *Industrial & Engineering Chemistry Research,* vol. 53, pp. 6569-6574, 2014/04/16 2014.

Zamora-Mora V., Velasco D., Hernández R., Mijangos C., and Kumacheva E., "Chitosan/agarose hydrogels: Cooperative properties and microfluidic preparation," *Carbohydrate Polymers,* vol. 111, pp. 348-355, 2014.

Zhang J., "Lattice Boltzmann method for microfluidics: models and applications," *Microfluidics and Nanofluidics,* vol. 10, pp. 1-28, 2011.

Zhang Q. J., Lin G. Y., Wang Y., Yang F. J., Ba L., and Fu D. G., "Formation of monodisperse cross-linked nanospherial condensates based on flow-focusing and droplet diffusion techniques," *Colloids and Surfaces a-Physicochemical and Engineering Aspects*, vol. 384, pp. 53-57, Jul 2011.

Zhang W., "Towards a New Paradigm of Theory for Having a Dynamic System: Operation Management Through Design (OMTD)," Shanghai University, Shanghai2010.

Zhang W. and Van Luttervelt C., "Toward a resilient manufacturing system," *CIRP Annals-Manufacturing Technology*, vol. 60, pp. 469-472, 2011.

Zhang W. J., Li Q., and Guo L. S., "Integrated design of mechanical structure and control algorithm for a programmable four-bar linkage," *Mechatronics, IEEE/ASME Transactions on*, vol. 4, pp. 354-362, 1999.

Zhou Q.-Z., Wang L.-Y., Ma G.-H., and Su Z.-G., "Preparation of uniform-sized agarose beads by microporous membrane emulsification technique," *Journal of Colloid and Interface Science*, vol. 311, pp. 118-127, 2007.

APPENDIX. COPYRIGHT PERMISSIONS

1 Permission for Figure 2.1:

ELSEVIER LICENSE
TERMS AND CONDITIONS

Jan 13, 2016

This is a License Agreement between lei lei ("You") and Elsevier ("Elsevier") provided by Copyright Clearance Center ("CCC"). The license consists of your order details, the terms and conditions provided by Elsevier, and the payment terms and conditions.

All payments must be made in full to CCC. For payment instructions, please see information listed at the bottom of this form.

Supplier	Elsevier Limited The Boulevard,Langford Lane Kidlington,Oxford,OX5 1GB,UK
Registered Company Number	1982084
Customer name	lei lei
Customer address	403-107 cumberland
	saskatoon, SK s7n2r6
License number	3786140632692
License date	Jan 11, 2016
Licensed content publisher	Elsevier
Licensed content publication	Chemical Engineering Research and Design
Licensed content title	Controlled Production of Emulsions Using a Crossflow Membrane Part I: Droplet Formation from a Single Pore
Licensed content author	S.J. Peng,R.A. Williams
Licensed content date	November 1998
Licensed content volume number	76
Licensed content issue number	8
Number of pages	8
Start Page	894
End Page	901
Type of Use	reuse in a thesis/dissertation
Intended publisher of new work	other
Portion	figures/tables/illustrations
Number of figures/tables/illustrations	1
Format	both print and electronic
Are you the author of this Elsevier article?	No
Will you be translating?	No
Original figure numbers	fig 1
Title of your thesis/dissertation	MODELING AND OPTIMIZATION OF THE MICROSPHERE GENERATION PROCESS
Expected completion date	Jan 2016
Estimated size (number of pages)	135
Elsevier VAT number	GB 494 6272 12
Permissions price	0.00 CAD
VAT/Local Sales Tax	0.00 CAD / 0.00 GBP
Total	0.00 CAD

2 Permission for Figure 2.8:

SPRINGER LICENSE
TERMS AND CONDITIONS

Jan 13, 2016

This is a License Agreement between lei lei ("You") and Springer ("Springer") provided by Copyright Clearance Center ("CCC"). The license consists of your order details, the terms and conditions provided by Springer, and the payment terms and conditions.

All payments must be made in full to CCC. For payment instructions, please see information listed at the bottom of this form.

License Number	3786140450196
License date	Jan 11, 2016
Licensed content publisher	Springer
Licensed content publication	Microfluids and Nanofluids
Licensed content title	A microfluidic cross-flowing emulsion generator for producing biphasic droplets and anisotropically shaped polymer particles
Licensed content author	Takasi Nisisako
Licensed content date	Jan 1, 2009
Volume number	9
Issue number	2
Type of Use	Thesis/Dissertation
Portion	Figures/tables/illustrations
Number of figures/tables/illustrations	1
Author of this Springer article	No
Order reference number	None
Original figure numbers	fig 1
Title of your thesis / dissertation	MODELING AND OPTIMIZATION OF THE MICROSPHERE GENERATION PROCESS
Expected completion date	Jan 2016
Estimated size(pages)	135
Total	0.00 CAD

3 Permission for Figure 2.21:

ELSEVIER LICENSE
TERMS AND CONDITIONS

Jan 13, 2016

This is a License Agreement between lei lei ("You") and Elsevier ("Elsevier") provided by Copyright Clearance Center ("CCC"). The license consists of your order details, the terms and conditions provided by Elsevier, and the payment terms and conditions.

All payments must be made in full to CCC. For payment instructions, please see information listed at the bottom of this form.

Supplier	Elsevier Limited The Boulevard,Langford Lane Kidlington,Oxford,OX5 1GB,UK
Registered Company Number	1982084
Customer name	lei lei
Customer address	403-107 cumberland
	saskatoon, SK s7n2r6
License number	3787391283495
License date	Jan 13, 2016
Licensed content publisher	Elsevier
Licensed content publication	Chemical Engineering Science
Licensed content title	Experiment and lattice Boltzmann simulation of two-phase gas–liquid flows in microchannels
Licensed content author	Zhao Yu,Orin Hemminger,Liang-Shih Fan
Licensed content date	December 2007
Licensed content volume number	62
Licensed content issue number	24
Number of pages	12
Start Page	7172
End Page	7183
Type of Use	reuse in a thesis/dissertation
Intended publisher of new work	other
Portion	figures/tables/illustrations
Number of figures/tables/illustrations	1
Format	both print and electronic
Are you the author of this Elsevier article?	No
Will you be translating?	No
Original figure numbers	fig 12
Title of your thesis/dissertation	MODELING AND OPTIMIZATION OF THE MICROSPHERE GENERATION PROCESS
Expected completion date	Jan 2016
Estimated size (number of pages)	135
Elsevier VAT number	GB 494 6272 12
Permissions price	0.00 CAD
VAT/Local Sales Tax	0.00 CAD / 0.00 GBP
Total	0.00 CAD

4 Permission for Figure 3.1:

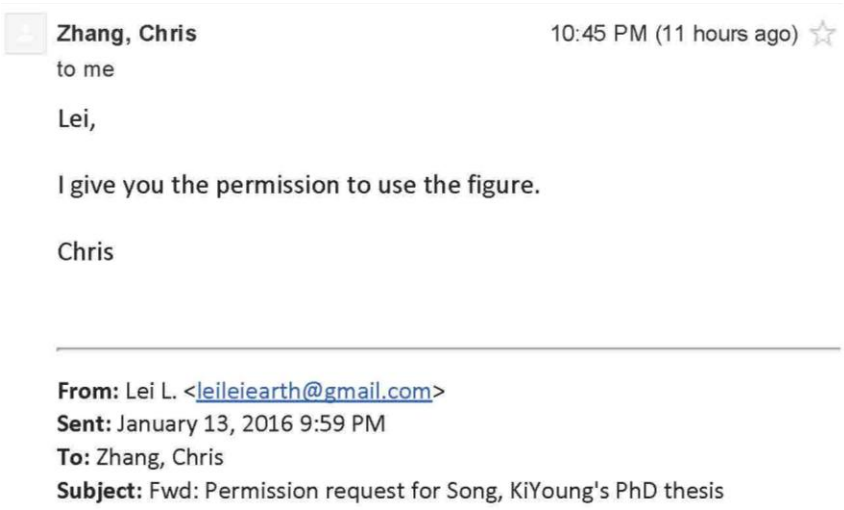

Zhang, Chris 10:45 PM (11 hours ago)
to me

Lei,

I give you the permission to use the figure.

Chris

From: Lei L. <leileiearth@gmail.com>
Sent: January 13, 2016 9:59 PM
To: Zhang, Chris
Subject: Fwd: Permission request for Song, KiYoung's PhD thesis

5 Permission for the following conference proceedings presented in the thesis:

Lei, L., Zhang, H., Bergstrom, D., Zhang, B., Song, K., Zhang, W. J., "Modeling and Validation of Microspheres Generation in the Modified T-Junction Device," in *Mechanical and Mechatronics Engineering*, 2015, 1(5), 696.

Lei, L., Zhang, H., Bergstrom, D., Zhang, B., Zhang, W. J., "Modeling Of Droplet Generation by a Modified T-Junction Device Using COMSOL," in *Applied Mechanics and Materials*, 2015, pp. 112-116

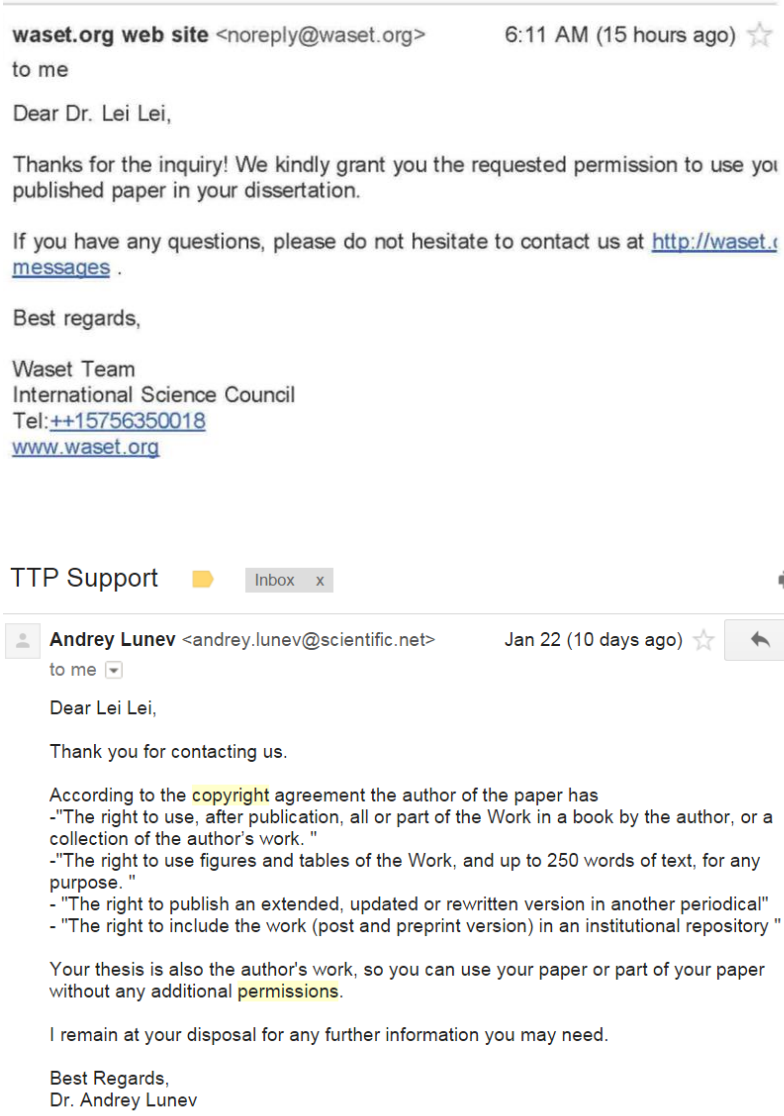

waset.org web site <noreply@waset.org> 6:11 AM (15 hours ago)

to me

Dear Dr. Lei Lei,

Thanks for the inquiry! We kindly grant you the requested permission to use you published paper in your dissertation.

If you have any questions, please do not hesitate to contact us at http://waset.c messages .

Best regards,

Waset Team
International Science Council
Tel:++15756350018
www.waset.org

TTP Support Inbox x

Andrey Lunev <andrey.lunev@scientific.net> Jan 22 (10 days ago)

to me

Dear Lei Lei,

Thank you for contacting us.

According to the copyright agreement the author of the paper has
-"The right to use, after publication, all or part of the Work in a book by the author, or a collection of the author's work. "
-"The right to use figures and tables of the Work, and up to 250 words of text, for any purpose. "
- "The right to publish an extended, updated or rewritten version in another periodical"
- "The right to include the work (post and preprint version) in an institutional repository "

Your thesis is also the author's work, so you can use your paper or part of your paper without any additional permissions.

I remain at your disposal for any further information you may need.

Best Regards,
Dr. Andrey Lunev